Eigenvalue Based Detector in Finite and Asymptotic Multi-antenna Cognitive Radio Systems

Hussein Kobeissi

N° d'ordre: 2016-36-TH

CentraleSupélec – Lebanese University

Ecole Doctorale MATISSE and Ecole Doctorale Science et Technologies

IETR Laboratory

DOCTORAL THESIS

Specialty: Telecommunications and Signal Processing

Defended the 13th of December 2016

by:

Hussein KOBEISSI

Eigenvalue Based Detector in Finite and Asymptotic Multi-Antenna Cognitive Radio Systems

Jury:

Supervisors:	Oussama BAZZI	Prof., Lebanese University (Lebanon)
	Yves LOUET	Prof., CentraleSupélec (France)
Co-supervisors:	Youssef NASSER	Ass. Prof., American Univ. of Beirut (Lebanon)
	Amor NAFKHA	Ass. Prof., CentraleSupélec (France)
President of jury:	Abed Ellatif SAMHAT	prof., Lebanese University (Lebanon)
Rapporteurs:	Inbar FIJALKOW	Prof., ETSI (France)
	Chafic MOKBEL	Prof., Balamand University (Lebanon)
Examiners:	Abed Ellatif SAMHAT	prof., Lebanese University (Lebanon)
	Maher JRIDI	Ass. Prof., ISEN (France)

Abstract

During the last decades, wireless communications have visualized an exponential growth due to rapidly expanding market of wireless broadband and multimedia users and applications. Indeed, the demand for more radio spectrum increased in order to support this growth which highlighted on the scarcity and under-utilization problems of the radio spectrum resources. To this end, Cognitive Radio (CR) technology has received an enormous attention as an emerging solution to the spectrum shortage problem for the next generation wireless communication systems. For the CR to operate efficiently and to provide the required improvement in spectrum efficiency, it must be able to effectively identifies the spectrum holes. Thus, Spectrum Sensing (SS) is the key element and critical component of the CR technology. In CR networks, Spectrum Sensing (SS) is the task of obtaining awareness about the spectrum usage. Mainly it concerns two scenarios of detection: (i) detecting the absence of the Primary User (PU) in a licensed spectrum in order to use it and (ii) detecting the presence of the PU to avoid interference. Several SS techniques were proposed in the literature. Among these, Eigenvalue Based Detector (EBD) has been proposed as a precious totally-blind detector that exploits the spacial diversity, overcome noise uncertainty challenges and performs adequately even in low SNR conditions. However, the complexity of the distributions of decision metrics of the EBD is one of the important challenges. Moreover, the use massive MIMO technology in SS is still not explored.

The first part of this study concerns the Standard Condition Number (SCN) detector and the Scaled Largest Eigenvalue (SLE) detector. The focus is on the complexity of the statistical distributions of the SCN and the SLE decision metrics since this will imply a complicated expressions for the performance probabilities as well as the decision threshold if it could be derived. We derive exact expressions for the Probability Density Function (PDF) and

the Cumulative Distribution Function (CDF) of the SCN using results from finite Random Matrix Theory (RMT). In addition, we derived exact expressions for the moments of the SCN and we proposed a new approximation based on the Generalized Extreme Value (GEV) distribution. Moreover, using results from the asymptotic RMT we further provide a simple forms for the central moments of the SCN and we end up with a simple and accurate expression for the CDF, PDF, Probability of False-Alarm (P_{fa}), Probability of Detection (P_d), Probability of Miss-Detection (Pmd) and the decision threshold that could be computed on the fly and hence provide a dynamic SCN detector that could dynamically change the threshold value depending on target performance and environmental conditions. On the other hand, we proved that the SLE decision metric could be modelled using Gaussian function and hence we derived its PDF, CDF, P_{fa}, P_d and decision threshold. In addition, we also considered the correlation between the largest eigenvalue and the trace in the SLE study.

The second part of this study concerns the massive MIMO technology and how to exploit the large number of antennas for SS and CRs. Two antenna exploitation scenarios are studied: (i) Full antenna exploitation and (ii) Partial antenna exploitation in which we have two options: (i) Fixed use or (ii) Dynamic use of the antennas. We considered the Largest Eigenvalue (LE) detector if noise power is perfectly known and the SCN and SLE detectors when noise uncertainty exists. For fixed approach, we derived the optimal threshold which minimizes the error probabilities. For the dynamic approach, we derived the equation from which one can compute the minimum requirements of the system. For full exploitation, asymptotic approximation of the threshold is considered using the GEV distribution. Finally, a comparisons between these scenarios and different detectors are provided in terms of system performance and minimum requirements. This work presents a novel study in the field of SS applications in CR with massive MIMO technology.

Acknowledgments

Firstly, I would like to express my sincere gratitude to my supervisors Professors Oussama Bazzi and Yves Louet for giving me the opportunity to pursue doctoral studies and providing an excellent work environment to carry out this research study. I am very much grateful to your continuous support, motivations, patience, insightful suggestions, and encouraging feedback.

Likewise, I am highly indebted to my co-supervisors Dr. Youssef Nasser and Dr. Amor Nafkha for your day to day supervision, excellent technical guidance and quick feedback on my research works. You have always motivated me in selecting valid research problems and modeling them correctly, and provided a lot of freedom in my research work while also keeping track in good directions with gentle pushes. Also, many thanks to my colleagues at the SCEE and HKS for their direct and indirect supports during my PhD period.

I would also like to thank the committee, Professors Abed Ellatif Samhat, Inbar Fijalkow, Chafic Mokbel and Maher Jridi, who supported with their precious time and useful suggestions.

Finally, This work was funded by a program of cooperation between the Lebanese University and the Azem & Saada social foundation (LU-AZM) and by CentraleSupélec (France).

Acronyms

AC Asymptotic Condition

CR Cognitive Radio

CC Critical Condition

CFAR Constant False Alarm Rate

CDF Cumulative Distribution Function

DCN Demmel Condition Number

DoF Degrees of Freedom

EBD Eigenvalue Based Detector

GEV Generalized Extreme Value

LE Largest Eigenvalue

LUT Lookup Table

MIMO Multiple Input Multiple Output

MGF Moment Generating Function

PU Primary User

PR Primary Receiver

PT Primary Transmitter

PDF Probability Distribution Function

RMT Random Matrix Theory

RF Radio Frequency

SS Spectrum Sensing

SU Secondary User

SR Secondary Receiver

ST Secondary Transmitter

SLE Scaled Largest Eigenvalue

SCN Standard Condition Number

SNR Signal-to-Noise Ratio

TW2 Tracy-Widom distribution order 2

List of Figures

List of Tables

Contents

Résumé des travaux de thèse

Motivation et chapitre 1

Le concept de la radio intelligente est apparu avec les travaux de J. Mitola [9]. Les études menées par Mitola visaient à rendre un équipement radio conscient de l'évolution de son environnement et aussi être capable d'adapter son comportement afin d'en collecter des informations permettant, au fur et à mesure des expériences, les meilleurs choix (bandes de fréquence, débits, performances, configurations, etc.).

L'objectif principal de la radio intelligente consiste à proposer une solution efficace et dynamique afin de palier à la politique rigide de gestion du spectre et au problème de pénurie et de sous-exploitation du spectre. Généralement, les allocations statiques du spectre radio conduisent à une utilisation inefficace du spectre en créant des trous dans le spectre à un instant donné et/ou une localité donnée. Afin de favoriser une meilleure utilisation du spectre radio, la radio intelligente permet d'envisager des scénarios d'accès dynamique au spectre permettant d'offrir plus de services. La technique d'accès dynamique au spectre est centrée autour de partage du spectre radio entre des utilisateurs licenciés (utilisateurs primaires) et des utilisateurs non licenciés (utilisateurs secondaires). Les utilisateurs primaires ont une priorité absolue pour accéder à la bande spectrale dont ils possèdent la licence. Les utilisateurs secondaires peuvent soit utiliser les bandes du spectre inutilisées par les utilisateurs primaires ou bien coexister dans les mêmes bandes que les utilisateurs primaires en garantissant un niveau d'interférence très faible de façon à ne pas affecter leurs communications. Les principales fonctions d'un équipement radio secondaire (utilisateur secondaire) sont : la détection des bandes inutilisées, l'analyse et décision sur le spectre et ladaptation. Ainsi, l'utilisateur secondaire doit interagir avec son environnement radio afin de s'y

adapter, d'y détecter les spectres libres et de les exploiter. Il doit veiller en priorité à minimiser ses erreurs d'observation pour réduire la probabilité de fausse alarme, c'est-à-dire la probabilité de détecter la présence d'un utilisateur primaire alors qu'il est en fait absent, et la probabilité de non-détection, c'est-à-dire la probabilité de détecter l'absence d'un utilisateur primaire alors qu'il est en fait présent. Généralement, les utilisateurs secondaires n'ont presque pas d'information a priori sur les caractéristiques des signaux des utilisateurs primaires et le taux d'occupation des bandes du spectre.

L'interaction récente entre la théorie des matrices aléatoires et le monde des radio communications a donné lieu à un développement rapide de plusieurs travaux théoriques tels que : la capacité asymptotique des canaux radio mobiles, la capacité des réseaux ad-hoc, les réseaux de neurones, l'estimation des directions d'arrivée dans les réseaux de capteurs. Cette théorie permet asymptotiquement la dérivation de la densité de probabilité des valeurs propres de matrices aléatoires, dont la dimension tend vers l'infini. Des progrès ont été réalisés sur le calcul de la capacité ergodique ainsi que la capacité de coupure. Le nombre d'antennes nécessaires pour atteindre les effets de Massive MIMO, ainsi que les aspects de l'efficacité énergétique ont été largement étudiés. Il y a eu un intérêt pour développer des méthodes de détection de bandes libres basées sur les valeurs propres. Les performances en terme de la probabilité de fausse alarme et probabilité de détection s'appuient uniquement sur les distributions asymptotiques des valeurs propres. Ces analyses ne sont pas exactes étant donné qu'on dispose d'un nombre fini d'échantillons.

Dans cette thèse, nous analysons l'impact de l'utilisation d'un nombre fini d'échantillons sur les performances de différents détecteurs utilisant des valeurs propres de la matrice de covariance.

Chapitre 2

Le chapitre 2 de la thèse constitue une introduction à la détection de spectre dans le contexte de la radio intelligente. Après avoir introduit la notion d'utilisateur primaire et secondaire, la notion d'hyper-espace est énoncée. Cet hyper-espace caractérise toutes les dimensions utiles d'un utilisateur : le temps (dans le sens temps d'occupation du canal), la fréquence (bande d'utilisation du canal), espace (notion de cellules), les angles d'arrivée, le code (si l'accès multi-utilisateurs est un système de type CDMA) et la polarisation (horizontale ou verticale). Dans le contexte de la thèse, un utilisateur sera

caractérisé par son occupation spectrale et l'objectif de la détection de spectre est alors de décider s'il y a présence ou non d'un utilisateur dans une bande donnée. La littérature est très abondante à ce sujet et le chapitre 2 en propose un état de l'art très précis. Après avoir insisté sur le caractère aveugle ou non aveugle des détecteurs, l'auteur présente un certain nombre de méthodes classiques de la littérature : (i) le détecteur d'énergie est la méthode la plus naturelle et la plus optimale mais nécessite la connaissance du niveau de bruit (ii) le détecteur de cyclostationnarités : tout signal de télécommunications étant composé de périodicités (fréquence symbole, porteuse, .), tout signature de telles périodicités permet d'affirmer qu'il y a un utilisateur présent dans une bande donnée. Plus complexe que le détecteur d'énergie, le détecteur cyclostationnaire est bien plus performant (iii) les détecteurs à base de valeurs propres : nécessitant plusieurs antennes en émission et/ou réception, ces détecteurs très performants permettent de détecter, à travers des variations des statistiques des valeurs propres d'une matrice de covariance du signal reçu, s'il y a présence ou pas d'un utilisateur. Un certain nombre de métriques sont associées à ce type de détecteur : le nombre de conditionnement, la valeur propre maximale pondérée, la valeur propre maximale pondérée par la variance du bruit.

Chapitre 3

Le chapitre 3 se concentre sur les performances du détecteur à base du nombre de conditionnement de la matrice de covariance du signal reçu. Une première contribution a été de proposer une formulation théorique de la distribution conjointe des valeurs propres de la matrice de corrélation dans le cas d'une matrice de Wishart centrée semi-corrélée dans le cas où les valeurs propres sont identiques. Les cas centrés/non centrés ont été ensuite étudiés et les résultats théoriques à faibles rapport signal à bruit sont tout à fait conformes aux simulations. A fort rapports signal à bruit, si le nombre d'échantillons est suffisamment grand, les relations obtenues permettent d'avoir une bonne mesure de la probabilité de détection. De plus dans le cas fini (non asymptotique), des relations théoriques du nombre de conditionnement ont été obtenues dans les cas centrés semi-corrélées et non centrés non corrélés. Pour réduire la complexité induite pour le calcul exact du nombre de conditionnement, nous en avons approximé la distribution grce à la distribution GEV basé sur la méthode d'équivalence des moments. Par conséquent, des expres-

sions simples des probabilités de fausse alarme, de probabilité de détection et du seuil de décision ont été proposées de telle façon qu'un système radio intelligent à grand nombre d'antennes puisse adapter en temps réel le seuil de décision en fonction des conditions de propagation.

Chapitre 4

Le chapitre 4 constitue une étude du détecteur SLE (Scaled Largest Eigenvalue) (le SLE est le rapport de la valeur propre la plus grande et de la moyenne des valeurs propres). Le SLE est le détecteur optimal dans le cas d'un seul utilisateur primaire dans le cas où la valeur du bruit est incertaine. Dans le chapitre 4, les expressions des densités de probabilités et de répartition ont été proposées dans le cas du SLE pour les probabilités de fausse alarme, la probabilité de détection et pour le seuil de détection. Ensuite les expressions des corrélations entre valeurs propres ont été proposées. Dans les deux cas (hypothèses H_0 et H_1), les expressions ont été validées avec les simulations.

Chapitre 5

Le dernier chapitre de la thèse aborde le problème de la détection de spectres dans un contexte multi-antennes (MIMO). Dans ce cas d'étude, on suppose qu'un système radio intelligent est équipé d'un nombre important d'antennes à la fois en émission et réception. En reprenant les détecteurs étudiés dans les chapitres précédents (LE, SCN, SLE), l'apport d'un système multi-antennes est abordé en considérant à la fois une exploitation totale puis partielle des informations fournies par les antennes. Des expressions des densités de probabilités et fonction de répartition du détecteur LE ont été proposées et approximées grâce à la densité GEV (à la fois dans le cas fini et asymptotique) pour obtenir des expressions simples du seuil de décision. Ceci a alors permis de détailler les caractéristiques requises par un système radio intelligent pour les détecteurs LE, SLE et SCN. Il a enfin été montré que l'approche dynamique aboutissait à de meilleurs résultats.

Publications de l'auteur

Publications dans des journaux

- Hussein Kobeissi, Youssef Nasser, Amor Nafkha, Oussama Bazzi, Yves Louet "On the detection probability of the standard condition number detector in finite dimensional cognitive radio context", EURASIP, Journal on Wireless Communications and Networking, DOI: 10.1186/s13638-016-0634-0, Published: 23 May 2016

- Hussein Kobeissi, Youssef Nasser, Amor Nafkha, Oussama Bazzi, Yves Louet, " On Approximating the Standard Condition Number for Cognitive Radio Spectrum Sensing with Finite Number of Sensors", DOI: 10.1049/iet-spr.2016.0146 , Online ISSN 1751-9683, Volume 11, Issue 2, p.145-154, Available online: 30 August 2016, IET Signal Processing, 2016

- Hussein Kobeissi, Amor Nafkha, Youssef Nasser, Oussama Bazzi, Yves Louet "On the Performance Analysis and Evaluation of Scaled Largest Eigenvalue in Spectrum Sensing: A Simple Form Approach" EAI Endorsed Transactions on Cognitive Communications 17(10): e5, Volume 3, Feb. 2017

- Hussein Kobeissi, Youssef Nasser, Amor Nafkha, Oussama Bazzi, Yves Louet, "Asymptotic Approximation of the Standard Condition Number Detector for Large Multi-Antenna Cognitive Radio Systems", EAI Endorsed Transactions on Cognitive Communications 17(11): e1, Volume 3, May 2017

Publications dans des conférences

- H. Kobeissi, Y. Nasser, A. Nafkha, O. Bazzi and Y. Louet, "A Simple formulation for the Distribution of the Scaled Largest Eigenvalue and application to Spectrum Sensing", 11th International Confere nce on Cognitive Radio Oriented Wireless Networks (Crowncom), GRENOBLE, May 2016.

- H. Kobeissi, A. Nafkha, Y. Nasser, O. Bazzi and Y. Louet, "Simple and Accurate Closed-Form Approximation of the Standard Condition

Number Distribution with Application in Spectrum Sensing", 11th International Conference on Cognitive Radio Oriented Wireless Networks (Crowncom), GRENOBLE, May 2016.

- H. Kobeissi, Y. Nasser, O. Bazzi, Y. Louet and A. Nafkha, "On the Performance Evaluation of the Eigenvalue-Based Spectrum Sensing Detector for MIMO Systems", URSI GASS 2014, Beijing, Aug. 2014.

- Hussein Kobeissi, Amor Nafkha, Yves Louet "Eigenvalue-based spectrum sensing with two receive antennas", GRETSI 2015, Lyon, France

Chapter 1

Introduction

1.1 Background and Motivation

During the last decades, wireless communications have visualized an exponential growth due to fast expanding market of wireless broadband and multimedia users and applications. Indeed, the demand for more radio spectrum increased in order to support this growth. In this regard, the traditional Static Spectrum Allocation (SSA) policy that assigns, via auctions, particular portions of the spectrum to licensees is successful in avoiding the interference between different services. However, since the radio frequency spectrum is a limited natural resource, this policy is not the best solution as the spectrum scarcity is being a critical problem. Nevertheless, several spectrum occupancy measurements have been conducted worldwide, for example in the U.S., Germany, Spain, China, New Zealand, Singapore, Qatar and India, revealed that most of the allocated spectrum remains under-utilized over a wide range of frequencies in both temporal and spatial domains [1–4]. Furthermore, measurements from the Federal Communications Commission (FCC) share the same results where up to 70% of the allocated spectrum is not utilized [5, 6]. In other words, the frequency in 70% of the time-area is not exploited although there is another operator that requires a new band but has no space to accommodate it. In this context, the need for adopting new spectrum access techniques with capability of efficiently and effectively exploiting the available spectrum resources arises. This motivates the introduction of the Dynamic Spectrum Access (DSA), which allows the use of part of the spectrum in a flexible manner under consideration of regularity

and technical restrictions [7]. It is about using the spectrum wherever and whenever it is unoccupied by allowing the unlicensed users to share or reuse the same spectrum band, such as UHF/VHF TV bands, originally allocated to licensed users [7, 8].

Cognitive radio (CR), firstly introduced in [9], has emerged as a novel wireless communication technology that brings a change into how the radio spectrum could be regulated. It is an enabling technology that enables the DSA networks to use the spectrum more efficiently in an opportunistic way without interfering with the licensed users known as Primary Users (PUs) [10]. Currently, there exists thousands of research papers in CR technology which illustrates its importance in the future. Moreover, various standardization activities have been led toward achieving ready-for-use CR technology. For example, IEEE 802.22 working group has published the IEEE 802.22 standards to enable spectrum sharing by using the vacant channels, known as spectrum holes or white spaces, in the UHF/VHF TV bands [11,12]. The European Telecommunication Standard Institute (ETSI) Reconfigurable Radio Systems (RRS) Working Group (WG1) has defined standards and operation requirements for the operation of the mobile broadband systems in the 2.3-2.4 GHz frequency band under the Licensed Shared Access (LSA) regime [13–15]. Further, U.S. FCC and United Kingdom (U.K.) Office of Communications (OFCOM) issued their milestone reports outlining governing regulations for unlicensed usage in TV spectrum holes and opened parts of the TV spectrum for unlicensed TV band devices [16–18]. On the other hand, important industry players, including Alcatel-Lucent, Ericsson and Motorola from the mobile equipment industry, Philips and Samsung from the consumer electronics industry, British Telecom and Orange from network operators, HP and Dell from the computer industry, and Microsoft and Google from the Internet/software industry, are putting effort toward the realization of the CR technology [19].

For the CR to operate effectively and to provide the required improvement in spectrum efficiency, it must be able to effectively detect the presence/absence of the PU to avoid interference if it exists and freely use the spectrum in the absence of the PU. Thus, Spectrum Sensing (SS), being responsible for the presence/absence detection process, is the key element in any CR guarantee. SS is the task of obtaining awareness about the spectrum usage. Mainly it concerns two scenarios of detection: (i) detecting the absence of the PU in a licensed spectrum in order to use it and (ii) detecting the presence of the PU to avoid interference. Hence, SS plays a major role

in the performance of the CR as well as the performance of the PU networks that coexist. In this regard, several SS techniques have been proposed in the literature [10, 20]. While energy detection (ED) is the most popular SS technique, it is indeed sensitive to noise power uncertainty which may cause significant performance degradation [21–24]. Cyclostationary feature detector (CFD) is robust against noise uncertainty, however, it requires the knowledge about the PU's signal and suffers from high computational complexity [25–31]. Matched filter detector (MFD) is the optimal if PU's signal is known, however, it requires perfect knowledge of the PU's signal features (i.e. operating frequency, modulation, pulse shaping etc.) and its implementation complexity is impractically large [32–35]. On the other hand, Eigenvalue Based Detector (EBD) circumvent the need of knowledge about the PU or the noise power and shows superior performance and robustness [36–43].

Eigenvalue based detector relies on the properties of the eigenvalues of the sample covariance matrix of the received signal. Several eigenvalue based techniques have been proposed including, but not limited to, the Largest Eigenvalue (LE) detector [36,42], the Scaled Largest Eigenvalue (SLE) detector [40,42] and the Standard Condition Number (SCN) detector [36,37,39,44]. Like ED, LE detector needs the knowledge about the noise power but however it outperforms the ED performance [36]. SCN and SLE does not require this information and have superior performance in noise uncertain environments [40, 44]. EBD techniques have been considered using results from the advances in Random Matrix Theory (RMT) [45, 46]. The performance probabilities and the decision threshold are usually determined after the analysis of the statistics of the detector's metrics which involves results from the finite and asymptotic RMT. Exact expressions could be derived in the finite case and beneficial approximations can be used in the asymptotic case. Based on these expressions, the main drawback of the EDB is the complexity of the analytical expressions of the performance probabilities and the decision threshold in case an expression could be provided. In fact, for a CR to dynamically change the threshold value according to certain performance/requirements/capabilities then the decision threshold must have simple analytical expression or alternatively Look-up Tables (LUT) should be constructed. However, as discussed through this thesis the implementation of the decision threshold must be dynamic and may rely on real-time computations rather than using LUTs. In this regard, a major part of this thesis considers this complexity in the EBD and provides simple and accurate expressions for the performance probabilities and the decision threshold

[J1-J4, C1, C2]. The SCN detector is considered and simple approximation is provided based on the Generalized Extreme Eigenvalue (GEV) distribution and results from finite and asymptotic RMT. Moreover, the SLE detector is also considered and a simple Gaussian formulation is provided.

On the other hand, the implementation of the EBD is based on certain diversity techniques such as fractional sampling, multiple-antennas or cooperation. In this context, it is very likely that the SUs would be equipped with multiple antenna technology as mentioned in Sec. 2.4.4. However, the research community lacks of studies that considers massive Multiple-Input Multiple-Output (MIMO) technology in CR for SS. In this regard, we have considered a CR with massive MIMO technology and studied the efficient way of antenna exploitation for SS and other purposes [J6].

1.2 Thesis Organization and Main Contributions

The structure of the thesis can be summarized as follows:

- Chapter 2 provides a brief discussion of the spectrum sensing in cognitive radio systems.

- Chapter 3 focus on the SCN detector in finite and asymptotic cases [J1, J2, J4, C2, C3]. Since finite case rely on exact distributions, the joint distribution of the ordered eigenvalue of the Wishart matrices is studied as the first step toward the exact distribution analysis of the EBD decision metrics. The exact SCN distribution is then considered and derivations of the exact expressions for the Probability Density Function (PDF) and Cumulative Distribution Function (CDF) are provided. The complexity of these exact expressions and the use of extreme eigenvalues make the motivation of the use of the GEV distribution as a simple approximation for the SCN. The exact moments are derived and the approximation is proposed to end up with simple forms for the Probability of False-alarm (P_{fa}), Probability of Detection (P_d), Probability of Missed-Detection (P_{md}) and the decision threshold (λ_{SCN}). Asymptotically, the use of approximations due to large numbers from RMT was advantageous. The asymptotic central moments of the SCN are derived by the use of the asymptotic central moments of the extreme

eigenvalues of Wishart matrices. Finally, the objective is attained by providing a very accurate and simple form for λ_{SCN} that could be used for dynamic and real time computations. These analytical derivations are all validated through extensive Monte-Carlo simulations.

- Chapter 4 considers the complexity in the SLE detector as the main objective [J3, C1]. The focus was to provide a simple form for the distribution of the SLE decision metric which would results in simple forms for the P_{fa}, P_d, P_{md} and λ_{SLE}. The distribution of the trace of the Wishart matrices was considered which is proved to be Gaussian. Consequently, the SLE distribution is proved to have a Gaussian form which is also provided. This form is a function of the means and variances of the largest eigenvalue and the trace and the correlation between them. Accordingly, the correlation coefficient is studied using variable transformation. The analytical derivations are all validated through Monte-Carlo simulations.

- Chapter 5 studies the antenna exploitation efficiency of a CR system equipped with massive MIMO technology [J5]. Using the LE detector, two scenarios of antenna use could be considered: (i) Full antenna exploitation scenario and (ii) Partial antenna exploitation scenario. In the first scenario, asymptotic approximation for the LE detector's performance probabilities and decision threshold are derived. In the second scenario, two options are discussed: the fixed number of antenna use and the dynamic number of antenna use. In the fixed case, an optimal threshold is derived to minimize the error probabilities. For the dynamic case, the equation after which the minimum requirement of the system could be evaluated is provided. When the noise power is not perfectly known, this work is extended to the SLE and SCN detectors using result from previous chapters. The analytical derivations are all validated through Monte-Carlo simulations and a comparison between these different scenarios nad different detectors are also provided in terms of performance and number of antennas involved in the sensing process.

- Chapter 6 summarizes the thesis and draws the conclusions and the future recommendations.

1.3 List of Publications

The publication resulted during the course of this PhD are listed below with the index "C" refers to peer-reviewed conference paper and "J" refers for the journal paper.

J1. H. Kobeissi, Y. Nasser, A. Nafkha, O. Bazzi and Y. Louet, "On the detection probability of the standard condition number detector in finite-dimensional cognitive radio context", EURASIP, Journal on Wireless Communications and Networking, DOI: 10.1186/s13638-016-0634-0, Published: 23 May 2016.

J2. H. Kobeissi, A. Nafkha, Y. Nasser, O. Bazzi and Y. Louet, "On Approximating the Standard Condition Number for Cognitive Radio Spectrum Sensing with Finite Number of Sensors", DOI: 10.1049/iet-spr.2016.0146 , Online ISSN 1751-9683, Volume 11, Issue 2, p.145-154, Available online: 30 August 2016, IET Signal Processing, 2016.

J3. H. Kobeissi, A. Nafkha, Y. Nasser, O. Bazzi and Y. Louet, "On the Performance Analysis and Evaluation of Scaled Largest Eigenvalue in Spectrum Sensing: A Simple Form Approach", EAI Endorsed Transactions on Cognitive Communications 17(10): e5, Volume 3, Feb. 2017.

J4. H. Kobeissi, Y. Nasser, A. Nafkha, O. Bazzi and Y. Louet, "Asymptotic Approximation of the Standard Condition Number Detector for Large Multi-Antenna Cognitive Radio Systems", EAI Endorsed Transactions on Cognitive Communications 17(11): e1, Volume 3, May 2017.

J5. H. Kobeissi, Y. Nasser, A. Nafkha, O. Bazzi and Y. Louet, "Multi-antenna Based Spectrum Sensing: Approaching Massive MIMOs", Submitted for IEEE Transactions on Cognitive Communications and Networks (TCCN).

C1. H. Kobeissi, Y. Nasser, A. Nafkha, O. Bazzi and Y. Louet, "A Simple formulation for the Distribution of the Scaled Largest Eigenvalue and

application to Spectrum Sensing", 11th International Conference on Cognitive Radio Oriented Wireless Networks (Crowncom), GRENOBLE, May 2016.

C2. H. Kobeissi, A. Nafkha, Y. Nasser, O. Bazzi and Y. Louet, "Simple and Accurate Closed-Form Approximation of the Standard Condition Number Distribution with Application in Spectrum Sensing", 11th International Conference on Cognitive Radio Oriented Wireless Networks (Crowncom), GRENOBLE, May 2016.

C3. H. Kobeissi, Y. Nasser, O. Bazzi, Y. Louet and A. Nafkha, "On the Performance Evaluation of the Eigenvalue-Based Spectrum Sensing Detector for MIMO Systems", URSI GASS 2014, Beijing, Aug. 2014.

1.4 Mathematical Notations

Vectors and Matrices are represented, respectively, by lower and upper case boldface. The symbols $|\mathbf{.}|$ and $tr(\mathbf{.})$ indicate, respectively, the determinant and trace of a matrix while $(.)^{1/2}$, $(.)^T$, and $(.)^\dagger$ are the square root, transpose, and Hermitian symbols respectively. $\boldsymbol{I}_n$ is the $n \times n$ identity matrix and $\mathbf{1}_{KN}$ is a $K \times N$ ones matrix. Symbol $\sim$ stands for "distributed as" and $E[.]$ stands for the expected value, $\|.\|$ for the Frobenius norm and $\|.\|^2$ for the norm. Notation $[1, \cdots, K] - \{m\}$ denotes an ordered vector with $K-1$ elements from 1 to K except m.

Chapter 2

Spectrum Sensing in Cognitive Radios

2.1 Introduction

Radio spectrum is a limited natural resource that is coordinated by national regularity bodies like the Federal Communications Commission (FCC) in the United States (U.S.). The FCC assigns particular portions of spectrum to licensees, also known as Primary Users (PUs), on a long-term basis for large geographical regions. This approach is beneficial as it prevents from interference, guarantees adequate quality of service (QoS), and, from technical perspectives, it is easier to manufacture a system operating in a dedicated band rather than a system to operate in different bands over a large frequency range. However, a large portion of the assigned spectrum remains underutilized in a world that aspires for more radio resources [1]. To this end, Cognitive Radio (CR) technology has received an enormous attention as an emerging solution to the spectrum shortage problem for the next generation wireless communication systems [47]. It is a technology that brings a change in how the radio spectrum is regulated from the current static spectrum allocation into a dynamic frequency allocation scheme known as the Dynamic Spectrum Access (DSA) [7].

CR concept was firstly proposed by Joseph Mitola in [9]. Since then, several definitions for the CR have been provided based on different contexts [48–50]. For example, FCC defines the CR as: "*A radio or system that senses its operational electromagnetic environment and can dynamically*

and autonomously adjust its radio operating parameters to modify system operation, such as maximize throughput, mitigate interference, facilitate interoperability, access secondary markets" [6]. This is achieved by the two main characteristics of CR: (i) cognitive capability and (ii) reconfigurability. Cognitive capability refers to the ability to sense and gather information from the surrounding environment while reconfigurability refers to the ability to rapidly adapt the operational parameters according to the sensed information in order to achieve the optimal performance.

CR users, also known as Secondary Users (SUs), are unlicensed users that have lower priority to access the spectrum resources. They are authorized to exploit the spectrum in such a way that they do not cause harmful interference to the PUs. Hence, SUs need to be aware of their surrounding spectrum environment and to intelligently exploit this spectrum to serve their duty while guaranteeing the normal operation of the PUs. Being the focus of this chapter, spectrum sensing (SS) is the most important mechanism for the establishment of CR. It is the key to successful of CR systems in which it is responsible of identifying the spectrum holes and the occupied bands. In this regard, sec. 2.2 discusses the basic meaning of spectral opportunity and the spectrum holes in a wider space known as the transmission hyperspace. Sec. 2.3 discusses the importance of SS starting by the spectrum exploitation techniques and passing through other spectrum awareness techniques. The concept of SS is discussed in Sec. 2.4. Different SS categories and techniques are also provided. In addition, this section discussed the cooperation in SS, multiple-antenna use in SS and the main challenges facing SS techniques. In Sec. 2.5, the concept of Eigenvalue Based Detector (EBD) is discussed through the different diversity techniques used to implement EBD, the hypothesis analysis of EBD and the different techniques that are used in the literature. Finally, the conclusion is drawn in Sec. 2.6.

2.2 Transmission Hyperspace

The main purpose of a CR is to efficiently utilize the spectral opportunities without interfering on the PUs. Thus, defining the term "spectral opportunity" in CR is mandatory for any awareness technique. Spectral opportunity is, traditionally, defined as a vacant band of frequencies at a particular time and in a particular geographic area [20]. In other words, it is a vacant hole in the time-frequency-space dimensions. This actually borders the field of

operation of the SUs as it could not use vacant spectrum holes in a wider dimensional space. Based on this definition, the radio spectrum is not optimally utilized since it does not consider the advantage of orthogonality schemes or diversity that permits multiple users to jointly-operate without interference. For example, multiple-users may use the same frequency at the same time in the same area by using different orthogonal codes so it can be intercepted only by receivers having the same code. This additional dimension, i.e. code dimension, can be further explored and added to the aforementioned dimensions to form a new wider space seeking for superior spectral opportunities. Further, other dimensions, such as polarization and angle-of-arrival, could also be included to achieve an optimal exploration and exploitation of the spectral opportunities.

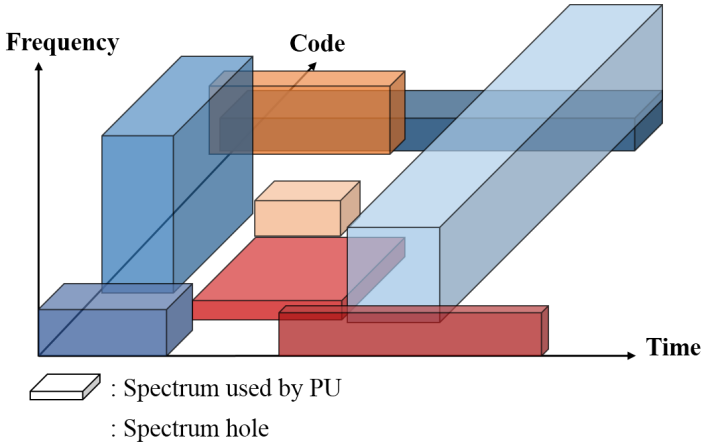

Figure 2.1: 3-D Spectrum Hyperspace and Spectrum holes within.

In this regard, 'Transmission Hyperspace' could be seen as an electromagnetic space bounded by all dimensions, i.e. time, frequency, space, code, polarization, angle-of-arrival, etc. [51]. Consequently, a spectral opportunity could be imagined as a vacant hole in such hyperspace in which it is still referred to as 'spectrum hole'. An imagination of a 3-dimensional transmission hyperspace is illustrated in Fig. 2.1 where the empty blocks refer to the spectrum holes in time-frequency-code-space dimensions. The SUs must be aware of these spectrum holes and use suitable access techniques depending on the available dimensions. However, the utilization of the dimensions of the spectrum hyperspace is mainly based on the available information at the

SUs. Here, the awareness needs not only the necessary information about the presence/absence of the PU in certain channels but also necessitates to identify the PU's waveform (e.g. radio access techniques, chip rates, preambles, etc.) and others [52]. Important dimensions of the transmission hyperspace are summarized in the following:

- *Frequency Dimension*: Frequency dimension is usually subdivided into spectrum bands that are typically matching the channelization of particular services such as the frequency division multiple access (FDMA) scheme [53]. Spectral opportunities, in this dimension, are the spectrum bands that are not utilized by the PUs.

- *Time Dimension*: The time dimension, depending on the application, is subdivided into periods such as the time-slots structure in time division multiple access (TDMA) systems [53]. Hence, SUs must be aware of the spectral opportunities available in the time domain, i.e. periods of time the spectrum band is not occupied with respect to other dimensions.

- *Space Dimension*: The space dimension refers to the physical geographical location and distance of PUs. As early discussed, the spectrum is under-utilized in the spatial domain. Hence, at a certain location, the spectrum may be unoccupied while it is occupied at another. Hence, spectrum opportunities could be found in some parts of the space dimension in which SUs can exploit.

- *Angle-of-Arrival Dimension*: Using advances in multiple-antenna technology, such as beamforming, the SUs can simultaneously use the same spectrum band with the PUs at the same time in the same location but through different direction than the direction of the PU radio signal [54]. This is usually known as the angle-of-arrival transmission in which different transmitters can simultaneously operate on the same frequency without interfering by forming the transmission beam in the direction of the intended receiver. Hence, a new spectral opportunity could be exploited if the SUs are aware of the position of the PU along with its beam direction (i.e. azimuth and elevation angle).

- *Code Dimension*: The spectrum may be used at a particular time and in a particular location and still could be considered as a spectral opportunity which might be used by the SUs thanks to the code division

access technique [53]. However, this assumes that both primary and secondary networks are using different orthogonal codes in which multiple PUs and/or SUs can access simultaneously the spectrum band without interfering. Accordingly, the SUs must be aware of the coding technology used (e.g. frequency-hopping, direct-sequence etc.) and the codes used by the PUs.

- *Polarization Dimension*: The electric field propagation determines the polarization of the electromagnetic wave. In general, most antennas radiate either linear (i.e. horizontal or vertical) polarization or circular (i.e. right-hand-circular or left-hand-circular) polarization. If the SUs are aware of the polarization state of the PUs, then it can transmit simultaneously in polarization state other than the polarization of the PUs as it is not causing harmful interference. The reader can refer to [55, 56] for examples on polarization exploitation in CRs.

Consequently, spectrum sensing must consider all the transmission hyperspace dimensions for an optimal utilization. From spectrum utilization efficiency perspective, the more dimensions the SUs are exploring the more efficient is the utilization of the spectrum holes and hence, a higher success level of the CR objective is achieved. In this regard, the focus of this thesis is the EBD using multiple antenna technology as discussed in Sec. 2.5. This detector allows the SUs to be aware of the spectrum holes in the time, frequency, space and angle-of-arrival dimensions.

2.3 Spectrum Sensing: Behind the Concept

Spectrum scarcity and under-utilization are the main motivations behind the concept of CR technology. To overcome these spectrum shortage problems, several spectrum exploitation models were proposed: (i) dynamic exclusive use model which include certain flexibility to improve spectrum efficiency while maintaining on the basic structure of the current spectrum allocation policy [57,58] and (ii) spectrum commons model which consists of a spectrum band for sharing between different users [59, 60]. These models improve the spectrum efficiency by providing unlicensed shared bands or an access to the licensed band for a certain time under the supervision of the primary network. However, the spectrum holes are still not exploited and the licensed bands are still considered underutilized.

In this regard, the third model is the hierarchical access model which is about allowing the SUs to access the PU's licensed bands if no harmful interference is caused. In other words, SUs are allowed to access the PU's band in any possible way that maintains the normal activity of the PU. This model can be broadly categorized into: (i) Underlay, (ii) Overlay and (iii) Interweave approaches [61]. An illustration of these approaches is considered in Fig. 2.2. The SU, based on its access technology and awareness about the PU, can use one or more of these techniques.

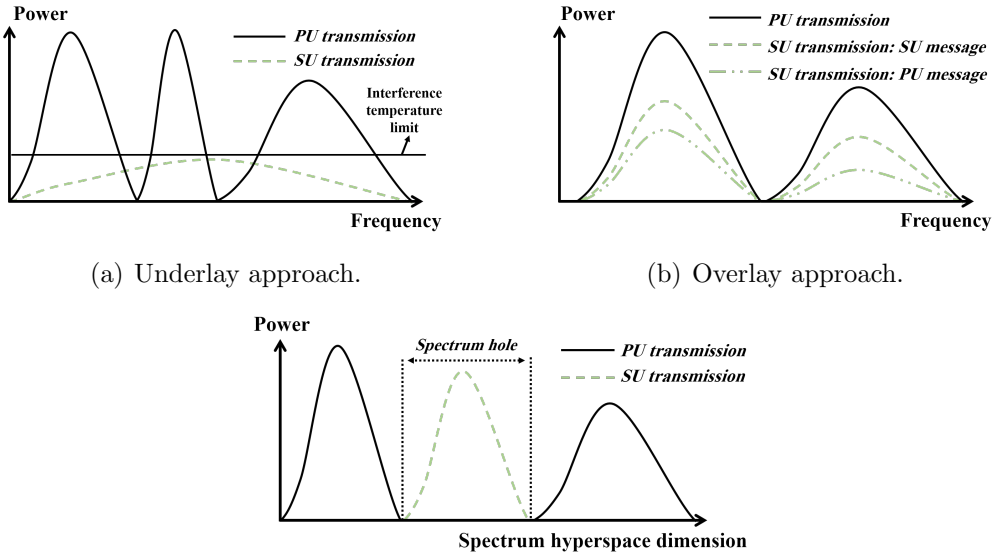

(a) Underlay approach.

(b) Overlay approach.

(c) Interweave approach.

Figure 2.2: Examples of different hierarchical access model approaches.

Both underlay and overlay approaches allow the SUs to communicate at the same time-frequency resources used by the PUs. In the underlay approach, the secondary transmitter (ST) must not significantly interfere with the primary receiver (PR) and hence, the coexistence of the SU and PU is realistic as the generated interference at the PR is below certain acceptable threshold [62]. Several methods could be used to support the SU to underlay its transmission simultaneously on the same band as the PU, such as beamforming [63], primary exclusion region [64,65], interference alignment [66,67] and spread spectrum signals [68]. However, the ST must be aware of the interference it causes to the PR which is not straightforward since it is actu-

ally happens at the PR side. In the overlay approach, the STs use advanced techniques in coding and transmission in order to mitigate the interference caused by such transmission. Basically, as shown in Fig. 2.2(b), the STs must relay the primary signals by using part of their power and the rest are used to transmit their own signals [61]. Accordingly, overlay approach needs advanced techniques in precoding, transmission and perfect power splitting, interference mitigation and time and frequency synchronization. Moreover, it also requires PU-SU cooperation, non-causal prior knowledge about the PU and could not be applied except in very few cases [69].

On the other hand, interweave approach is about the opportunistic utilization of the spectrum holes whenever and wherever it exists. It was the basic motivation behind the introduction of the CR systems as a solution for the under-utilization problem of the licensed spectrum bands. The SUs, in this approach, must be aware of the PU activity in its geographical area in order to identify the spectrum holes and exploit them for their own transmission. Further, SUs must also identify any reappearance of the PU and should, immediately, leave the channel by switching to another spectrum hole or stop transmission. This opportunistic use of the spectrum, ideally, causes no interference to the PU. Indeed, this is almost true if the used awareness method is capable of correctly identifying the spectrum hole with optimal performance. However, any incorrect identification will lead to a miss-utilization of the spectrum hole or harmful interference to the PU. Consequently, the performance of the awareness mechanism is a challenge in the interweave approach.

In general, most of the aforementioned exploitation techniques could be jointly used. For example, SUs can underlay their transmission until a spectrum hole is detected and then shift to the interweave approach to transmit with higher power according to the dimensions of the spectrum hole. However, interweave is the most efficient and effective approach for exploiting the underutilized spectrum by targeting the spectrum holes in the transmission hyperspace. In this regard, different spectrum awareness methods exist in order to serve the SUs and make them aware of the surrounding environment. On a large scale, spectrum awareness can be classified into passive and active awareness [70]. In passive awareness, the SU receives the spectral information needed from an outside agent. On the other hand, in active awareness the SUs need to sense the radio environment and make their own measurements.

Different passive awareness techniques are proposed to inform the SU

about its surrounding spectrum status. Such techniques include (i) Beacon Signals [71–73], (ii) Control Channel [74–78], (iii) Geolocation databases [79–82], (iv) Policy based [83] and (v) Spectrum broker [71]. In fact, passive awareness can ensure interference-free communication to the PUs and a simple secondary transceiver. However, it may require modification to the PU systems, control channels and the establishment of costly infrastructure. Moreover, passive awareness leads to a static SU that strongly depends on how frequent the outside agent is updated. On the other hand, active awareness could be either detecting a PR or a PT. Methods for detecting the PR are based on detecting the Local Oscillator (LO) leakage power [10, 84] or the interference at the PR [85]. Since LO leakage and interference are actually happening at the receiver side, then CR active awareness based on these approaches must focus on the receiver activity of the PU. To fulfill such approach, it is more likely that the secondary network should establish a large grid of sensors to cover all its communication region. Hence, without PU-SU cooperation assumption, it is easier to detect the PT than the detection of PR. In this regard, Spectrum sensing (SS) is the active awareness approach that is responsible on detecting the PT by taking certain measures from the SU surrounding environment and decide whether a spectrum hole exists or not. The main advantage of SS approach is that the SUs may not need to rely on any external source of knowledge to take a transmit/no-transmit decision.

Based on this discussion, SS is considered as the most practical, efficient and effective approach in spectrum awareness. It permits the detection of spectrum holes in order to be exploited using the interweave approach. This concept is basic in CR since it takes the spectrum bands from the underutilized state to a more efficiently-utilized state. There exists a massive number of researches that provide this approach with worthy different detection techniques to identify the spectrum holes. In the next section, we discuss the concept of SS and different aspects related to it.

2.4 Spectrum Sensing: literature review

Spectrum sensing is a crucial stage that must be performed by the SUs in order to identify the spectrum holes. To this end, a variety of techniques has been proposed in literature. In general, these techniques are based on

detection problem with binary hypothesis model defined as:

$$\mathcal{H}_0 : \ y(n) = \eta(n), \tag{2.1}$$
$$\mathcal{H}_1 : \ y(n) = s(n) + \eta(n), \tag{2.2}$$

where $y(n)$ is the sample received at instant n; $\eta(n)$ represents the additive white Gaussian noise with zero mean and variance σ_η^2; $s(n)$ is the PU's transmitted signal samples passed through a wireless channel. This represents a binary signal detection problem in which SUs need to decide between the two hypotheses, $\mathcal{H}_0$ or $\mathcal{H}_1$. $\mathcal{H}_0$ is the only noise hypothesis, i.e. the PU does not exist, while $\mathcal{H}_1$ indicates that the considered spectrum band is occupied.

The detection performance is commonly determined on the basis of two probabilities, namely, the probability of false-alarm (P_{fa}) and the probability of detection (P_d). P_{fa} denotes the probability that the SU falsely decide that the PU is present when actually it is absent and P_d denotes the probability of correctly deciding the presence of the PU. An alternative to P_d and another important probability is the missed-detection probability (P_{md}) which denotes the decision of a vacant band when the PU is actually presents. P_{fa} represents a miss-utilization of the spectrum hole whereas P_{md} results in interference on the PUs. Hence, the key challenge of any SS technique is to minimize the error probabilities, i.e. P_{fa} and P_{md}, and, thus, maximizing P_d. Denote by X the decision metric used by the SS technique, then these probabilities are given by:

$$P_{fa} = P(X \geq \lambda_X / \mathcal{H}_0), \tag{2.3}$$
$$P_d \ = P(X \geq \lambda_X / \mathcal{H}_1), \tag{2.4}$$
$$P_{md} = P(X < \lambda_X / \mathcal{H}_1) = 1 - P_d, \tag{2.5}$$

where λ_X is the decision threshold. Further, denote by $f_i(x)$ and $F_i(x)$ the Probability Density Function (PDF) and the Cumulative Distribution Function (CDF) of X respectively under the hypothesis $i \in \{0, 1\}$, then P_{fa}, P_d and P_{md}, as represented in Fig. 2.3, are respectively given by:

$$P_{fa} = 1 - F_0(\lambda_X), \tag{2.6}$$
$$P_d = 1 - F_1(\lambda_X), \tag{2.7}$$
$$P_{md} = F_1(\lambda_X), \tag{2.8}$$

Before getting into the details of SS methods in Sec. 2.4.2, different SS categories are summarized in the following subsection.

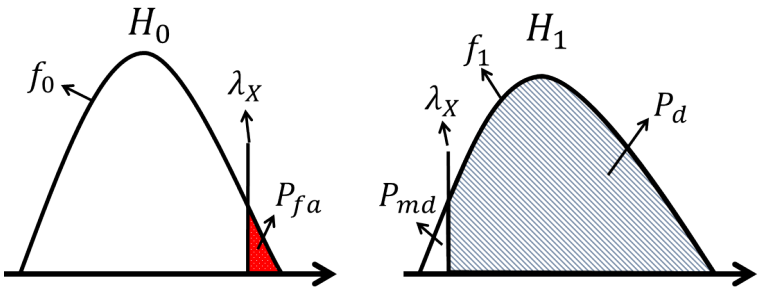

Figure 2.3: False-alarm, detection and miss-detection probabilities.

2.4.1 Spectrum Sensing Categories

Spectrum sensing techniques can be categorized upon different basis which reflect certain requirement/property/application/target as shown in Fig. 2.4. In the following, a summary of different categories is provided:

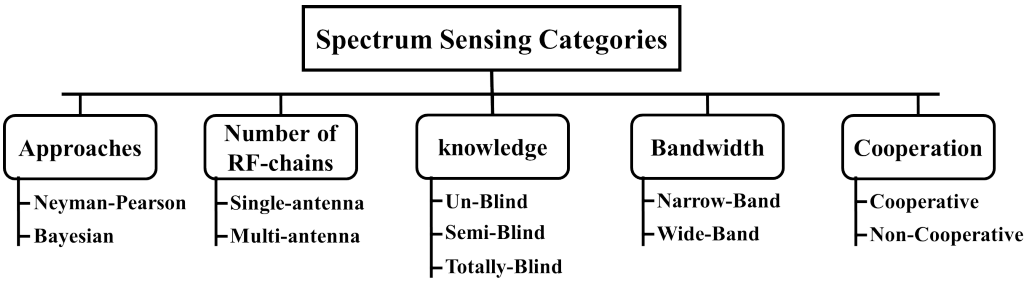

Figure 2.4: Different Sensing Categories.

Neyman-Pearson vs. Bayesian: These are two general approaches for the hypothesis testing. Neyman-Pearson is a classical approach that assumes no prior knowledge about the probabilities of occurrence of the hypotheses. On the other had, the Bayesian approach is based on minimizing the Bayes risk by employing prior knowledge about the probabilities of occurrence of the hypotheses [86].

Cooperative vs. Non-cooperative: In non-cooperative based approach, SUs decide the presence/absence of the PU based on its local observations only. In contrast, the cooperative based approach is based on the cooperation between multiple SUs, by sharing their information in a centralized or distributed manner, to decide about the spectrum availability. More

about cooperation is provided by Sec. 2.4.3.

Un-blind vs. Semi-blind vs. Totally-blind: These categories reflect the amount of prior knowledge required at the SU. Un-blind detectors require a prior knowledge about the PU signal's characteristics as well as the noise power to accurately make a decision. Semi-blind detectors are more practical as they require a prior knowledge about the noise power only. This power could be estimated, however, a further performance study for such detectors in the presence of noise uncertainty is required. On the other hand, totally-blind detectors are the detectors that do not require any prior information regarding both the PU signal and the noise power. These techniques are the most practical and preferable techniques in SS.

Multi-antenna vs. Single-antenna: It is about the number of antennas at the RF part of the SU that are used for the SS process. In comparison with single-antenna SS, multi-antenna SS utilize the spatial correlation of PU signal received by different antennas for spectrum holes detection. Moreover, several multi-antenna SS techniques have been shown to be totally-blind and thus, provide robustness against noise uncertainty problems. On the other hand, multi-antenna SS requires additional hardware components and an increase in the computational complexity. More about multi-antenna is provided by Sec. 2.4.4.

Wide-band vs. Narrow-band: Herein, the detectors are categorized based on the bandwidth of the channel to be sensed. Narrow-band (NB) SS techniques are detectors that could be used to sense a sufficiently narrow frequency range band such that a flat channel frequency response could be considered, i.e. the sensed bandwidth is less than the channel coherence bandwidth [87]. On the other hand, wide-band (WB) SS techniques aim to sense a wider frequency band. It is worth noting that the NB SS techniques cannot be directly used in WB sensing, however, they can be extended for WB context.

In addition, categories, such as **proactive** (i.e. periodic sensing) or **reactive** (i.e. on-demand sensing), **In-band** (i.e. sensing the band currently used by the SUs) or **Out-of-band** (i.e. sensing other bands for possible backup) and **sequential** (i.e. sensing several bands sequentially) or **parallel** (i.e. sensing several bands in parallel), also exists. However, the fundamental of all these categories is to detect the spectrum holes in order to be used by the SUs. In this regard, different methods were proposed in literature and are discussed next.

2.4.2 Spectrum Sensing Techniques

Several SS techniques exist as shown in Fig. 2.6. Each have distinct capabilities, requirements, performances and complexities. A detailed survey of the existing SS techniques could be found in [10, 20, 87, 88] and a comparative study, in terms of performance, complexity and requirements, could be found in [89]. In the following, we summarize methods considered in PU detection and most of the existing SS techniques. It is worth mentioning that some of the techniques in Fig. 2.6 are discussed in Sec. 2.5. Moreover, Fig. 2.6 considered two basis, namely the knowledge and the number of RF-chains, in illustrating the SS techniques due to their importance in this thesis.

1. **Energy Detection**: The concept of energy detection is to measure the energy of the received signal in a certain spectrum band of interest, then compare this energy with a pre-computed threshold value to decide whether the PU is present in this spectrum band or not [21–24, 90–92].

1.1. *Traditional Energy Detector*: the traditional energy detector (ED) is, usually, a single-antenna and narrowband detector and its decision metric is given by:

$$X = \frac{1}{N} \sum_{n=1}^{N} |y(n)|^2. \tag{2.9}$$

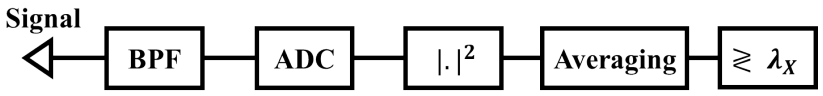

Figure 2.5: Traditional energy detector block diagram.

Figure 2.5 illustrates the implementation of ED. The exact distribution of the ED decision metric is a chi-squared distribution; however, due to the large number of samples, N, involved in the detection, it has been shown that in practical scenarios the distribution of X, using Central Limit Theorem (CLT), can be accurately assumed to follow the

Gaussian distribution [93]. Consequently, one can obtain the following:

$$\mathcal{H}_0 : X \sim \mathcal{N}\left(\sigma_\eta^2, \frac{\sigma_\eta^4}{N}\right), \tag{2.10}$$

$$\mathcal{H}_1 : X \sim \mathcal{N}\left(\sigma_\eta^2 + \sigma_s^2, \frac{(\sigma_\eta^2 + \sigma_s^2)^2}{N}\right), \tag{2.11}$$

where σ_s^2 is the energy of the signal at the SR (i.e. including channel effect). Hence, P_{fa}, P_d and P_{md}, using (2.6), (2.7) and (2.8), are straightforwardly formulated as follows:

$$P_{fa} = Q\left(\frac{\lambda_X - \sigma_\eta^2}{\sigma_\eta^2/\sqrt{N}}\right), \tag{2.12}$$

$$P_d = Q\left(\frac{\lambda_X - \sigma_\eta^2(1+\rho)}{\sigma_\eta^2(1+\rho)/\sqrt{N}}\right). \tag{2.13}$$

where $Q(.)$ is the standard Gaussian complementary CDF and ρ is the signal to noise ratio. The optimal decision threshold, λ_X, is selected by minimizing both P_{fa} and P_{md}. However, this requires the knowledge of noise and received signal powers.

ED is the most popular technique for SS due to its low implementation and computational complexities. In practice, the threshold is chosen so as to maintain a predefined false-alarm probability, i.e. Constant False Alarm Rate (CFAR) [94]. Hence, ED is considered a semi-blind detector as it is sufficient to know the noise variance for calculating λ_X. Despite the simplicity of ED, its main drawback lies in its sensitivity on noise power uncertainty. Any small error in the noise power estimation may cause a significant performance degradation.

The threshold of the ED, for a CFAR, is straightforward from (2.12) as:

$$\lambda_X = \sigma_\eta^2\left(1 + \frac{Q^{-1}(P_{fa})}{\sqrt{N}}\right), \tag{2.14}$$

where $Q^{-1}(.)$ is the inverse Q-function. In perfect operating conditions, i.e. σ_η^2 is perfectly known, ED can achieve any detection performance by increasing N. For a targeted P_{fa} and P_d, the minimum required N is straightforward derived from (2.12) and (2.13) as:

$$N = \left[Q^{-1}(P_{fa}) - Q^{-1}(P_d)(1+\rho)\right].\rho^{-2}. \tag{2.15}$$

Hence, if σ_η^2 is known, the ED can detect any PU at arbitrarily low SNR by increasing N. Conversely, due to noise uncertainty the PU could not be detected if the SNR is under certain SNR wall regardless the value of N [95, 96]. To address this issue, accurate noise estimation methods [91, 97] and hybrid detectors [98] were proposed for ED.

1.2. *Teager-Kaiser based ED*: As presented for the ED, the most widely used approach for the energy estimation is based on the squared energy operator whereby the desired energy given by (2.9) or the squares of the magnitude of the frequency samples of the same signal segment after discrete Fourier transform (DFT). Alternatively, a simple and fast approach is based on the Teager-Kaiser energy operator which was first proposed by Teager in [99] and further investigated by Kaiser [100]. A comparison between both energy estimation approaches in presence of additive noise is reported in [101]. In CR, Teager-Kaiser based ED has been used in detecting the wireless microphone signals in narrowband and wideband frequency domains [24, 92].

2. *Feature Detection*:

   In general, Feature Detector (FD) distinguishes the PU by matching features extracted from the received signal with a priori known features that characterize the PU transmission such as Cyclostationarity, idle guard interval of OFDM, location, channel bandwidth and its shape, etc. [25–31, 98, 102–107].

2.1 **Cyclostationary Feature Detector:** Cyclostationary Feature Detector (CFD) is an effective FD that exploits the cyclostationary features of the primary signals [27–31, 98, 102–107]. Unlike the noise, PU signals are modulated signals that carry cyclostationary features due to the periodicity in its statistics such as the mean and the autocorrelation. In this regard, the cyclic spectrum density (CSD) function is defined as the Fourier series expansion of the cyclic autocorrelation function of the received signal. If PU is present, the CSD function shows peak values when the cyclic frequencies are equal to the fundamental frequencies of the PU signals. This approach is robust against noise uncertainty and shows high detection performance at the cost of high computational complexity. However, CFD is very sensitive to cyclic frequency mismatch [108].

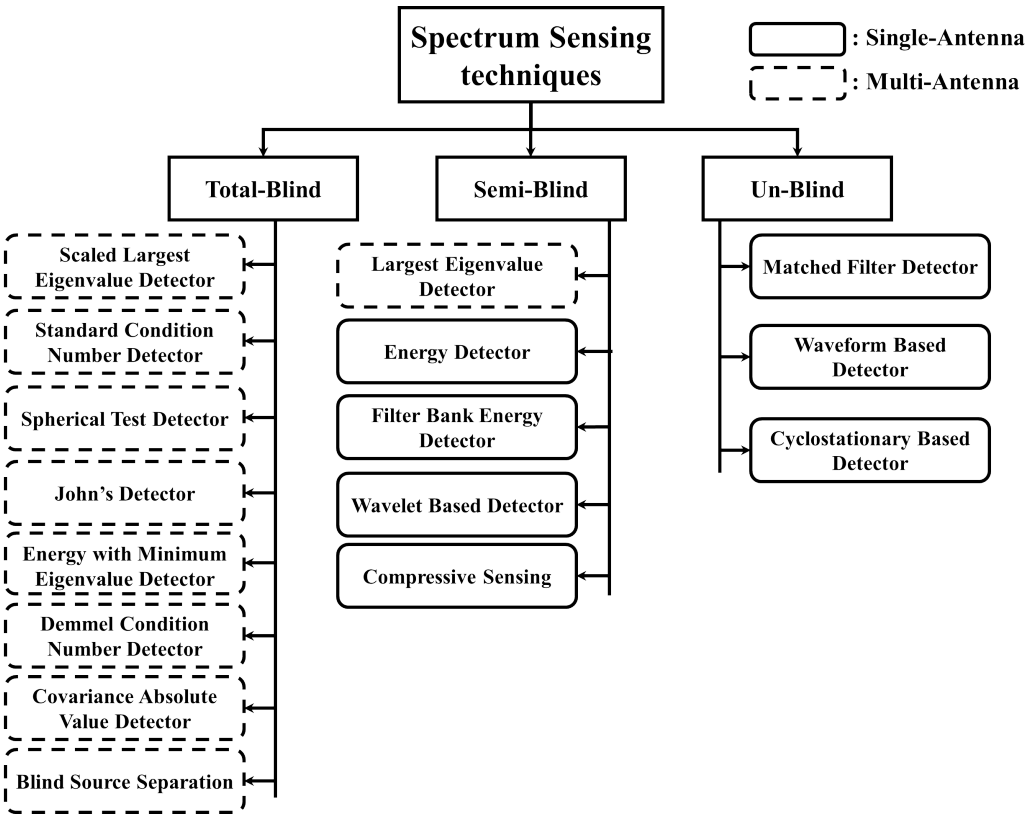

Figure 2.6: Spectrum sensing techniques categorized upon knowledge and number of RF-chains.

3. *Coherent Detection*: Coherent detection uses a known patterns in the PU's signal to detect its presence [89]. If the SU has a perfect knowledge about the PU's signal then matched filter detector could be used. However, if this knowledge is not attained and a certain pattern is still known then waveform-based detector could be used [32–35, 109–114].

3.1 **Matched Filter Detector**: Matched filter detector (MFD) is an unblind detector that correlates the apriori known PU's signal with the received signal to detect the presence of the PU [32–35, 109]. In comparison with other detectors, MFD has many advantages; it is the optimal detector if PU's signal is known and thus, it maximizes the SNR in presence of additive noise. Further, it requires short time to achieve certain performance probabilities. On the other hand, MFD is

not considered as relevant choice in CR due to several disadvantages; first, MFD requires perfect knowledge of PU's signal features such as operating frequency, bandwidth, modulation, pulse shaping etc. and thus, it suffers from high performance degradation if wrong information regarding PU signal is used in the detection. Moreover, its implementation complexity is impractically large as it needs a dedicated receiver for every primary system type which also results in high power consumption.

3.2 **Waveform-Based Detector**: Pilots, spreading codes, preambles and midambles are examples of patterns used by most wireless communication systems for synchronization, equalization and other purposes. If PU signal features are not perfectly known by the SU, such patterns might still be a priori known. Waveform-based detector correlates the received signal with a copy of the known pattern for PU detection [110, 111]. The performance of this detector improves as the length of the known pattern increases. It can be seen as a simplified version of MFD however, synchronization between the primary signal and the detector is still required and thus, any synchronization error can degrade the detection performance. Moreover, SUs must have knowledge of patterns of all primary system in its coverage area. *Cyclic prefix correlation detector* [112, 113] and *pilot detector* [114] are examples of waveform-based detector.

4. *Covariance Based Detection*: Covariance based approach is based on the sample covariance matrix of the received signal at the SR in which it exploits the difference in the statistical covariances of the received signal and the noise.

4.1 **Covariance Absolute Value Detector**: In the covariance based approach, the authors in [115] proposed Covariance Absolute Value (CAV) detector which is a totally-blind detector that rely on the fact that if PU is not present then the off-diagonal elements of the covariance matrix are all zeros whereas if the PU's signal exists and the samples are correlated then the covariance matrix is not diagonal. The distribution of the ratio of the sum of absolute values of the non-diagonal elements to that of the diagonal elements were further studied in [116] in order to obtain mathematical expressions for the P_{fa} and P_d.

4.2 **Eigenvalue Based Detector**: Eigenvalue based detector (EBD) could be considered as an advanced method in the covariance based detection approach. It relies on the eigenvalues of the sample covariance matrix of the signal received using certain diversity technique such as the fractional sampling, cooperation or multi-antenna [36–43, 117]. EBD consists of several detection techniques whose properties are studied using recent results from advances in random matrix theory (RMT). Some of the these techniques are totally-blind and outperform the ED especially in noise uncertain environment. A detailed description of this approach is provided in Sec. 2.5.

5. *Wide-Band Detection*: Two main approaches in wide-band SS are the Nyquist wide-band SS and the sub-Nyquist wide-band SS [87]. In Nyquist Wide-band SS, the signal is directly acquired using a high sampling rate analog-to-digital converter (ADC), i.e. at or above Nyquist rate, and then uses some signal processing techniques to detect the spectrum holes. In contrast, sub-Nyquist wide-band SS detects the spectrum holes using acquisitions at sampling rate lower than the Nyquist rate. Various wide-band techniques were proposed in literature and used in SS such as:

5.1 **Compressive Sensing**: Compressive sensing is a powerful approach that enables the analysis and recovery of a wideband signal while it is sampled at a sub-Nyquist rate [27, 98, 118–123]. Compressive sensing exploits the fact that many natural signals are sparse or compressible and can be represented shortly when expressed in a proper basis. Sparsity represents the property that the "information rate" of a continuous-time signal could be much smaller than proposed by its bandwidth [118].

5.2 **Wavelet Based Detector**: Wavelet detection is an effective technique used in image processing for edge detection. In SS, wavelet detection is applied on the wideband power spectral density (PSD) to detect the edges which represents the transitions between occupied and vacant bands [124]. Once the edges are detected, the bands between the edges are further analyzed to identify the spectrum holes.

5.3 **Filter-Bank Based Detector**: In multi-carrier communication systems, spectrum sensing can be performed by measuring the power at

the output of the sub-carrier bands [125]. In this regard, **Multitaper Based Detector** can be seen as a filter-bank spectrum estimation with multiple filter banks or filter-bank is a simplified version of the multitaper by using only one prototype filter for each band [10, 126, 127].

6. *Examples of Other Detectors*: In addition to the mentioned techniques, other detectors also exists. The reader may refer to the surveys such as [10, 20] for others detection techniques. Here we refer for two examples:

6.1 **Blind Source Separation detection**: Blind Source Separation (BSS) was recently proposed in CR networks for SS [128–130]. Several methods were used to separate the mixed signal of CR with the PU or to sense multi frequency bands by separating different signals in different frequency bands such as the independent component analysis [129] and the Kurtosis applied on the separated signals [130]. The advantage of such techniques is their ability to sense the channel even if the SU is operating. However, BSS assumes the statistical independence of the sources. Moreover, other detectors, like EBD, are used with the BSS to improve its performance [130].

6.2 **High-order statistics based detection**: High-order statistics represent the third and higher order in which two basic statistics the moments and cumulants exist. While the first-order and second-order statistics are used to detect the signals in most of the CR applications, high-order moment based detectors have been considered to detect signals have certain properties. For example, second-, fourth- and six-order moments were used in [131], ratio of the second and fourth moments were used in [132] and the third- and higher odd moments were used in [133].

2.4.3 Cooperation in Spectrum Sensing

In general, any wireless communication channel may be characterized by multi-path fading, path-loss, shadowing, noise uncertainty and interference in which the detection performance of the SS techniques may significantly degrade. To overcome these challenges, cooperative sensing was proposed to enhance the detection performance by exploiting the spatial location of different SUs. By means of cooperation, SUs sense certain spectrum band and share their sensing information toward achieving a combined and more

accurate decision [134]. In this regard, cooperation gain is the term that defines any benefit achieved due to this cooperation such as the improvement in the detection performance and overcoming multi-path and shadowing effects such as hidden node problem (HNP) as illustrated in Fig. 2.7. Therein, SU1 and SU3 exists in a place that shadowing effect makes no possible detection of the primary transmission. This is known as the HNP and results in harmful interference. However, SU2 has a good line of sight with primary BS and can inform the others by means of cooperation. In contrast to the cooperation gain, cooperation overhead refers to any additional operation or performance degradation caused by the cooperation in comparison with the non-cooperative sensing such as the need for a control channel and/or a reporting channel, synchronization and reporting delays [103, 135].

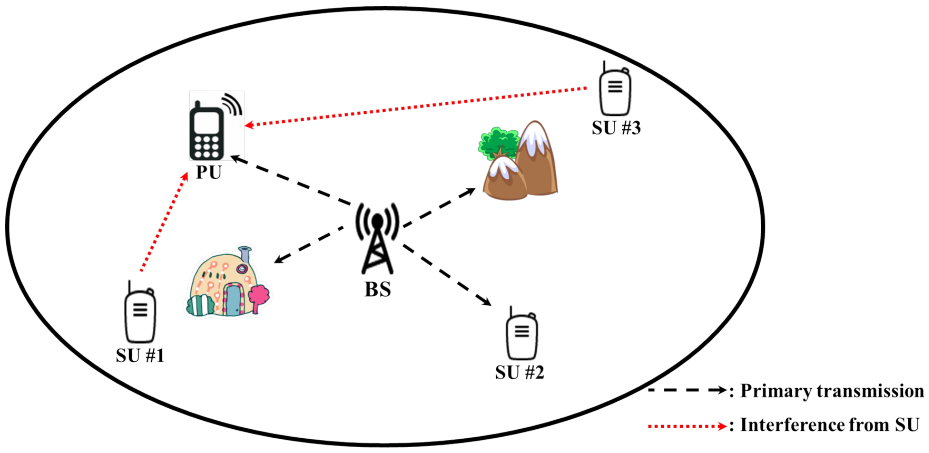

Figure 2.7: Shadowing Effect and Hidden Node problem.

Cooperation could be done in a centralized manner or a distributed one [136]. In centralized cooperation, a fusion center collects the sensed information from all the secondary nodes, decides about the spectrum holes and then broadcasts the decision to all SUs or manages the exploitation of the spectrum holes in the secondary network. In distributed cooperation, SUs share information among themselves and converge to a global decision iteratively. In both centralized and distributed approaches, the bandwidth allocated for the reporting channel limits the amount of information transmitted by the SU nodes. In this regard, three data fusion techniques are defined: (i) Soft combining in which the SUs transmit the entire local sensed samples or the decision metric, (ii) Quantized soft combining in which the

SUs quantize the local sensed samples or the decision metric before sharing and (iii) Hard combining where the shared information is a one bit local decision [135]. For more information regarding cooperative SS, the reader may refer to [135].

2.4.4 Multi-antenna Spectrum Sensing

Antenna diversity or multi-antenna techniques have been widely deployed and are used in communications to improve the transmission/reception by increasing channel capacity without bandwidth expansion and overcoming the effects of fading by space-time coding [137]. In CR context, one of the major objectives and the main motivation is to improve the spectrum utilization [9]. Hence, it is very likely for CRs to exploit the advantages offered by the multiple-input multiple-output (MIMO) technologies to improve secondary communications [138, 138–143]. Further, multi-antenna techniques are also beneficial for the SS process since it can significantly improve the sensing performance by exploiting the spacial diversity. Methods, such as maximum ratio combining, equal gain combining and selection combining, are applied using energy detector to better sense the spectrum [144–146]. The resultant detectors still require the knowledge of the noise power and their performance degrades in noise uncertain environments. However, using multiple antennas it is possible to overcome this problem. Indeed, it is possible to derive optimal totally-blind detectors in multi-antenna scenarios by using the properties of the covariance matrix such as in the EBD approach [40–42]. Moreover, introducing multiple antenna architecture for CR will extend the spectrum awareness and exploitation dimensions to include the angle-of-arrival dimension. For example, beamforming with power control in CR have been jointly considered to control the interference towards PUs and to improve channel capacity in SUs communication [138, 141–143]. In SS, beamforming could offer solution for directed environment detection, i.e. the angle-of-arrival [140].

2.4.5 Challenges in Spectrum Sensing

CR is an intelligent network that must be aware of the changes in its surrounding to adapt its transmission parameters accordingly. Hence, SS is a vital task among other CR tasks that represents the key element for CR realization. Indeed, SS is facing a number of challenges that may cause negative

impact on spectrum detection if they are not well considered. Such challenges includes the hardware implementations, complexity, synchronization, uncertainties, hidden node problem etc. [20]. In this regard, noise uncertainty and very low SNR environments are critical problems that may significantly degrade the performance of any SS detector. To overcome these problems, SUs must use detectors that overcome noise uncertainty problems and performs adequately even in low SNR conditions. EBD is, in general, a totally-blind detector that is not effected by noise uncertainty and robust in low SNR conditions. Moreover, extending SS to detect spectrum holes in a wider space as discussed in Sec. 2.2 is also a challenge. In this regard, the exploitation the diversity of multiple antennas along with the EBD is useful for efficiently detecting the spectrum holes in frequency, time, space and angle-of-arrival dimensions.

In the next section, the concept of EBD is considered since it is the focus of the thesis. Different metrics are considered and the hypothesis tests are analyzed. Different diversity techniques are also discussed such as the cooperation and multiple antennas.

2.5 Eigenvalue Based Detector

Spectrum Sensing techniques with superior performance and robustness can be designed using the eigenvalues of the received signals covariance matrix. These detectors, classified under the name of "eigenvalue based detector" (EBD), rely on the use of random matrix theory (RMT) and different eigenvalue properties of the sample covariance matrix in decision making. For the implementation of the EBD, the SUs have to collect the signal's sample matrix in the first step, determine the sample covariance matrix in the second and then perform the EBD. Several diversity techniques have been introduced in literature in which the SUs can collect the signal's samples in a $K \times N$ matrix form, where K represents the diversity order and N the number of samples collected for the sensing process. Such diversity techniques are:

i. Fractional sampling: Fractional sampling can convert a single-input single-output (SISO) system into a virtual single-input multiple-output (SIMO) system and it has been exploited in the literature to acquire diversity gains over frequency-selective fading channels [147, 148]. In

CR, the received signal is sampled, using fractional sampling, with the rate higher than the Nyquist rate in order to achieve diversity as illustrated in Fig. 2.8 where T_{FS} is the fractional sampling rate.

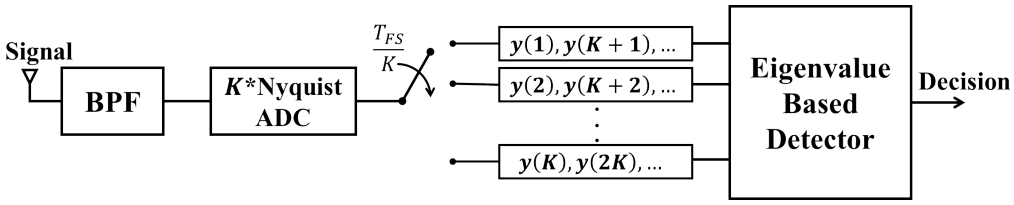

Figure 2.8: Eigenvalue based detector using fractional sampling.

ii. Multi-antenna: SU equipped with multiple antenna, as illustrated in Fig. 2.9, uses these antennas to achieve diversity and acquire the signal independently from each antenna to perform EBD.

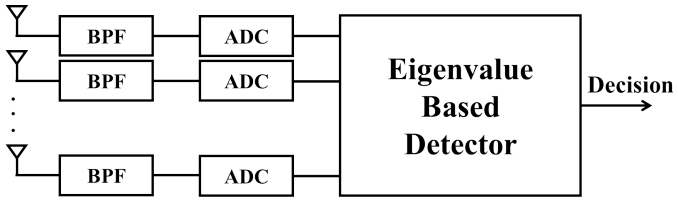

Figure 2.9: Eigenvalue based detector using multiple antennas.

iii. Cooperation: In general, several SUs or nodes can achieve diversity through cooperation by transmitting their raw data to the fusion center where the EBD is performed as illustrated in Fig. 2.10.

Moreover, any combination from these diversity techniques could also be used in performing the EBD. The use of fractional sampling at the receiver requires a high rate ADC and results in colored noise [149]. On the other hand, the use of cooperative approach requires a reporting channel with huge bandwidth and the use of multiple antenna requires multiple RF chains. In this regard, it is very likely that the SUs would be equipped with multiple antenna technology as mentioned in Sec. 2.4.4. To this end, multi-antenna approach is considered as the diversity technique used by SUs for implementing EBD in this report. However, most of the results provided can be directly applied for EBD using any of the mentioned diversity techniques.

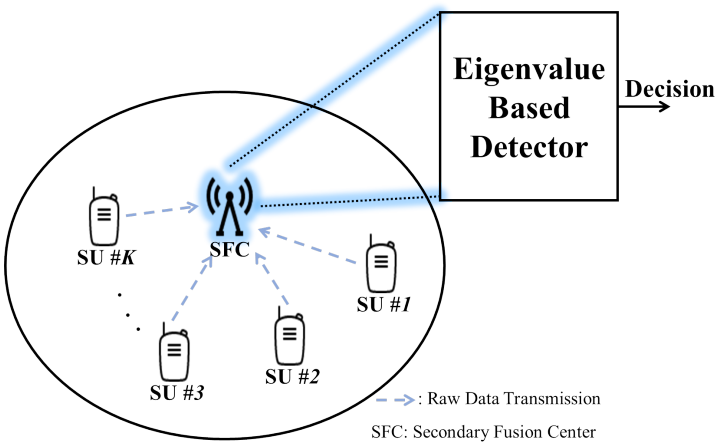

Figure 2.10: Eigenvalue based detector using cooperative technique.

2.5.1 Concept of EBD

Consider a multi-antenna CR system equipped with K receiving antennas aiming to detect the presence/absence of a single PU in a narrowband channel B with the central carrier frequency f_c. The received signal at the SR is sampled at the sampling frequency f_s and denote by N the number of samples acquired at each antenna for the sensing process. Hence, the sensing time, T_s, is given by: $T_s = {}^{N}/_{f_s}$ and the received signal matrix, $\boldsymbol{Y}$, is given by:

$$\boldsymbol{Y} = \begin{pmatrix} y_1(1) & y_1(2) & \cdots & y_1(N) \\ y_2(1) & y_2(2) & \cdots & y_2(N) \\ \vdots & \vdots & \ddots & \vdots \\ y_K(1) & y_K(2) & \cdots & y_K(N) \end{pmatrix}, \tag{2.16}$$

where $y_k(n)$ is the baseband sample at antenna $k = 1 \cdots K$ and instant $n = 1 \cdots N$.

For this detection problem, the received vector, at instant n, under both hypotheses, $\mathcal{H}_0$ and $\mathcal{H}_1$, is given by:

$$\begin{cases} \mathcal{H}_0 & : \ y_k(n) = \eta_k(n), \\ \mathcal{H}_1 & : \ y_k(n) = h_k(n)s(n) + \eta_k(n), \end{cases} \tag{2.17}$$

with $\eta_k(n)$ is a complex circular white Gaussian noise with zero mean and unknown variance σ_η^2, $h_k(n)$ is the channel coefficient between the PU and

antenna k at instant n, and $s(n)$ stands for the primary signal sample modeled as a zero mean Gaussian random variable with variance σ_s^2. Without loss of generality, we suppose that $K \leq N$ and the channel is considered flat-fading, i.e. constant during the sensing time.

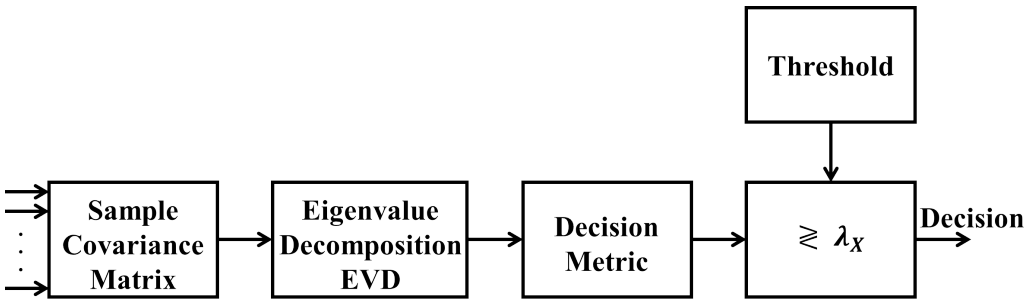

Figure 2.11: General Eigenvalue based detector.

Let $\boldsymbol{W}$ be the sample covariance matrix, $\boldsymbol{W} = \boldsymbol{Y}\boldsymbol{Y}^{\dagger}$, and denote by $\lambda_1 \geq \lambda_2 \geq \cdots \geq \lambda_K > 0$ its ordered eigenvalues. Depending on these eigenvalues and their properties, various decision metrics can be derived. The general EBD block diagram is illustrated in Fig. 2.11. However, depending on the decision metric used in the third block, the second block may not involve eigenvalue decomposition (EVD) algorithm where instead another methods could be applied to reduce the complexity such as direct computation of the trace or the computation of the largest eigenvalue using iterative method (i.e. Power method).

2.5.2 Hypothesis Analysis

In order to decide between the two hypothesis mentioned in (2.17), the decision metric statistics must differ from the $\mathcal{H}_0$ hypothesis to the $\mathcal{H}_1$ hypothesis. In the following, we analyze the statistics of the sample covariance matrix under both hypotheses.

$\mathcal{H}_0$ hypothesis

Consider the following definition of the central Wishart matrix [45]:

Definition 2.1. *The $K \times K$ random matrix $\boldsymbol{W} = \boldsymbol{Y}\boldsymbol{Y}^{\dagger}$ is a central real/complex Wishart matrix with N degrees of freedom and of covariance matrix $\boldsymbol{\Sigma}$ if the*

columns of the $K \times N$ matrix $\boldsymbol{Y}$ are zero-mean independent real/complex Gaussian vectors with covariance matrix $\boldsymbol{\Sigma}$.

Under $\mathcal{H}_0$ hypothesis, the entries of matrix $\boldsymbol{Y}$ are complex Gaussian with zero mean and variance σ_η^2. The interest of the Wishart matrix is primarily due to the sample covariance matrix, $\boldsymbol{W}$, associated with the receiver signal random matrix $\boldsymbol{Y}$. Consequently, and with particular importance of the case where $\boldsymbol{\Sigma} = \sigma_\eta^2 \boldsymbol{I}_K$, $\boldsymbol{W}$, is a $K \times K$ central uncorrelated complex Wishart matrix and is denoted by:

$$\mathbf{W} \sim \mathcal{CW}_K(N, \sigma_\eta^2 \mathbf{I}_K). \tag{2.18}$$

$\mathcal{H}_1$ hypothesis

Under $\mathcal{H}_1$ hypothesis, an unknown single PU is considered and its signal amplitude is independently drawn from a Gaussian process for every sample. The channel is considered flat-fading during the sensing time. Accordingly, the mean matrix, $\boldsymbol{M}$, of the received signal matrix is given by [150, 151]:

$$\boldsymbol{M} = \boldsymbol{h}\boldsymbol{s}^T, \tag{2.19}$$

where $\boldsymbol{h} = [h_1 h_2 \cdots h_K]^T$ and $\boldsymbol{s} = [s(1)s(2) \cdots s(N)]^T$.

In this regard, the definition of the non-central Wishart matrix is an extension of that of the central Wishart matrix when it is originated from a matrix with non-central (i.e. nonzero-mean) Gaussian entries as follows:

Definition 2.2. *The $K \times K$ random matrix $\boldsymbol{W} = \boldsymbol{Y}\boldsymbol{Y}^\dagger$ is a non-central real/complex Wishart matrix with N degrees of freedom, covariance matrix $\boldsymbol{\Sigma}$ and non-centrality matrix $\boldsymbol{\Omega}$ if the columns of the $K \times N$ matrix $\boldsymbol{Y}$ are nonzero-mean independent real/complex Gaussian vectors with covariance matrix $\boldsymbol{\Sigma}$.*

Hence, by considering the special case when $\boldsymbol{\Sigma} = \sigma_\eta^2 \mathbf{I}_K$ then the sample covariance matrix, $\boldsymbol{W}$, under the $\mathcal{H}_1$ hypothesis follows a non-central uncorrelated complex Wishart distribution which is denoted as:

$$\boldsymbol{W} \sim \mathcal{CW}_K(N, \sigma_\eta^2 \mathbf{I}_K, \boldsymbol{\Omega}), \tag{2.20}$$

then the non-centrality matrix can be derived by:

$$\boldsymbol{\Omega} = \boldsymbol{\Sigma}^{-1}\boldsymbol{M}\boldsymbol{M}^\dagger = \frac{1}{\sigma_\eta^2}\|\boldsymbol{s}\|^2 \boldsymbol{h}\boldsymbol{h}^\dagger, \tag{2.21}$$

where $\boldsymbol{\Sigma}$ is the covariance matrix of $\boldsymbol{Y}$, defined as $\boldsymbol{\Sigma} = E[(\boldsymbol{Y} - \boldsymbol{M})(\boldsymbol{Y} - \boldsymbol{M})^{\dagger}] = \sigma_{\eta}^2 I_K$, and $\boldsymbol{M}$ is the mean matrix given by (2.19). Obviously, $\boldsymbol{\Omega}$ is a rank-1 matrix where the nonzero eigenvalue is denoted by ω_1. The average signal to noise ratio (SNR) is defined by:

$$\rho = \frac{\sigma_s^2 \sigma_h^2}{\sigma_{\eta}^2}, \tag{2.22}$$

where the PU signal power, σ_s^2, could be estimated by[1] $(\|\boldsymbol{s}\|^2/N)$, and the channel power $\sigma_h^2 = (\|\boldsymbol{h}\|^2/K)$. As a result, and by using the property that the trace of a matrix equals the sum of its eigenvalues, then ω_1 could be written as:

$$\begin{aligned} \omega_1 &= tr(\boldsymbol{\Omega}) = \frac{1}{\sigma_{\eta}^2}\|\boldsymbol{s}\|^2 tr(\boldsymbol{h}\boldsymbol{h}^{\dagger}) = \frac{1}{\sigma_{\eta}^2}\|\boldsymbol{s}\|^2\|\boldsymbol{h}\|^2 \\ &= NK\rho. \end{aligned} \tag{2.23}$$

2.5.3 EBD decision metrics

Various decision metrics can be derived from the eigenvalues of the sample covariance matrix. In the following, existing approaches are described.

1. ***Standard Condition Number Detector:*** Standard condition number (SCN) detector, also known as maximum-to-minimum eigenvalue detector or the condition number detector, is the ratio of the largest eigenvalue, λ_1, to the smallest eigenvalue, λ_K, of the sample covariance matrix and it is given by:

$$X_{SCN} = \frac{\lambda_1}{\lambda_K}. \tag{2.24}$$

   It is another total-blind detector from the EBD class where no a priori information is required [36, 37]. Let λ_{SCN} be the decision threshold of the SCN detector, then the decision is expressed as follows:

$$D_{SCN} = \begin{cases} \mathcal{H}_0 & \text{if } X_{SCN} \leq \lambda_{SCN} \\ \mathcal{H}_1 & \text{else} \end{cases}. \tag{2.25}$$

[1]The norm of the PU signal, $\|\boldsymbol{s}\|^2$, is still a random variable, however, this randomness decreases fast as N increases and $(\|\boldsymbol{s}\|^2/N)$ can be well approximated by σ_s^2 for sufficient N.

This detector has received a great attention in literature and an enormous work has been done in its analysis. The detailed description of this detector is provided in Ch. 3

2. ***Scaled Largest Eigenvalue Detector:*** Scaled largest eigenvalue (SLE) detector is the ratio of the largest eigenvalue, λ_1, to the normalized trace of the sample covariance matrix and is expressed as follows:

$$X_{SLE} = \frac{\lambda_1}{\frac{1}{K}\sum_{i=1}^{K}\lambda_i}. \tag{2.26}$$

It is a total-blind detector as no a priori information regarding the PU or the noise power is required. In noise uncertainty environments, SLE is proved to be the optimal detector under the generalized likelihood ratio (GLR) criterion [40, 41]. Let λ_{SLE} be the decision threshold of the SLE detector, then the decision is expressed as follows:

$$D_{SLE} = \begin{cases} \mathcal{H}_0 & \text{if } X_{SLE} \leq \lambda_{SLE} \\ \mathcal{H}_1 & \text{else} \end{cases}. \tag{2.27}$$

A more detailed description of the SLE detector is provided in Ch. 4

3. ***Largest Eigenvalue Detector:*** Largest eigenvalue (LE) detector, also known as Roy's Largest Root test, is the largest eigenvalue of the sample covariance matrix normalized by the noise power as follows:

$$X_{LE} = \frac{\lambda_1}{\sigma_\eta^2}. \tag{2.28}$$

It is a semi-blind detector as it requires the noise power knowledge, however, if perfect knowledge is available then LE is the optimal detector [36, 42]. Let λ_{LE} be the decision threshold of the LE detector, then the decision is expressed as follows:

$$D_{LE} = \begin{cases} \mathcal{H}_0 & \text{if } X_{LE} \leq \lambda_{LE} \\ \mathcal{H}_1 & \text{else} \end{cases}. \tag{2.29}$$

A more detailed description of the LE detector is provided in Ch. 5

4. *Other Total-blind EBD metrics:*

4.1 *Spherical Test:* Spherical test (ST) detector, or the sphericity test, is the ratio of the geometric mean to the arithmetic mean of the eigenvalues of the sample covariance matrix [39, 43, 152]. It is a total-blind detector and its decision metric is expressed as follows:

$$X_{ST} = \frac{(det(W))^{1/K}}{\frac{1}{K}tr(W)} = \frac{(\Pi_{i=1}^{K}\lambda_i)^{1/K}}{\frac{1}{K}\sum_{i=1}^{K}\lambda_i}. \tag{2.30}$$

4.2 *Energy with Minimum Eigenvalue:* Energy with minimum eigenvalue (EME) detector is based on the ratio of the average of all eigenvalues of the sample covariance matrix to the minimum eigenvalues which results a total-blind detector [38]. Since the average of the eigenvalues is almost the same as the signals energy [38], then the decision metric is given by:

$$X_{EME} = \frac{\frac{1}{KN}\sum_{k=1}^{K}\sum_{n=1}^{N}|y_k(n)|^2}{\lambda_K}. \tag{2.31}$$

4.3 *John's Detector:* John's detector (JD) is the ratio of the quadratic mean to the arithmetic mean of the eigenvalues of the sample covariance matrix [43, 153]. The decision metric is given by:

$$X_{JD} = \frac{\sum_{k=1}^{K}\lambda_i^2}{(\sum_{k=1}^{K}\lambda_k)^2}. \tag{2.32}$$

4.4 *Demmel Condition Number Detector:* Demmel condition number (DCN) detector is defined by the ratio of the trace to the minimum eigenvalue of the sample covariance matrix [117, 154–158]. The decision metric is given by:

$$X_{DCN} = \frac{tr(W)}{\lambda_K} = \frac{\sum_{k=1}^{K}\lambda_k}{\lambda_K}. \tag{2.33}$$

2.6 Conclusion

CR users use the spectral opportunities as they are not causing harmful interference to the PUs. In this regard, several spectrum exploitation techniques

exist as provided by Sec. 2.3. Interweave approach is the exploitation technique that allows the SUs to dynamically access the spectrum holes wherever and whenever detected in the transmission hyperspace and provide an efficient and effective way in utilizing the spectrum. To do so, SUs must be aware of their surrounding environment and the changes in the spectrum usage instantaneously. Various spectrum awareness approaches exist in the literature as mentioned. In passive awareness, the behavior of the SUs is totally dependent on the outside agent that is responsible of providing the SU by spectrum hyperspace information. This results a static SU that relies on information that might not be up-to-date and may not be useful in the sense of time received. Moreover, the realization of any passive awareness approach requires the establishment of a costly infrastructure, cooperation with the primary network and a dedicated communication channel or an access method to the information source. Likewise, the realization of active awareness approach based on receiver detection, assuming no PU-SU cooperation, may not be applicable as it requires PR position knowledge, a dedicated sensor network and a communication channel. Spectrum sensing, the active PT detection approach, is a powerful approach that does not necessitate the mentioned requirements as it, may only, requires the capability to sense a target channel.

Several SS techniques were proposed in literature as provided in sec. 2.4.2. These techniques are facing challenges such as noise uncertainty, very low SNR, complexities and sensing time that may degrade their performance and shorten the transmission time of the ST. From knowledge perspective, some of these techniques rely on a priori PU information, others rely on noise information and few techniques do not require any a priori knowledge, denoted as "Totally-blind detectors". Totally-blind detectors are applicable in any situation and could effectively be used in detecting spectrum holes without being affected by noise uncertainty. Moreover, under non-cooperative detection assumption, most of the mentioned SS techniques do not exploit the spatial diversity on one hand and on the other hand cannot be extended to new dimensions other than the time-frequency-space dimensions. In this regard, EBD is a multi-antenna based blind detector that is efficient in low SNR environments and could be used for detecting spectrum holes in the time-frequency-space-angle-of-arrival transmission hyperspace without any a prior knowledge regarding the PU and the noise variance. However, the main disadvantage of the EBD is the complexity of its performance probabilities and its decision threshold which cannot be evaluated on the fly. In this re-

gard, the following chapters considers this complexity problem and provides simple and accurate approximations for the SCN, SLE and LE detectors. Moreover, the concept of large multiple-antenna CR systems (i.e. massive MIMO) is considered in Ch. 5 using the EBD to study the efficient way of antenna exploitation.

Chapter 3

Standard Condition Number Detector: Performance Probabilities and Threshold

This chapter considers the performance probabilities and the decision threshold of the SCN detector in finite and asymptotic cases. Consequently, it discusses the statistics of the SCN decision metric of the SCN detector. To this end, the concept of joint distribution of the ordered eigenvalues is presented in Sec. 3.2 where our contribution is provided. Then the contributions for the SCN in the finite case is illustrated in Sec. 3.3. The contributions regarding the SCN in the asymptotic case is illustrated in Sec. 3.4. The problem and the general contributions of this work is illustrated in Fig. 3.1.

3.1 Standard Condition Number Detector

In the last few years, EBD has been proposed as a precious totally-blind detector that exploits the spacial diversity, overcome noise uncertainty challenges and performs adequately even in low SNR conditions. Several EBD decision metrics were proposed in the literature as provided in Sec. 2.5. Among these metrics, the SCN ratio has been extensively studied and has many applications mainly in the context of MIMO systems and SS for CR systems [36–38, 44, 159–163].

Recall that the SU is equipped with K antennas and is acquiring N

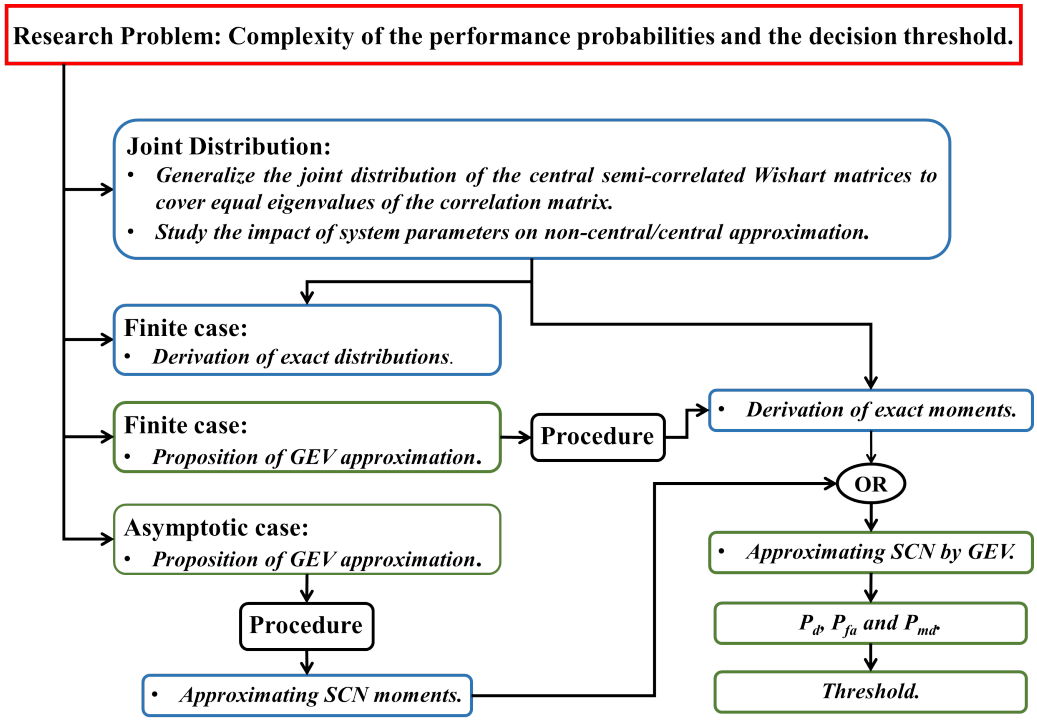

Figure 3.1: Main problem and general contributions.

samples per antenna for the sensing process where $N > K$. The sample covariance matrix is $\boldsymbol{W} = \boldsymbol{Y}\boldsymbol{Y}^{\dagger}$ and $\boldsymbol{Y}$ is the received signal matrix. The SCN is the ratio of the largest to the smallest eigenvalues of $\boldsymbol{W}$ and is given by:

$$X_{SCN} = \frac{\lambda_1}{\lambda_K}. \tag{3.1}$$

In MIMO systems, the SCN has an effective connection with MIMO receiver performance in spatial multiplexing systems [159–161] and it indicates the multipath richness of the MIMO channel [162, 163]. In CR systems, the SCN detector compares this ratio to a threshold to decide whether the PU is present or not. SCN detector is totally-blind detector, not affected by noise power uncertainty and outperform the ED in noise uncertainty environments. For a given decision threshold, $\hat{\lambda}_{SCN}$, the SCN detector algorithm is summarized in Algorithm 3.1.

Despite the mentioned characteristics of the SCN detector, its main drawback primarily lies in the complexity of its performance probability expres-

Algorithm 3.1: SCN Detector

Input: $\boldsymbol{Y}$, $\hat{\lambda}_{SCN}$
Output: D_{SCN}
compute $\boldsymbol{W} = \boldsymbol{Y}\boldsymbol{Y}^{\dagger}$;
get λ_1 and λ_K of $eig(\boldsymbol{W})$;
evaluate $X = \lambda_1/\lambda_K$;
decide $D_{SCN} = X_{SCN} \underset{\mathcal{H}_0}{\overset{\mathcal{H}_1}{\gtrless}} \hat{\lambda}_{SCN}$;

sions and consequently, the expression of its decision threshold. More precisely, the P_{fa}, P_d and P_{md} expressions are directly related to the CDF expression of the decision metric as provided by (2.6), (2.7) and (2.8) respectively. Hence, this drawback is indeed due to the complexities of the CDF expressions.

Consequently, we aim to study the SCN metric and to provide the research community with a simple and accurate forms for the SCN distribution. In this regard, we consider the following two cases in this work:

1. Finite Case: this case represents a SU that is detecting the spectrum holes with finite small number of antenna.

2. Asymptotic Case: this case represents a SU with a large number of antennas aiming to detect the presents of spectrum holes.

Before getting into the details of these cases, the joint distribution of the ordered eigenvalues of the Wishart matrix and the non-central/central approximation are discussed first. In the following section we will consider the Joint PDF of the ordered eigenvalues of the Wishart matrices as it is a key element in deriving the SCN distributions. Problems and contributions are also discussed with some numerical results.

3.2 Joint Distribution of the Ordered Eigenvalues

In the EBD, the decision metrics are the eigenvalues or a combination of the eigenvalues of the sample covariance matrix. When the number of antennas, K, takes a finite values, then results from the finite random matrix

theory (RMT) are involved in the derivation of the decision metrics' exact CDF expressions. Marginal distributions, condition number distributions, moments and several statistical characteristics of the EBD decision metrics usually requires the joint distribution of the eigenvalues of the Wishart matrix. In this regard, the joint distributions of the ordered and unordered eigenvalues of the real/complex central/non-central correlated/uncorrelated Wishart matrices have been derived in [164–177]. The joint distribution of the ordered eigenvalues, denoted by $\lambda_1 \geq \lambda_2 \geq \cdots \geq \lambda_K > 0$, of the central and non-central uncorrelated complex Wishart matrices are considered for $\mathcal{H}_0$ and $\mathcal{H}_1$ hypotheses respectively.

Under $\mathcal{H}_0$, $\boldsymbol{W}$ is a central uncorrelated complex Wishart matrix. The joint distribution of the ordered eigenvalues of $\boldsymbol{W}$ is given by the following Lemma:

Lemma 3.1. *Let $\boldsymbol{W} \sim \mathcal{CW}_K(N, \boldsymbol{I}_K)$ be a central uncorrelated complex Wishart matrix with N Degrees of Freedom (DoF) and correlation matrix $\boldsymbol{I}_K$. Then, the joint distribution of the ordered eigenvalues, $\lambda_1 \geq \lambda_2 \geq \cdots \geq \lambda_K$, of $\boldsymbol{W}$ is given by [178]:*

$$f(\boldsymbol{\lambda}) = \mathcal{K}_{cu} |\boldsymbol{V}(\boldsymbol{\lambda})|^2 \prod_{l=1}^{K} \lambda_l^{N-K} e^{-\lambda_l}, \tag{3.2}$$

with $\boldsymbol{\lambda} = [\lambda_1, \lambda_2, \cdots, \lambda_K]^T$ is the vector of ordered eigenvalues of $\boldsymbol{W}$, $\boldsymbol{V}(\boldsymbol{\lambda})$ is a Vandermonde matrix with (i,j)-th entries $v_i(\lambda_j) = \lambda_j^{i-1}$ and $\mathcal{K}_{cu}$ is a normalization constant given by (3.3) with $\Gamma_n(m) = \prod_{i=0}^{n}(m-i)!$

$$\mathcal{K}_{cu} = [\Gamma_K(N)\Gamma_K(K)]^{-1} \tag{3.3}$$

Under $\mathcal{H}_1$, $\boldsymbol{W}$ is a non-central uncorrelated complex Wishart matrix with rank-1 non-centrality matrix. The joint distribution of the ordered eigenvalues of $\boldsymbol{W}$ is given by the following Lemma:

Lemma 3.2. *Let $\boldsymbol{W} \sim \mathcal{CW}_K(N, \sigma_\eta^2 \boldsymbol{I}_K, \boldsymbol{\Omega})$ be a non-central uncorrelated complex Wishart matrix with N DoF, correlation matrix $\sigma_\eta^2 \boldsymbol{I}_K$ and non-centrality matrix $\boldsymbol{\Omega}$ of eigenvalues $\omega_1 > \omega_2 = \cdots = \omega_K = 0$. Then, the joint distribution of the ordered eigenvalues, $\lambda_1 \geq \lambda_2 \geq \cdots \geq \lambda_K$, of $\boldsymbol{W}$ is given by:*

$$f(\boldsymbol{\lambda}) = \mathcal{K}_{nu} |\boldsymbol{U}(\boldsymbol{\lambda})| \times |\boldsymbol{F}(\boldsymbol{\lambda}, \omega_1)| \prod_{i=1}^{K} \lambda_i^{N-K} \cdot e^{-\lambda_i} \tag{3.4}$$

where $\boldsymbol{U}(\boldsymbol{\lambda})$ *and* $\boldsymbol{F}(\boldsymbol{\lambda}, \omega_1)$ *are* $K \times K$ *matrices of* (i,j)*-th entries given respectively by* $u_i(\lambda_j) = \lambda_j^{K-i}$ *and (3.5). In (3.5),* ${}_0F_1(.,.)$ *is the generalized hypergeometric function defined in [179, Eq. 9.14.1].* $\mathcal{K}_{nu}$ *is defined in (3.6).*

$$f_i(\lambda_j) = \begin{cases} {}_0F_1(N-K+1, \omega_1\lambda_j) & i = 1 \\ \frac{\lambda_j^{K-i} \cdot (N-K)!}{(N-i)!} & i = 2, \cdots, K \end{cases} \tag{3.5}$$

$$\mathcal{K}_{nu} = \frac{e^{-\omega_1} \cdot [(N-K)!]^{-K}}{\Gamma_{K-1}(K-1) \cdot \omega_1^{K-1}} \tag{3.6}$$

Proof. Particularize [180, App. I] with $\boldsymbol{\Omega}$ is a rank-1 matrix. □

Under $\mathcal{H}_1$ hypothesis, one can sometimes obtain explicit solutions for the distributional properties of the non-central Wishart matrices. However, these expressions are usually more complicated than that of the central Wishart matrices. For example, the exact general form of the distribution of SCN of the non-central uncorrelated complex Wishart matrix with full rank non-centrality matrix is derived in [157], however, further numerical evaluation would either require Nuttall-Q function which could be replaced by Marcum Q-function and a finite weighted sum of Bessel functions [181] or by hypergeometric functions that could be expanded to an infinite sum (See, for example, [182] for $K = 2$ and $N = 2$) [157]. In this regard, using certain method that approximates a non-central Wishart distribution by a central Wishart distribution would be practical. In this light, consider the following Lemma that approximate the non-central Wishart distribution with a central Wishart distribution by modifying its correlation matrix.

Lemma 3.3. *[183] The non-central uncorrelated complex Wishart matrix* $\boldsymbol{W} \sim \mathcal{CW}_K(N, \sigma_\eta^2 \boldsymbol{I}_K, \boldsymbol{\Omega})$ *and the central semi-correlated complex Wishart matrix* $\boldsymbol{W} \sim \mathcal{CW}_K(N, \widehat{\boldsymbol{\Sigma}})$ *with effective correlation matrix* $\widehat{\boldsymbol{\Sigma}} = \sigma_\eta^2 I_K + {}^{\boldsymbol{\Omega}}/_N$ *have the same first and second-order moments differing by* ${}^{\boldsymbol{\Omega}}/_N$*.*

Yet, Lemma 3.3 was used in the approximation of several marginal distributions and condition numbers such as the LE, SCN and DCN where the Ricean fading MIMO channel matrix has been studied [157,184]. It has been reported that the accuracy of this approximation deteriorates at high Ricean K-factors [157]. From SS perspective, this approximation has been also used to replace the CDF of the SCN of the dual non-central Wishart matrices by

that of the dual central Wishart matrices under $\mathcal{H}_1$ hypothesis [44]. However, the impact of CR system parameters, such as the SNR, N and K, on the accuracy of this approximation for P_d or P_{md} has not been studied.

Moreover, work done on the joint distribution of the ordered eigenvalues of the central semi-correlated Wishart matrices has considered that the eigenvalues of the correlation matrix, $\mathbf{\Sigma}$, are all distinct [157]. Indeed, these eigenvalues may coincide as the case in SS. Recall that under $\mathcal{H}_1$ hypothesis the non-centrality matrix, $\mathbf{\Omega}$, is a rank-1 matrix where the nonzero eigenvalue is denoted by ω_1 and is given by:

$$\omega_1 = NK\rho. \tag{3.7}$$

Consequently, the correlation matrix of the corresponding central semi-correlated Wishart matrix, due to Lemma 3.3, is given by:

$$\mathbf{\Sigma} = \sigma_\eta^2 I_K + \frac{1}{N}\mathbf{\Omega}. \tag{3.8}$$

Accordingly, all but one eigenvalue of the eigenvalues of $\mathbf{\Sigma}$ are equal to σ_η^2 while σ_1, the remaining eigenvalue, is given by:

$$\sigma_1 = \sigma_\eta^2 + \frac{\omega_1}{N}. \tag{3.9}$$

Therefore, by considering the non-central/central approximation, results based on assuming all the eigenvalues of the correlation matrix are distinct could not be used. Next, we consider the joint distribution of the ordered eigenvalues of the central semi-correlated complex Wishart matrices where the correlation matrix have some coincide eigenvalues. Moreover, the impact of the SNR, K and N on the non-central/central approximation is also studied via simulations.

3.2.1 Central Semi-correlated Wishart Case

As mentioned, all but one of the eigenvalues of the correlation matrix are equal. In this section, we generalize the joint distribution of the ordered eigenvalues of the central semi-correlated Wishart matrix. This new form considers any number L of equal eigenvalues positioned anywhere in vector of eigenvalues of the correlation matrix $\boldsymbol{\sigma}$ and is given in Theorem 3.1 below.

Theorem 3.1. *Let $\boldsymbol{W}$ be a central semi-correlated complex Wishart matrix $\boldsymbol{W} \sim \mathcal{CW}_K(N, \boldsymbol{\Sigma})$, and denote by $\sigma_1 > \sigma_2 > \cdots > \sigma_p = \cdots = \sigma_q > \cdots > \sigma_K > 0$ the ordered eigenvalues of $\boldsymbol{\Sigma}$ assumed full rank with L equal eigenvalues (from p to q with $q = p + L - 1$), then the joint PDF of $\boldsymbol{\lambda}$ could be written as:*

$$f(\boldsymbol{\lambda}) = \mathcal{K}_{cc1} |\boldsymbol{V}(\boldsymbol{\lambda})| \times |\boldsymbol{E}(\boldsymbol{\lambda}, \boldsymbol{\sigma})| \prod_{i=1}^{K} \lambda_i^{N-K}, \tag{3.10}$$

where $\mathcal{K}_{cc1}$ is a normalization constant given by:

$$\mathcal{K}_{cc1} = \frac{\prod_{i<j}^{K} \sigma_i \sigma_j}{\prod_{i=1}^{K} (N-i)! \sigma_i^N \prod\limits_{\substack{i<j \\ \sigma_i \neq \sigma_j}}^{K} (\sigma_j - \sigma_i)\, \Gamma_L(L)}, \tag{3.11}$$

and $\boldsymbol{E}(\boldsymbol{\lambda}, \boldsymbol{\sigma})$ is a $K \times K$ matrix with (i,j)-th entry:

$$\{\boldsymbol{E}(\boldsymbol{\lambda}, \boldsymbol{\sigma})\}_{i,j} = \begin{cases} \frac{\partial^{q-i}(e^{-\frac{\lambda_j}{\sigma_p}})}{\partial \sigma_p^{q-i}} & p \leq i \leq q \\ e^{-\frac{\lambda_j}{\sigma_i}} & otherwise \end{cases}, \tag{3.12}$$

where the n-th partial derivative in (3.12) is given by (3.13) and the Lah number is defined by $\mathcal{L}(n,k) = \binom{n}{k}\binom{n-1}{k-1}(n-k)!$.

$$\frac{\partial^n (e^{-\frac{\lambda_j}{\sigma_p}})}{\partial \sigma_p^n} = \begin{cases} e^{-\frac{\lambda_j}{\sigma_p}} \sum\limits_{k=1}^{n} \frac{(-1)^{k+n} \cdot \mathcal{L}(n,k) \cdot \lambda_j^k}{\sigma_p^{n+k}} & if\ n > 0 \\ e^{-\frac{\lambda_j}{\sigma_p}} & if\ n = 0 \end{cases} \tag{3.13}$$

Proof. See Appendix A.1. □

It can be easily shown that by taking $L = 1$, the parameters in theorem 3.1 will be equivalent to the case of all distinct eigenvalues in the literature [157, Table I].

3.2.2 Numerical Results and Discussion

In this section, we discuss the analytical results through Monte-Carlo simulations. We, firstly, validate the theoretical analysis presented in Theorem

3.1. Given the non-central/central approximation in Lemma 3.3, we study the approximation accuracy as well as the impact of the SNR on this approximation. Since the probability of detection is the main target, we study the effect of the approximation accuracy and the impact of system parameters on P_d. The results are discussed using P_d from the CDF expressions of the SCN of the Wishart matrices derived in App. B.

For this purpose, we, first, generate 10^5 central semi-correlated Wishart matrices. In our simulation setup, the entries of $\boldsymbol{Y}$ are complex standard Gaussian with $K = 2$ and $N = 20$ and we have considered a correlation matrix with eigenvalues $\sigma_1 = \sigma_2$.

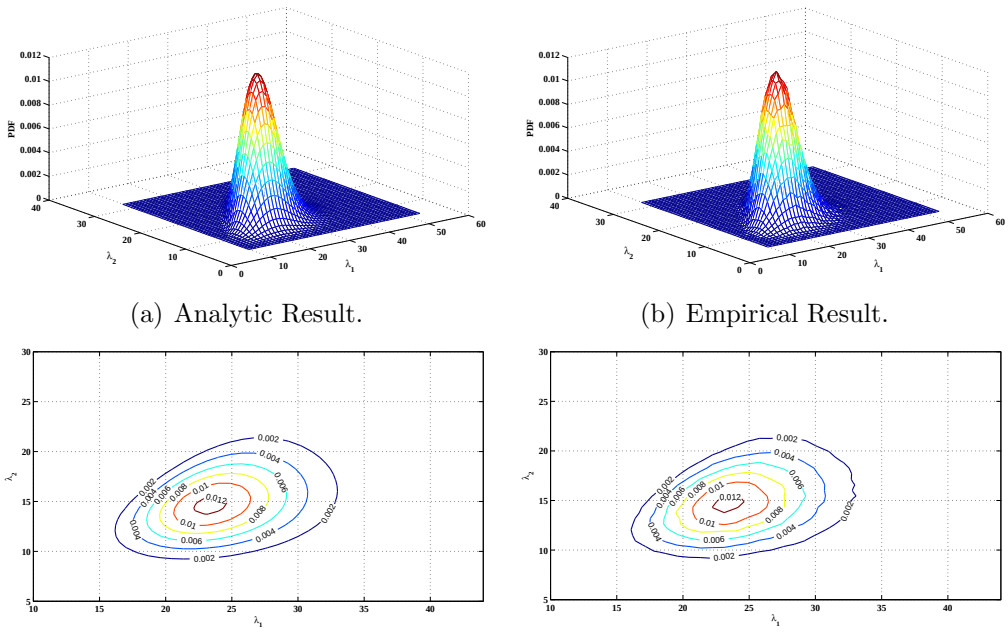

(a) Analytic Result.

(b) Empirical Result.

(c) Analytic Result.

(d) Empirical Result.

Figure 3.2: Joint distribution and its corresponding contour of the ordered eigenvalues of central semi-correlated Wishart matrix with $K = 2$, $N = 20$ and $\sigma_1 = \sigma 2$.

Figure 3.2 shows the joint distribution of the ordered eigenvalues, $\lambda_1 > \lambda_2$, of the central semi-correlated Wishart matrix derived in Theorem 3.1. Figures 3.2(a) and 3.2(b) show the analytical joint PDF and its corresponding empirical result respectively and Figures 3.2(c) and 3.2(d) show the corresponding contours. It is clear that both figures show a perfect match between

the empirical and analytical results.

Non-central/central approximation accuracy is shown in Figure 3.3. The Figure shows the empirical distribution of the SCN of non-central uncorrelated Wishart matrices (under $\mathcal{H}_1$ hypothesis) and its corresponding analytical approximation using Lemma 3.3 for different SNR values (ρ). It is worth mentioning that the analytical expressions are provided in App. B. Results show a perfect match between the empirical results and the analytical approximation at low SNR values, however, approximation accuracy degrades as SNR increases ($\rho > -2dB$).

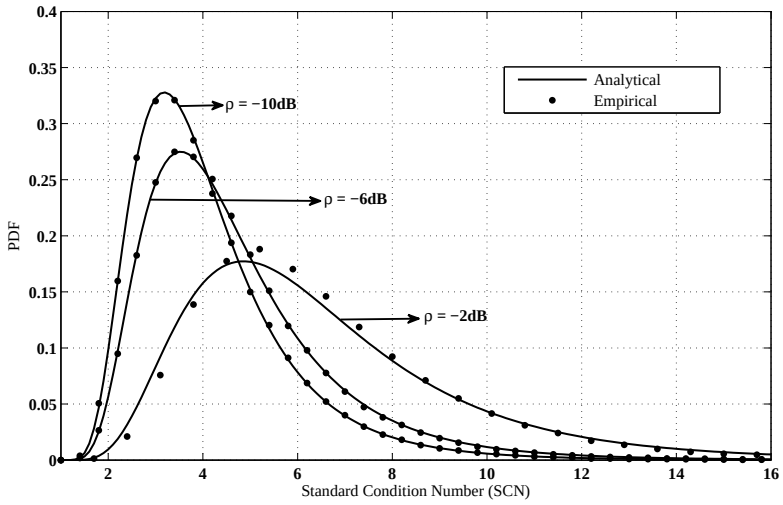

Figure 3.3: Empirical PDF of the SCN of non-central uncorrelated Wishart matrices and the corresponding analytical PDF of central semi-correlated Wishart matrices using normalized non-central/central approximation.

Figures 3.4 and 3.5 present the impact of the system parameters (K, N, and ρ) on the approximation in terms of the performance of the SCN detector for a preset target $\hat{P}_{fa}$. Figure 3.4 shows the P_d of SCN detector of 3-antenna CR as a function of SNR for different number of samples ($N = \{10, 30, 50, 100\}$) while in Fig. 3.5 we vary K ($K = \{2, 3\}$) with the false alarm being set to $\hat{P}_{fa} = 0.1$. Both figures show perfect accuracy for low SNR values ($\rho < -2dB$), however, as SNR increases the approximation starts to show dissimilarity with the empirical results until both probabilities reach 1 (both distributions, the empirical and the analytical, are totally to the right of the considered threshold).

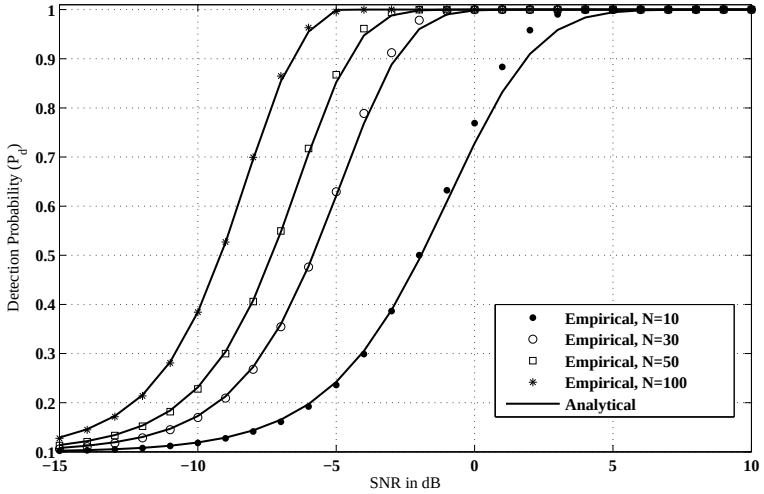

Figure 3.4: Empirical P_d of the SCN metric and its corresponding analytical P_d using normalized non-central/central approximation as a function of SNR for $K = 3$ and $\hat{P}_{fa} = 0.1$.

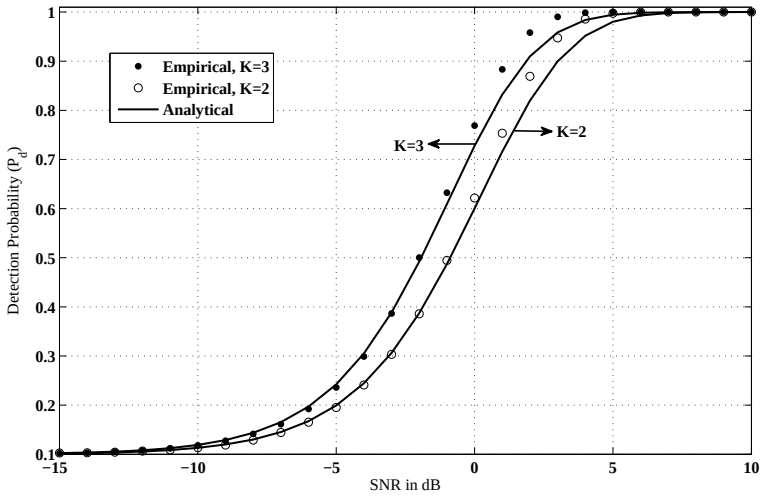

Figure 3.5: Empirical P_d of the SCN metric and its corresponding analytical P_d using normalized non-central/central approximation as a function of SNR for $N = 10$ and $\hat{P}_{fa} = 0.1$.

Figure 3.4 shows that the dissimilarity between the curves decreases as N

increases and becomes very close to zero at $N = 100$. This is related to the threshold selection criteria which is usually based on a constant false-alarm rate (CFAR) [94]. As N increases, P_d is improved since the part to the right of the threshold of the PDF under $\mathcal{H}_1$ increases. This reveals that, in the sense of detection performance, the non-central/central approximation could be considered as a good fit for the empirical distribution of the SCN for sufficiently large values of N. Indeed, both distributions perfectly match at low SNR values and exceed the threshold for higher SNR values where the approximation accuracy degrades. Moreover, same result could be deduced from Fig. 3.5 where the performance of the detector increases as K increases.

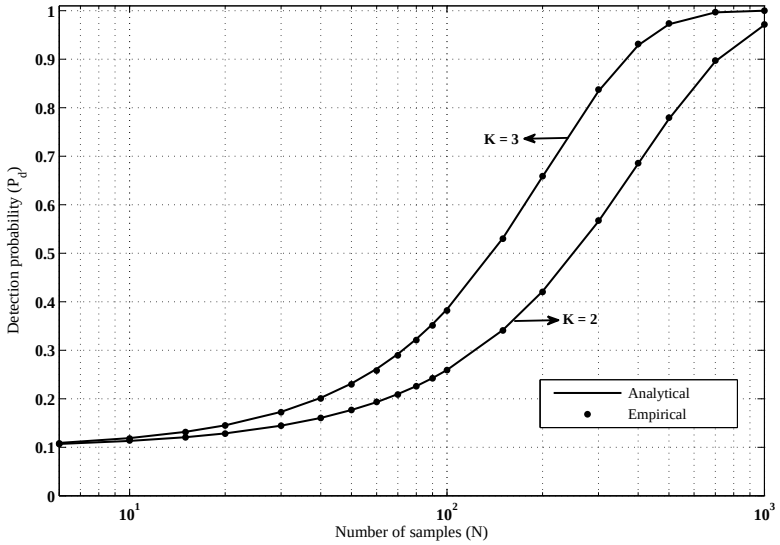

Figure 3.6: Empirical P_d of the SCN metric and its corresponding analytical P_d using normalized non-central/central approximation as a function of the number of received samples for $\rho = -10dB$, and $\hat{P}_{fa} = 0.1$.

To stand on the previous results and to validate the approximation accuracy obtained at low SNR for different values of N and K, we present in Fig. 3.6 the P_d of SCN metric for different N and K with SNR fixed at $\rho = -10dB$ and $\hat{P}_{fa} = 0.1$. The figure shows a perfect match between the empirical and the analytical results for all values of K and N. As it could be seen from the figure, the distribution under $\mathcal{H}_1$ hypothesis partially exceeds the threshold ($P_d < 1$), therefore, the approximation perfectly fits the empirical distribution. Thus, at an acceptable SNR value, the approximation

doesn't show any degradation as N and K values change.

3.2.3 Section Conclusion

Through this section, we have considered the joint distribution of the ordered eigenvalue of different Wishart matrices. Under $\mathcal{H}_1$ hypothesis, the non-central/central approximation is considered as a practical solution to avoid the difficult manipulation and the complicated analytical results when using the non-central uncorrelated Wishart matrix statistical properties. In this regard, we have derived the expression of the joint PDF of the ordered eigenvalues of the central semi-correlated complex Wishart matrices when the correlation matrix exhibit equal eigenvalues. Based on these results, we study the impact of system parameters on P_d when using the non-central/central approximation. Results have shown that this approximation has perfect accuracy for low SNR values and could be considered as a good fit for P_d for sufficiently large values of N when the SNR is high.

3.3 Finite Case

Herein, we consider the SCN detector in the finite case where $K > 1$ takes small values. In literature, the authors in [157] provided the exact generic form of the distribution of the SCN based on the joint distribution of the ordered eigenvalues of Wishart matrices. Consequently, [44] provides the exact forms of the P_{fa} of the SCN detector for CR with two antenna (i.e. dual case). In addition, the P_d for 2-dimensional systems was approximated using the non-central/central approximation and provided in [44] following the results in [157].

In this section, we first derive the exact distribution of the SCN metric using the joint distributions provided by Sec. 3.2. A general nested form for the CDF and the PDF of the SCN of the central uncorrelated, non-central uncorrelated and central semi-correlated complex Wishart matrices are derived. Consequently, it could be easily deduced that lookup tables (LUT) must be constructed and used to avoid computational complexity. In this regard, we provide an alternative solution as we propose a new approximation for the SCN based on the generalized extreme value (GEV) distribution. For this purpose, we derive the exact form of the p-th moment of the SCN to match the first three moments of the GEV distribution. This approxi-

mation is simple and accurate even though the computational complexity of the SCN moments still exists. However, as we need only the first three moments, the latter could be computed offline and saved. Moreover, we show that by using the non-central/central approximation along with the proposed approximation, the result is still accurate with a simpler moments form.

It is worth mentioning that $\sigma_\eta^2 = 1$ is reasonable value since the SCN is not effected by the noise power value. Moreover, the use of Lemma 3.3 for SCN distribution approximation requires the normalization by σ_η^2 if it is else than 1, i.e. $\boldsymbol{W}_n = \sigma_\eta^{-2}\boldsymbol{W}$ where $\boldsymbol{W}_n$ is normalized Wishart matrix.

3.3.1 SCN Exact Distribution

Under $\mathcal{H}_0$ hypothesis, the sample covariance matrix follows a central uncorrelated Wishart distribution, i.e. $\boldsymbol{W} \sim \mathcal{CW}_K(N, \sigma_\eta^2 \boldsymbol{I}_K)$. Then, the general form of the CDF of the SCN of $\boldsymbol{W}$ is given by [157]:

$$F_0(x) = \mathcal{K}_{cu} \sum_{n=1}^{K} \int_0^\infty |\boldsymbol{\Upsilon}_n^{cu}(x)| \, d\lambda_K \tag{3.14}$$

with

$$\Upsilon_n^{cu}(x)_{i,j} = \begin{cases} \gamma(N-K+i+j-1, x\lambda_K) - \gamma(N-K+i+j-1, \lambda_K), & i \neq n \\ \lambda_K^{N-K+i+j-2} e^{-\lambda_K}, & i = n \end{cases} \tag{3.15}$$

where $\gamma(.,.)$ is the lower incomplete gamma function [179, Eq.(8.350.1)], $\mathcal{K}_{cu}$ defined by (3.3).

Corollary 3.1. *Let $\boldsymbol{W} \sim \mathcal{CW}_K(N, \sigma_\eta^2 \boldsymbol{I}_K)$ be a central uncorrelated complex Wishart matrix with N DoF and correlation matrix $\sigma_\eta^2 \boldsymbol{I}_K$. Then, the exact general form of the CDF and PDF of the SCN of $\boldsymbol{W}$ are given, respectively, by:*

$$\begin{aligned} F_0(x) = \mathcal{K}_{cu} \sum_{n,m=1}^{K} (-1)^{n+m} \sum_{\delta \in \mathbb{P}_1} sgn(\delta) \prod_{i=1}^{K-1} (N + r_{\delta(i),n} + r_{i,m} - K - 2)! \\ \times \sum_{\boldsymbol{s} \in \mathbb{S}_1} (-1)^{|\boldsymbol{s}|} \sum_{l_1 \cdots l_{K-1}} \frac{x^{\Sigma \boldsymbol{s}} \cdot (\Sigma l_i + N + n + m - K - 2)!}{\Pi l_i! \cdot (|\boldsymbol{s}|x - |\boldsymbol{s}| + K)^{\Sigma l_i + N + n + m - K - 1}} \end{aligned} \tag{3.16}$$

$$f_0(x) = \mathcal{K}_{cu} \sum_{n,m=1}^{K} (-1)^{n+m} \sum_{\delta \in \mathbb{P}_1} sgn(\delta) \prod_{i=1}^{K-1} (N + r_{\delta(i),n} + r_{i,m} - K - 2)! \sum_{\boldsymbol{s} \in \mathbb{S}_1} (-1)^{|\boldsymbol{s}|}$$
$$\times \sum_{l_1 \cdots l_{K-1}} \frac{x^{\Sigma \boldsymbol{s}} [\Sigma \boldsymbol{s} x^{-1} (|\boldsymbol{s}| x - |\boldsymbol{s}| + K) - |\boldsymbol{s}| (\Sigma l_i + N + n + m - K - 1)]}{\Pi l_i! \cdot [(\Sigma l_i + N + n + m - K - 2)!]^{-1} \cdot (|\boldsymbol{s}| x - |\boldsymbol{s}| + K)^{\Sigma l_i + N + n + m - K}} \tag{3.17}$$

where $\mathbb{P}_1$ *and* $\mathbb{S}_1$ *are, respectively, the set of all possible permutations and subsets of the vector* $[1, \cdots, K-1]$. $sgn(\delta)$ *is the permutation sign and* $|\boldsymbol{s}|$ *is the cardinality.* $\sum_{l_1 \cdots l_{K-1}} = \sum_{l_1}^{L_1} \cdots \sum_{l_{K-1}}^{L_{K-1}}$ *with* $L_j = N + r_{\delta(j),n} + r_{j,m} - K - 2$*;* $\Sigma \boldsymbol{s}$, Σl_i *and* $\Pi l_i!$ *are, respectively, the sum of the values of* $l_i \in \boldsymbol{s}$*, the sum of the values of* $l_{1 \leq i \leq K-1}$ *and the product of the factorial of the values of* $l_{1 \leq i \leq K-1}$*. Finally,* $r_{i,j}$ *is defined as:*

$$r_{i,j} = \begin{cases} i & i < j \\ i+1 & i \geq j \end{cases} \tag{3.18}$$

Proof. Refer to Appendix A.2. □

Under $\mathcal{H}_1$ hypothesis, the sample covariance matrix follows a non-central uncorrelated Wishart distribution, $\boldsymbol{W} \sim \mathcal{CW}_K(N, \sigma_\eta^2 \boldsymbol{I}_K, \boldsymbol{\Omega})$, with rank-1 non-centrality matrix $\boldsymbol{\Omega}$. Then, the exact generic form of the SCN CDF under $\mathcal{H}_1$ hypothesis is given by the following Theorem:

Theorem 3.2. *Let* $\boldsymbol{W} \sim \mathcal{CW}_K(N, \sigma_\eta^2 \boldsymbol{I}_K, \boldsymbol{\Omega})$ *be a non-central uncorrelated complex Wishart matrix with* N *DoF, correlation matrix* $\sigma_\eta^2 \boldsymbol{I}_K$ *and non-centrality matrix* $\boldsymbol{\Omega}$ *of eigenvalues* $\omega_1 > \omega_2 = \cdots = \omega_K = 0$*. Then, the CDF of the SCN of* $\boldsymbol{W}$ *is given by:*

$$F_1(x) = \mathcal{K}_{nu} \sum_{n=1}^{K} \int_0^\infty |\boldsymbol{\Upsilon}_n^{nu}(x)| \, d\lambda_K \tag{3.19}$$

with

$$\Upsilon_n^{nu}(x)_{i,j} = \begin{cases} \mathcal{I}_{i,j}^{nu} = \int_{\lambda_K}^{x\lambda_K} f_j(u) u^{N-i} e^{-u} du, & i \neq n \\ f_j(\lambda_K) \lambda_K^{N-i} e^{-\lambda_K}, & i = n \end{cases} \tag{3.20}$$

where $f_j(.)$ is given in (3.5) and the integral in (3.20) has analytical solution given by:

$$\mathcal{I}_{i,j}^{nu} = \begin{cases} \sum_{l=0}^{\infty} \frac{\omega_1^l}{(N-K+1)_l l!} \Big[\gamma(N-i+l+1, x\lambda_K) - \gamma(N-i+l+1, \lambda_K)\Big] & j=1 \\ \frac{(N-K)!}{(N-j)!} \Big[\gamma(N+K-i-j+1, x\lambda_K) - \gamma(N+K-i-j+1, \lambda_K)\Big] & j=2,\cdots,K \end{cases} \tag{3.21}$$

Proof. Refer to Appendix A.3. □

Corollary 3.2. *Let $\boldsymbol{W} \sim \mathcal{CW}_K(N, \sigma_\eta^2 \boldsymbol{I}_K, \boldsymbol{\Omega})$ be a non-central uncorrelated complex Wishart matrix with N DoF, correlation matrix $\sigma_\eta^2 \boldsymbol{I}_K$ and non-centrality matrix $\boldsymbol{\Omega}$ of eigenvalues $\omega_1 > \omega_2 = \cdots = \omega_K = 0$. Then, the exact general form of the CDF and PDF of the SCN of $\boldsymbol{W}$ is given, respectively, by:*

$$F_1(x) = \mathcal{K}'_{nu} \sum_{n,m=1}^{K} (-1)^{n+m} \sum_{h=0}^{\infty} \frac{\omega_1^h}{(N-K+h)!h!} \sum_{\delta \in \mathbb{P}_1} sgn(\delta) \prod_{i=1}^{K-1} (N - r_{\delta(i),n} + g_{r_{i,m},1}(h,K))!$$
$$\times \sum_{\boldsymbol{s} \in \mathbb{S}_1} (-1)^{|\boldsymbol{s}|} \sum_{l_1 \cdots l_{K-1}} \frac{x^{\Sigma \boldsymbol{s}} \cdot (\Sigma l_i + N - n + g_{m,1}(h,K))!}{\Pi l_i! \cdot (|\boldsymbol{s}|x - |\boldsymbol{s}| + K)^{\Sigma l_i + N - n + g_{m,1}(h,K)+1}} \tag{3.22}$$

$$f_1(x) = \mathcal{K}'_{nu} \sum_{n,m=1}^{K} (-1)^{n+m} \sum_{h=0}^{\infty} \frac{\omega_1^h}{(N-K+h)!h!} \sum_{\delta \in \mathbb{P}_1} sgn(\delta) \prod_{i=1}^{K-1} (N - r_{\delta(i),n} + g_{r_{i,m},1}(h,K))!$$
$$\times \sum_{\boldsymbol{s} \in \mathbb{S}_1} (-1)^{|\boldsymbol{s}|} \sum_{l_1 \cdots l_{K-1}} \frac{x^{\Sigma \boldsymbol{s}} [\Sigma \boldsymbol{s} x^{-1} (|\boldsymbol{s}|x - |\boldsymbol{s}| + K) - |\boldsymbol{s}| (\Sigma l_i + N - n + g_{m,1}(h,K) + 1)]}{\Pi l_i! \cdot [(\Sigma l_i + N - n + g_{m,1}(h,K))!]^{-1} \cdot (|\boldsymbol{s}|x - |\boldsymbol{s}| + K)^{\Sigma l_i + N - n + g_{m,1}(h,K)+2}} \tag{3.23}$$

with

$$\mathcal{K}'_{nu} = \left[\Gamma_{K-1}(K-1) \prod_{i=2}^{K} (N-i)! \omega_1^{K-1} e^{\omega_1} \right]^{-1}, \tag{3.24}$$

and $\sum_{l_1 \cdots l_{K-1}} = \sum_{l_1}^{L_1} \cdots \sum_{l_{K-1}}^{L_{K-1}}$ with $L_j = N - r_{\delta(j),n} + g_{r_{j,m},1}(h,K)$ and we define $g_{i,j}(a,b)$ as:

$$g_{i,j}(a,b) = \begin{cases} a & i = j \\ b - i & i \neq j \end{cases} \tag{3.25}$$

Proof. Refer to Appendix A.2. □

Under $\mathcal{H}_1$ hypothesis and using Lemma 3.1, the sample covariance matrix could be approximated by a central semi-correlated Wishart distribution, $\boldsymbol{W} \sim \mathcal{CW}_K(N, \boldsymbol{\Sigma})$, with correlation matrix having $K-1$ equal eigenvalues. The exact generic form of the SCN CDF for the $\mathcal{H}_1$ hypothesis is given by the following Theorem:

Theorem 3.3. *Let $\boldsymbol{W} \sim \mathcal{CW}_K(N, \boldsymbol{\Sigma})$ be a Central Semi-Correlated Wishart matrix with N DoF and correlation matrix $\boldsymbol{\Sigma}$ of eigenvalues $\sigma_1 > \sigma_2 = \cdots = \sigma_K$. Then, the CDF of the SCN of $\boldsymbol{W}$ is given by:*

$$F_1(x) = \mathcal{K}_{cc} \sum_{n=1}^{K} \int_0^{\infty} |\boldsymbol{\Upsilon}_n^{cc}(x)| \, d\lambda_K \tag{3.26}$$

with

$$\Upsilon_n^{cc}(x)_{i,j} = \begin{cases} \mathcal{I}_{i,j}^{cc} = \int_{\lambda_K}^{x\lambda_K} e_j(u) u^{N+i-K-1} du, & i \neq n \\ e_j(\lambda_K) \lambda_K^{N+i-K-1}, & i = n \end{cases} \tag{3.27}$$

where $e_j(.)$ is given in (A.6) and the integral in (3.27) has an analytical solution given by:

$$\mathcal{I}_{i,j}^{cc} = \begin{cases} \left[\gamma(N+i-K, \frac{x\lambda_K}{\sigma_1}) - \gamma(N+i-K, \frac{\lambda_K}{\sigma_1})\right] \cdot \sigma_1^{N+i-K} & j = 1 \\ (-1)^{K-j} \left[\gamma(N+i-j, \frac{x\lambda_K}{\sigma_2}) - \gamma(N+i-j, \frac{\lambda_K}{\sigma_2})\right] \sigma_2^{N+i-j} & j = 2, \cdots, K \end{cases} \tag{3.28}$$

Proof. Refer to Appendix A.3. □

Corollary 3.3. *Let $\boldsymbol{W} \sim \mathcal{CW}_K(N, \boldsymbol{\Sigma})$ be a Central Semi-Correlated Wishart matrix with N DoF and correlation matrix $\boldsymbol{\Sigma}$ of eigenvalues $\sigma_1 > \sigma_2 = \cdots = \sigma_K$. Then, the exact general form of the CDF and PDF of the SCN of $\boldsymbol{W}$ is given, respectively, by:*

$$\begin{aligned} F_1(x) = \mathcal{K}'_{cc} \sum_{n,m=1}^{K} (-1)^{n+m} \sum_{\delta \in \mathbb{P}_1} sgn(\delta) \prod_{i=1}^{K-1} \frac{(N + r_{\delta(i),n} - g_{r_{i,m},1}(K, 2i) - 1)!}{\sigma_{r_{i,m}}^{-(N+r_{\delta(i),n} - g_{r_{i,m},1}(K,2i))}} \\ \times \sum_{\boldsymbol{s} \in \mathbb{S}_1} (-1)^{|\boldsymbol{s}|} \sum_{l_1 \cdots l_{K-1}} \frac{x^{\Sigma \boldsymbol{s}} \cdot (\Sigma l_i + N + n - g_{m,1}(K, 2i) - 1)!}{\Pi l_i! \cdot \Pi \sigma_{r_{i,m}}^{l_i} \cdot (\Sigma_{\boldsymbol{s}} \frac{x}{\sigma_{s_i,m}} + \Sigma_{\bar{\boldsymbol{s}}} \frac{1}{\sigma_{\bar{s}_i,m}} + \frac{1}{\sigma_m})^{\Sigma l_i + N + n - g_{m,1}(K,2i)}} \end{aligned} \tag{3.29}$$

$$f_1(x) = \mathcal{K}'_{cc} \sum_{n,m=1}^{K} (-1)^{n+m} \sum_{\delta \in \mathbb{P}_1} sgn(\delta) \prod_{i=1}^{K-1} \frac{(N - r_{\delta(i),n} + g_{r_{i,m},1}(K,2i) - 1)!}{\sigma_{r_{i,m}}^{-(N-r_{\delta(i),n}+g_{r_{i,m},1}(K,2i))}} \sum_{\boldsymbol{s} \in \mathbb{S}_1} (-1)^{|\boldsymbol{s}|}$$
$$\times \sum_{l_1 \cdots l_{K-1}} \frac{\Pi l_i! \cdot \Pi \sigma_{r_{i,m}}^{l_i}}{(\Sigma l_i + N + n - g_{m,1}(K,2i) - 1)!} \cdot$$
$$\frac{x^{\Sigma \boldsymbol{s}} [\Sigma \boldsymbol{s} x^{-1} (\Sigma_{\boldsymbol{s}} \frac{x}{\sigma_{s_i,m}} + \Sigma_{\bar{\boldsymbol{s}}} \frac{1}{\sigma_{\bar{s}_i,m}} + \frac{1}{\sigma_m}) - (\Sigma l_i + N + n - g_{m,1}(K,2i)) \Sigma_{\boldsymbol{s}} \frac{1}{\sigma_{s_i,m}}]}{(\Sigma_{\boldsymbol{s}} \frac{x}{\sigma_{s_i,m}} + \Sigma_{\bar{\boldsymbol{s}}} \frac{1}{\sigma_{\bar{s}_i,m}} + \frac{1}{\sigma_m})^{\Sigma l_i + N + n - g_{m,1}(K,2i) + 1}} \tag{3.30}$$

with

$$\mathcal{K}'_{cc} = \frac{(-1)^{(K-1)(K-2)/2} \sigma_1^{K-N-1} \ \sigma_2^{(N-1)(1-K)}}{\Gamma_K(N) \Gamma_{K-1}(K-1)(\sigma_2 - \sigma_1)^{K-1}} \tag{3.31}$$

Proof. Refer to Appendix A.2. □

The results provided are the exact expressions of the SCN distributions. One can easily notice the complexity of these expressions in which it is impossible for the system to dynamically compute the threshold online. Indeed, it is even very complicated to find such threshold starting by these expressions. Accordingly, finding a simple form approximation for the distribution of SCN metric is extremely important. In this regard, we start by deriving the exact p-th moment form of the SCN metric in the next section to be used later in the approximation.

3.3.2 SCN Moments

Under $\mathcal{H}_0$ hypothesis, the exact expression of the $p-th$ moment of the SCN of the central uncorrelated complex Wishart matrix is given by the following Theorem:

Theorem 3.4. *Let $\boldsymbol{W} \sim \mathcal{CW}_K(N, \sigma_\eta^2 \boldsymbol{I}_K)$ be a central uncorrelated complex Wishart matrix with N DoF and correlation matrix $\sigma_\eta^2 \boldsymbol{I}_K$. Then, the p-th moment of the SCN of $\boldsymbol{W}$ is given by:*

$$M(p) = \mathcal{K}_{cu} \sum_{\delta \in \mathbb{P}_0} sgn(\delta) \sum_{\alpha \in \mathbb{P}_0} sgn(\alpha) \sum_{l_1 \cdots l_{K-1}} \frac{\Pi_i (N - K - 2 + \delta(i) + \alpha(i) + l_{i-1} + C_{i,p})!}{\Pi_i l_i! \cdot \Pi_i i^{N-K-1+\delta(i)+\alpha(i)+l_{i-1}-l_i+C_{i,p}}} \tag{3.32}$$

with

$$C_{i,p} = \begin{cases} p & i = 1 \\ 0 & 1 < i < K \\ -p & i = K \end{cases} \tag{3.33}$$

and $\sum\limits_{l_1 \cdots l_{K-1}} = \sum\limits_{l_1=0}^{L_1} \cdots \sum\limits_{l_{K-1}=0}^{L_{K-1}}$ *with* $L_j = N - K - 2 + \delta(j) + \alpha(j) + l_{j-1} + C_{j,p}$, $\Pi_i(.)$ *denotes the multiplication over* $i = 1 \cdots K$ *and* $l_0 = l_K = 0$.

Proof. Refer to Appendix A.4. □

Under $\mathcal{H}_1$ hypothesis, the exact expression of the p-th moment of the SCN under $\mathcal{H}_1$ hypothesis is given by the following Theorem:

Theorem 3.5. *Let* $\boldsymbol{W} \sim \mathcal{CW}_K(N, \sigma_\eta^2 \boldsymbol{I}_K, \boldsymbol{\Omega})$ *be a non-central uncorrelated complex Wishart matrix with* N *DoF, correlation matrix* $\sigma_\eta^2 \boldsymbol{I}_K$ *and non-centrality matrix* $\boldsymbol{\Omega}$ *of eigenvalues* $\omega_1 > \omega_2 = \cdots = \omega_K = 0$. *Then, the* p*-th moment,* $M(p)$*, of the SCN of* $\boldsymbol{W}$ *is given by:*

$$\begin{aligned} M(p) = \mathcal{K}'_{nu} \sum_{n=1}^{K} (-1)^{n+1} \sum_{\delta \in \mathbb{P}_0} sgn(\delta) \sum_{\alpha \in \mathbb{P}_1} sgn(\alpha) \sum_{h=0}^{\infty} \frac{\omega_1^h}{(N-K+h)!h!} \\ \times \sum_{l_1 \cdots l_{K-1}} \frac{\Pi_i (N - \delta(i) + G_{i,n}(h, K, \alpha) + l_{i-1} + C_{i,p})!}{\Pi_i l_i! \cdot \Pi_i i^{N - \delta(i) + G_{i,n}(h,K,\alpha) + C_{i,p} + l_{i-1} - l_i + 1}} \end{aligned} \tag{3.34}$$

with

$$G_{i,n}(h, K, \alpha) = \begin{cases} K - r_{\alpha(i),1} & i < n \\ h & i = n \\ K - r_{\alpha(i-1),1} & i > n \end{cases} \tag{3.35}$$

and $\sum\limits_{l_1 \cdots l_{K-1}} = \sum\limits_{l_1=0}^{L_1} \cdots \sum\limits_{l_{K-1}=0}^{L_{K-1}}$ *with* $L_j = N - \delta(j) + G_{j,n}(h, K, \alpha) + l_{j-1} + C_{j,p}$.

Proof. Refer to Appendix A.4. □

Under $\mathcal{H}_1$ hypothesis and using Lemma 3.3, the sample covariance matrix could be approximated by a central semi-correlated Wishart distribution, $\boldsymbol{W} \sim \mathcal{CW}_K(N, \boldsymbol{\Sigma})$, with correlation matrix having $K - 1$ equal eigenvalues. The exact expression of the p-th moment of the SCN of $\boldsymbol{W} \sim \mathcal{CW}_K(N, \boldsymbol{\Sigma})$ is given by the following Theorem:

Theorem 3.6. *Let $\boldsymbol{W} \sim \mathcal{CW}_K(N, \boldsymbol{\Sigma})$ be a Central Semi-Correlated Wishart matrix with N DoF and correlation matrix $\boldsymbol{\Sigma}$ of eigenvalues $\sigma_1 > \sigma_2 = \cdots = \sigma_K$. Then, the p-th moment, $M(p)$, of the SCN of $\boldsymbol{W}$ is given by:*

$$\begin{aligned} M(p) =& \mathcal{K}'_{cc} \sum_{n=1}^{K} (-1)^{n+1} \sum_{\delta \in \mathbb{P}_0} sgn(\delta) \sum_{\alpha \in \mathbb{P}_1} sgn(\alpha) \\ & \times \sum_{l_1 \cdots l_{K-1}} \frac{\Pi_i (N + \delta(i) + G_{i,n}(0, K, \alpha) + l_{i-1} + C_{i,p} - K - 1)!}{\Pi_i l_i! \cdot \Pi_i [\sum_{j=1}^{i} \frac{1}{\sigma_{b_{j,n}}}]^{N + \delta(i) + G_{i,n}(0,K,\alpha) + C_{i,p} + l_{i-1} - l_i - K}} \end{aligned} \tag{3.36}$$

with

$$b_{i,n} = \begin{cases} 1 & i = n \\ 2 & i \neq n \end{cases} \tag{3.37}$$

and $\sum_{l_1 \cdots l_{K-1}} = \sum_{l_1=0}^{L_1} \cdots \sum_{l_{K-1}=0}^{L_{K-1}}$ *with* $L_j = N + \delta(j) + G_{j,n}(0, K, \alpha) + l_{j-1} + C_{j,p} - K - 1$.

Proof. Refer to Appendix A.4. □

Based on these moments, we propose the SCN approximation. Indeed, we approximate the SCN distribution using moment matching method. Specifically, we consider the first three central moments and match them with the first three moments of the GEV distribution. This approximation is considered in the next subsection.

3.3.3 SCN Distribution Approximation

This section provides an approximation for the SCN distribution based on the GEV distribution. The approximation framework is based on the moment-matching method where the exact expressions of the moments of the SCN are derived in previous subsection.

By considering the moments of the SCN, in Theorems 3.4, 3.5 and 3.6, the mean, variance and skewness of the SCN of each of the considered Wishart

matrices are written as follows:

$$\mu_{X_{SCN}} = M(1) \tag{3.38}$$

$$\sigma^2_{X_{SCN}} = M(2) - \mu^2_{X_{SCN}} \tag{3.39}$$

$$\mathcal{S}_{X_{SCN}} = \frac{M(3) - 3M(2)\mu_{X_{SCN}} + 2\mu^3_{X_{SCN}}}{\sigma^3_{X_{SCN}}} \tag{3.40}$$

Accordingly, we give the following Proposition that approximate the distribution of the SCN of the central uncorrelated, non-central uncorrelated and central semi-correlated Wishart matrices using the GEV distribution as follows:

Proposition 3.1. *Let X_{SCN} be the SCN of $\boldsymbol{W}$ and consider the following three cases:*

Case 1: $\boldsymbol{W} \sim \mathcal{CW}_K(N, \sigma^2_\eta \boldsymbol{I}_K)$ *is a central uncorrelated Wishart matrix.*

Case 2: $\boldsymbol{W} \sim \mathcal{CW}_K(N, \sigma^2_\eta \boldsymbol{I}_K, \boldsymbol{\Omega})$ *is a non-central uncorrelated Wishart matrix with $\boldsymbol{\Omega}$ has only one non-zero eigenvalue ω_1.*

Case 3: $\boldsymbol{W} \sim \mathcal{CW}_K(N, \boldsymbol{\Sigma})$ *is a central semi-correlated Wishart matrix with $\boldsymbol{\Sigma}$ has $K-1$ equal eigenvalues ($\sigma_1 > \sigma_2 = \cdots = \sigma_K$).*

Then, the CDF and PDF of X_{SCN} can be tightly approximated respectively by:

$$F(x;\theta,\beta,\xi) = e^{-(1+(\frac{x-\theta}{\beta})\xi)^{-1/\xi}} \tag{3.41}$$

$$f(x;\theta,\beta,\xi) = \frac{1}{\beta}(1+(\frac{x-\theta}{\beta})\xi)^{\frac{-1}{\xi}-1} e^{-(1+(\frac{x-\theta}{\beta})\xi)^{-1/\xi}} \tag{3.42}$$

where ξ, β and θ are defined respectively as:

$$\xi = -0.06393\mathcal{S}^2_{X_{SCN}} + 0.3173\mathcal{S}_{X_{SCN}} - 0.2771 \tag{3.43}$$

$$\beta = \sqrt{\frac{\sigma^2_{X_{SCN}}\xi^2}{g_2 - g_1^2}} \tag{3.44}$$

$$\theta = \mu_{X_{SCN}} - \frac{(g_1-1)\beta}{\xi} \tag{3.45}$$

where $g_i = \Gamma(1-i\xi)$; the mean, the variance and the skewness are, respectively, given by (3.38), (3.39) and (3.40) with $M(p)$ is the p-th moment of the SCN given, respectively for each case, by Theorems 3.4, 3.5 and 3.6.

Proof. The result comes after using Lemma C.1 in Appendix C. □

3.3.4 Performance Probabilities and Decision Threshold

According to cases 1 and 2 of Proposition 3.1 and using (2.6), (2.7) and (2.8), then P_{fa}, P_d and P_{md} are, respectively, given by:

$$P_{fa} = 1 - e^{-(1+(\frac{\lambda_{SCN}-\theta_0}{\beta_0})\xi_0)^{-1/\xi_0}} \tag{3.46}$$

$$P_{md} = 1 - P_d = e^{-(1+(\frac{\lambda_{SCN}-\theta_1}{\beta_1})\xi_1)^{-1/\xi_1}} \tag{3.47}$$

where ξ_0, β_0 and θ_0 are the shape, scale and location parameters respectively under $\mathcal{H}_0$ hypothesis and are evaluated using (3.43), (3.44) and (3.45) respectively by considering the moments in Theorem 3.4; ξ_1, β_1 and θ_1 are the shape, scale and location parameters respectively under $\mathcal{H}_1$ hypothesis and are evaluated using (3.43), (3.44) and (3.45) respectively by considering the moments in Theorem 3.5.

An alternative approximation could be provided for P_{md} and P_d using both Lemma 3.3 and case 3 of Proposition 3.1 which we refer to by the 2-step approximation. In this approach, we first approximate the SCN of the non-central uncorrelated Wishart matrix by the SCN of central semi-correlated Wishart matrix due to Lemma 3.3 and then we approximate the later using GEV approximation. Then, P_{md} and P_d is still given by (3.47); however, the moments used in calculating θ_1, β_1 and ξ_1 are given by Theorem 3.6.

Accordingly, the threshold could be calculated. For example, for a CFAR, the threshold is given by:

$$\lambda_{SCN} = \theta_0 + \frac{\beta_0}{\xi_0}\Big(-1 + \big[-\ln(1-P_{fa})\big]^{-\xi_0}\Big) \tag{3.48}$$

3.3.5 Comments on the Complexity

In practice, channel conditions are not stable and K and N may frequently change. Consequently, the implementation of the decision threshold must be dynamic and may rely on real-time computations rather than using LUTs.

The real-time computations are satisfied using the proposed threshold in (3.48). However, the complexity still exists in the computation of the GEV parameters due to the complexity of the exact SCN moments. This complexity could be avoided by an offline computations of these parameters.

As a comparison; the exact SCN distribution needs a 1-D LUT for every (K, N) value under $\mathcal{H}_0$ hypothesis whereas only three values are needed in the proposed GEV approximation (i.e. the 3 parameters). Further step is to approximate the SCN central moments using a simple formulation, and thus no need for the offline computation. This approach is provided in the Asymptotic case section.

3.3.6 Numerical Results and Discussion

In this section, the analytical results provided by Sections 3.3.1, 3.3.2, 3.3.3 and 3.3.4 are discussed and validated through Monte-Carlo simulations. The simulation results are obtained by generating 10^5 random realizations of $\boldsymbol{Y}$. To validate the results of central semi-correlated Wishart matrices, we have considered a correlated complex Gaussian noise with zero mean and correlation matrix as defined in Lemma 3.3.

Figure 3.7 validates the analytical form of the distribution of the SCN of the three considered Wishart cases derived in Section 3.3.1. Figures 3.7(a), 3.7(b) and 3.7(c) plot the empirical CDF of the SCN of central uncorrelated, non-central uncorrelated and central semi-correlated complex Wishart matrices respectively with the corresponding analytical form given by Theorems 3.2 and 3.3 and by Corollaries 3.1, 3.2 and 3.3. The simulations are given for different number of antennas ($K = \{2, 3, 4\}$), $N = 10$ and $SNR = -10dB$. Results show a perfect match between the empirical SCN distribution and the corresponding analytical form in each case.

Table 3.3.6 validates the analytical expressions of the p-th moment of the SCN of the central uncorrelated, non-central uncorrelated and central semi-correlated Wishart matrices provided in Theorems 3.4, 3.5 and 3.6 by considering the first moment. The SNR value is set to $-10dB$. Table 3.3.6 shows a perfect accuracy in the analytical representation in each case. Moreover, from the table and Figures 3.7(b) and 3.7(c), results also show a high accuracy in the non-central/central approximation presented in Lemma 3.3.

Figure 3.8 shows the accuracy of the GEV approximation of the SCN of the three considered Wishart cases in Proposition 3.1. Figures 3.8(a), 3.8(b) and 3.8(c) plot the empirical CDF of the SCN and its corresponding GEV approximations for different number of antennas ($K = \{2, 3, 4\}$), $N = 10$ and $SNR = -10dB$. The results show high accuracy in the GEV approximation in all cases for different number of sensors.

The performance of the cognitive radio system is considered in Figures

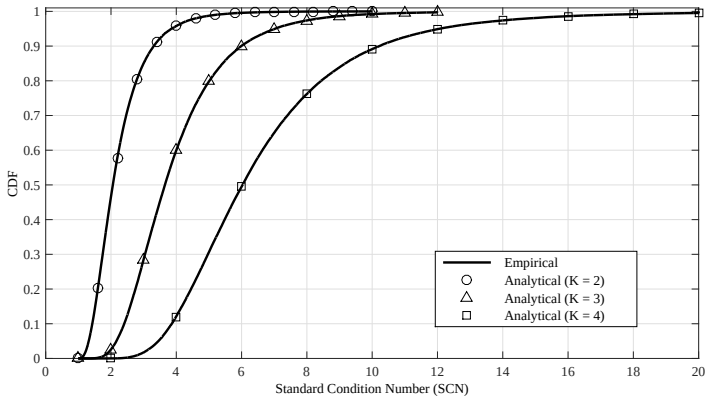

(a) Central Uncorrelated Wishart Case.

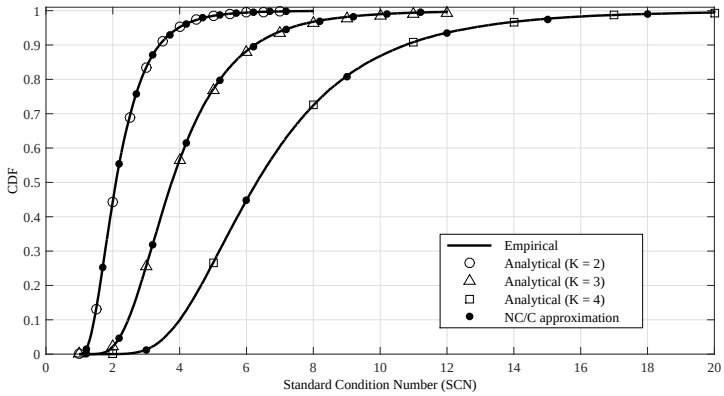

(b) Non-central Uncorrelated Wishart Case.

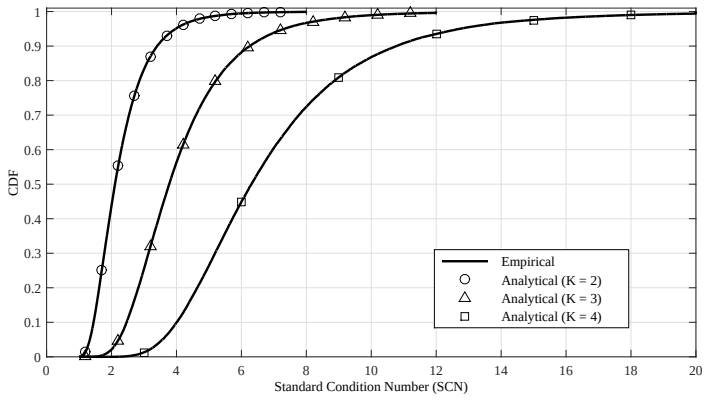

(c) Central Semi-correlated Wishart Case.

Figure 3.7: Empirical and analytical CDF of the SCN of Wishart matrices for different number of sensors $K = \{2, 3, 4\}$, $N = 10$ and $SNR = -10dB$.

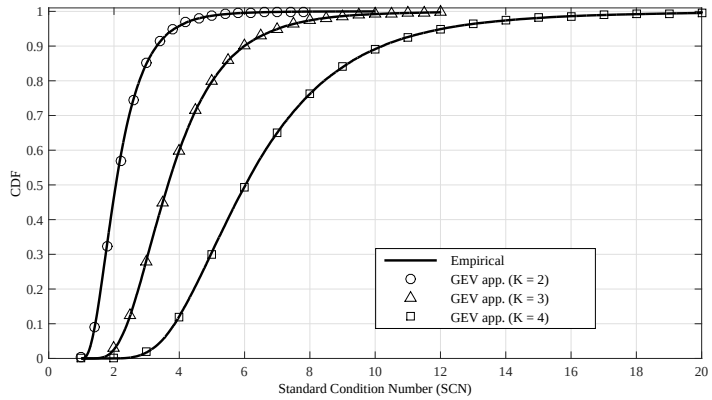

(a) Central Uncorrelated Wishart Case.

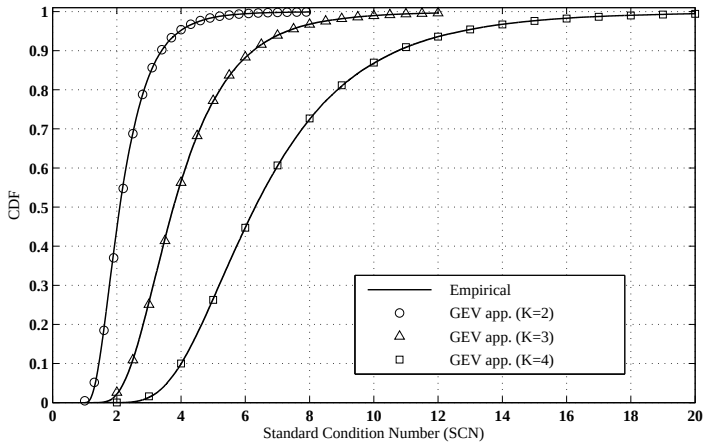

(b) Non-central Uncorrelated Wishart Case.

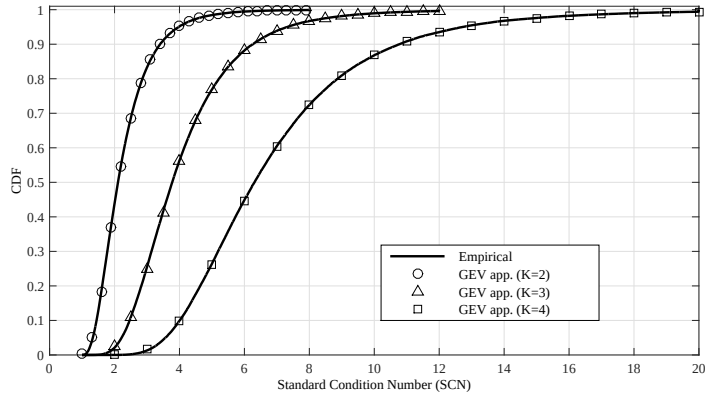

(c) Central Semi-correlated Wishart Case.

Figure 3.8: Empirical CDF of the SCN of Wishart matrices and its corresponding GEV approximation.

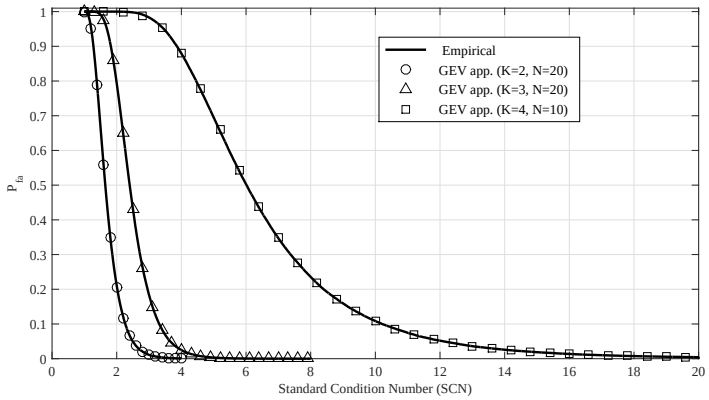

(a) Probability of false-alarm (P_{fa}).

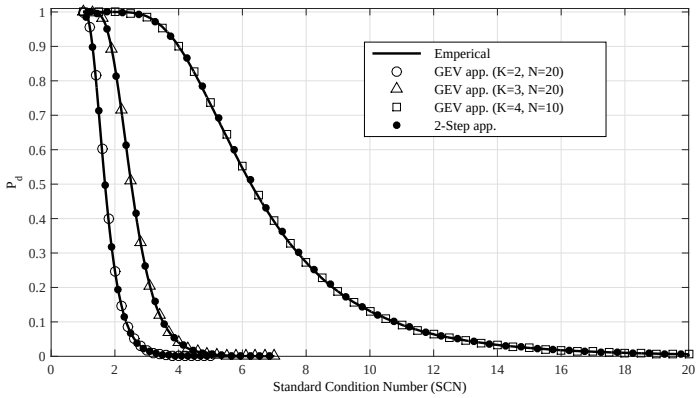

(b) Probability of detection (P_d).

Figure 3.9: Empirical performance probabilities of the SCN detector and its corresponding GEV and 2-step approximations for different K, N and $SNR = -10dB$.

Table 3.1: Empirical and Analytical Mean of the SCN of Wishart matrices.

	N	10		20	
	K	2	3	2	3
Central Uncorr.	Empirical	2.2527	4.002	1.7243	2.5021
	Analytical	2.2560	4.0041	1.7239	2.5020
Non-central Uncorr.	Empirical	2.3025	4.1495	1.7723	2.6267
	Analytical	2.3036	4.1442	1.7743	2.6271
Central Semi-corr.	Empirical	2.3041	4.1489	1.7780	2.6311
	Analytical	2.3060	4.1529	1.7760	2.6308

3.9 and 3.10. Figures 3.9(a) and 3.9(b) show the empirical P_{fa} and P_d of the SCN and its corresponding GEV approximation and the 2-step approximation given by Section 3.3.4. Figure 3.10(a) shows the empirical results of the P_d as a function of SNR and its corresponding GEV approximation and 2-step approximation. Figure 3.10(b) shows the empirical Receiver Operating Characteristics of the SCN detector and its corresponding approximation using GEV for P_{fa} and the GEV or the 2-step approximation for P_d. Results show that the proposed approximations are perfect and match the empirical results with high accuracy. In addition, results show that the 2-step approximation could be used as an alternative for the GEV approximation of P_d since both have approximately same accuracy, especially as N increases, and since the moments of the SCN of central semi-correlated Wishart matrix are simpler than those of non-central uncorrelated Wishart matrix.

3.3.7 Section Conclusion

In this section, we have considered the finite case of the SCN detector. We have derived the exact distribution of the SCN of the central uncorrelated, central semi-correlated and non-central uncorrelated Wishart matrices. In addition, the p-th moment of the SCN is considered as we derived the exact form for the pre-mentioned Wishart matrices. To overcome the computational complexity of the exact SCN distribution, we have proposed to approximate it using the GEV distribution based on moment matching criteria. Accordingly, an approximation for the performance probabilities of the SCN detector and its decision threshold are given through simple ex-

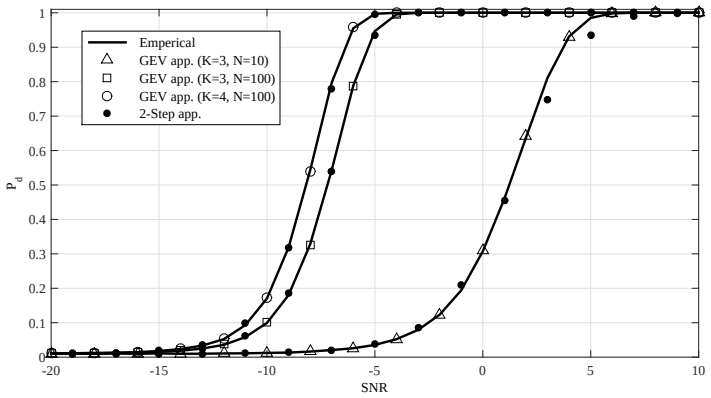

(a) P_d versus SNR.

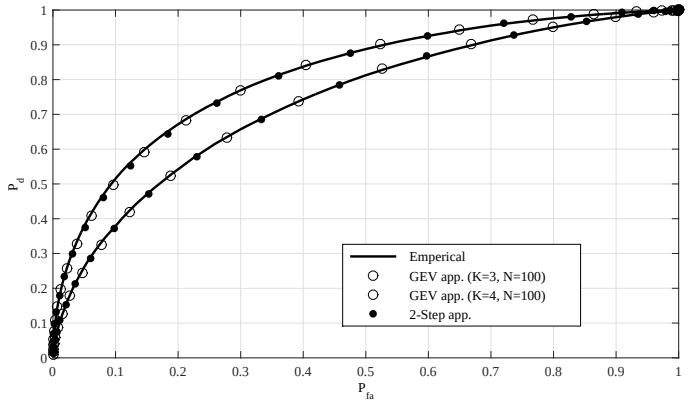

(b) ROC at -10dB.

Figure 3.10: Empirical P_d function of SNR and ROC of the SCN detector and its corresponding GEV and 2-step approximations for different K, N and $SNR = -10dB$.

pressions. Moreover, and using the non-central/central approximation we have proposed a 2-step approximation for the detection probability of the SCN detector which provides analogous accuracy with simpler moment complexity. The analytical results are validated through extensive Monte-Carlo simulations with different system parameters. Results have shown that the proposed GEV approximation perfectly fits the empirical results.

3.4 Asymptotic Case

In literature, the SCN metric was studied asymptotically in [36] and the threshold was presented according to Marchenko-Pastur (MP) law [185]. If the size of the receiver's matrix is $K \times N$, then MP law proves that the largest and the smallest eigenvalues of the receiver's covariance matrix converge to constants as $(K, N) \to \infty$ with $c = {}^{K}/_{N}$ [46]. These constants are simply determined by the constant c and the noise and signal powers. In [38], the authors improved the accuracy of the asymptotic statistical distribution of the SCN by using the Tracy-Widom (TW) distribution to model the largest eigenvalue [186] while maintaining the MP representation of the smallest one. TW distribution is a limiting distribution of the largest eigenvalue of a central Wishart matrix as $(K, N) \to \infty$ [187]. This approximation of the SCN, by TW distribution for the numerator and MP law for the denominator, results in an approximated relation between the decision threshold and the P_{fa}. This work was further extended in [37, 188] by using Curtiss formula for the distribution of the ratio of random variables [189] where both the largest and the smallest eigenvalues converge to Tracy-Widom distributions when $(K, N) \to \infty$ as shown in [186, 190]. Moreover, by the exploitation of the normal and TW distributions and using the Curtiss formula, the authors in [191] provided an analytical expression for the probability of P_{md} for sufficiently large values of K and N. However, all these expressions include TW distribution and Curtiss formula that are hard to evaluate numerically online.

The importance of the GEV approximation provided by the previous section is indeed due to its accuracy and simplicity. However, the exact expressions of the moments are still complicated and need to be computed offline. In this section, we will show that a simple form approximation for these moments could be derived under certain conditions. We will first consider some statistical properties of the extreme eigenvalues of $\boldsymbol{W}$ and analyze

these properties under both detection hypothesis in Sec. 3.4.1.

Since SCN is not affected by the noise power, let $\sigma_\eta^2 = 1$ and we define the Asymptotic Condition (AC) and the Critical Condition (CC) as follows:

$$\textbf{AC}: \qquad (K,N) \to \infty \text{ with } K/N \to c \in (0,1), \tag{3.49}$$

$$\textbf{CC}: \qquad \rho > \rho_c = \frac{1}{\sqrt{KN}}. \tag{3.50}$$

3.4.1 Assymptotic Moments of Extreme Eigenvalues

This section considers the statistical analysis of the extreme eigenvalues, λ_1 and λ_K, of the sample covariance matrix, $\boldsymbol{W}$, by considering both hypotheses $\mathcal{H}_0$ and $\mathcal{H}_1$.

$\mathcal{H}_0$ hypothesis

Let $\lambda_1^{\mathcal{H}_0}$ be the largest eigenvalue of $\boldsymbol{W}$ under $\mathcal{H}_0$ and denote the centered and scaled version of $\lambda_1^{\mathcal{H}_0}$ of the central uncorrelated complex Wishart matrix $\boldsymbol{W} \sim \mathcal{CW}_K(N, \boldsymbol{I}_K)$ by:

$$\lambda_1' = \frac{\lambda_1^{\mathcal{H}_0} - a_1(K,N)}{b_1(K,N)} \tag{3.51}$$

with $a_1(K,N)$ and $b_1(K,N)$, the centering and scaling coefficients respectively, are defined by:

$$a_1(K,N) = (\sqrt{K} + \sqrt{N})^2 \tag{3.52}$$

$$b_1(K,N) = (\sqrt{K} + \sqrt{N})(K^{-1/2} + N^{-1/2})^{\frac{1}{3}} \tag{3.53}$$

then, as AC is satisfied, λ_1' follows a TW distribution of order 2 (TW2) [192].

Now let $\lambda_K^{\mathcal{H}_0}$ be the smallest eigenvalue of $\boldsymbol{W}$ under $\mathcal{H}_0$ and denote the centered and scaled version of $\lambda_K^{\mathcal{H}_0}$ of the central uncorrelated complex Wishart matrix $\boldsymbol{W} \sim \mathcal{CW}_K(N, \boldsymbol{I}_K)$ by:

$$\lambda_K' = \frac{\lambda_K^{\mathcal{H}_0} - a_2(K,N)}{b_2(K,N)} \tag{3.54}$$

with $a_2(K,N)$ and $b_2(K,N)$, the centering and scaling coefficients respectively, are defined by:

$$a_2(K,N) = (\sqrt{K} - \sqrt{N})^2 \tag{3.55}$$

$$b_2(K,N) = (\sqrt{K} - \sqrt{N})(K^{-1/2} - N^{-1/2})^{\frac{1}{3}} \tag{3.56}$$

then, as AC is satisfied, λ'_K follows a TW2 [190].

Accordingly, the mean, the variance and the skewness of λ'_1 and λ'_K are that of the TW2. They are given by $\mu_{TW2} = -1.7710868074$, $\sigma^2_{TW2} = 0.8131947928$ and $\mathcal{S}_{TW2} = 0.2240842036$ respectively [193]. Accordingly, using (5.17), the mean, the variance and the skewness of $\lambda_1^{\mathcal{H}_0}$ are, respectively, given by:

$$\mu_{\lambda_1^{\mathcal{H}_0}} = b_1(K,N)\mu_{TW2} + a_1(K,N), \tag{3.57}$$

$$\sigma^2{}_{\lambda_1^{\mathcal{H}_0}} = b_1^2(K,N)\sigma^2_{TW2}, \tag{3.58}$$

$$\mathcal{S}_{\lambda_1^{\mathcal{H}_0}} = \mathcal{S}_{TW2}, \tag{3.59}$$

and using (3.51), the mean, the variance and the skewness of $\lambda_K^{\mathcal{H}_0}$ are, respectively, given by:

$$\mu_{\lambda_K^{\mathcal{H}_0}} = b_2(K,N)\mu_{TW2} + a_2(K,N), \tag{3.60}$$

$$\sigma^2{}_{\lambda_K^{\mathcal{H}_0}} = b_2^2(K,N)\sigma^2_{TW2}, \tag{3.61}$$

$$\mathcal{S}_{\lambda_K^{\mathcal{H}_0}} = -\mathcal{S}_{TW2}. \tag{3.62}$$

$\mathcal{H}_1$ hypothesis

Let $\lambda_1^{\mathcal{H}_1}$ be the largest eigenvalue of $\boldsymbol{W}$ under $\mathcal{H}_1$ and denote the centered and scaled version of $\lambda_1^{\mathcal{H}_1}$ of the central semi-correlated Wishart matrix $\boldsymbol{W} \sim \mathcal{CW}_K(N, \boldsymbol{\Sigma})$ by:

$$\lambda''_1 = \frac{\lambda_1^{\mathcal{H}_1} - a_3(K,N,\boldsymbol{\sigma})}{\sqrt{b_3(K,N,\boldsymbol{\sigma})}} \tag{3.63}$$

with $a_3(K,N)$ and $b_3(K,N)$, the centering and scaling coefficients respectively, are defined by:

$$a_3(K,N,\boldsymbol{\sigma}) = \sigma_1(N + \frac{K}{\sigma_1 - 1}) \tag{3.64}$$

$$b_3(K,N,\boldsymbol{\sigma}) = \sigma_1^2(N - \frac{K}{(\sigma_1 - 1)^2}) \tag{3.65}$$

then, as AC and CC are satisfied, λ''_1 follows a standard normal distribution ($\lambda''_1 \sim \mathcal{N}(0,1)$) [194].

On the other hand, as mentioned in [195], when $\boldsymbol{\Sigma}$ has only one non-unit eigenvalue such that CC is satisfied, then only one eigenvalue of $\boldsymbol{W}$ will be pulled up. In other words, and as it could be deduced from [196, Proof of Lemma 2], the remaining $K-1$ eigenvalues of $\boldsymbol{W}$ (i.e. $\lambda_2^{\mathcal{H}_1}, \cdots, \lambda_K^{\mathcal{H}_1}$) have the same distribution as the eigenvalues of $\boldsymbol{W} \sim \mathcal{CW}_{K-1}(N, \boldsymbol{I}_{K-1})$ under $\mathcal{H}_0$ hypothesis.

Now let $\lambda_K^{\mathcal{H}_1}$ be the smallest eigenvalue of $\boldsymbol{W}$ under $\mathcal{H}_1$ and denote the centered and scaled version of $\lambda_K^{\mathcal{H}_1}$ of the central semi-correlated Wishart matrix $\boldsymbol{W} \sim \mathcal{CW}_K(N, \boldsymbol{\Sigma})$ by:

$$\lambda_K'' = \frac{\lambda_K^{\mathcal{H}_1} - a_2(K-1, N)}{b_2(K-1, N)} \tag{3.66}$$

with $a_2(K, N)$ and $b_2(K, N)$ are, respectively, given by (3.55) and (3.56). Then, as the AC and CC are satisfied, λ_K'' follows a TW2.

It is worth mentioning that as CC is not satisfied and AC is satisfied, then $\lambda_1^{\mathcal{H}_1}$ follows TW2 distribution of $\lambda_1^{\mathcal{H}_0}$ [194]. Thus, $\lambda_K^{\mathcal{H}_1}$ follows TW2 distribution of $\lambda_K^{\mathcal{H}_0}$. Accordingly, the PU signal has no effect on the eigenvalues and could not be detected. It follows that the same analysis under $\mathcal{H}_0$ hypothesis is applied for this case.

Accordingly, the mean, the variance and the skewness of $\lambda_1^{\mathcal{H}_1}$ are, due to (3.63), given respectively by:

$$\mu_{\lambda_1^{\mathcal{H}_1}} = a_3(K, N, \boldsymbol{\sigma}), \tag{3.67}$$

$$\sigma^2{}_{\lambda_1^{\mathcal{H}_1}} = b_3(K, N, \boldsymbol{\sigma}), \tag{3.68}$$

$$\mathcal{S}_{\lambda_1^{\mathcal{H}_1}} = 0, \tag{3.69}$$

and using (3.66), the mean, the variance and the skewness of $\lambda_K^{\mathcal{H}_1}$ are respectively given by:

$$\mu_{\lambda_K^{\mathcal{H}_1}} = b_2(K-1, N)\mu_{TW2} + a_2(K-1, N), \tag{3.70}$$

$$\sigma^2{}_{\lambda_K^{\mathcal{H}_1}} = b_2^2(K-1, N)\sigma_{TW2}^2, \tag{3.71}$$

$$\mathcal{S}_{\lambda_K^{\mathcal{H}_1}} = -\mathcal{S}_{TW2}. \tag{3.72}$$

As a result, this section provides a simple form for the central moments of the extreme eigenvalues. These moments are used, in the next section, to derive an approximation for the mean, the variance and the skewness of the SCN under both hypotheses.

3.4.2 Asymptotic Central Moments of the SCN

The bi-variate first order Taylor expansion of the function $X = g(\lambda_1, \lambda_K) = \lambda_1/\lambda_K$ about any point $\theta = (\theta_{\lambda_1}, \theta_{\lambda_K})$ is written as:

$$X = g(\theta) + g'_{\lambda_1}(\theta)(\lambda_1 - \theta_{\lambda_1}) + g'_{\lambda_K}(\theta)(\lambda_K - \theta_{\lambda_K}) + O(n^{-1}), \tag{3.73}$$

with g'_{λ_i} is the partial derivative of g over λ_i.

Let $\theta = (\mu_{\lambda_1}, \mu_{\lambda_K})$ with μ_{λ_1} and μ_{λ_K} are the means of λ_1 and λ_K respectively, then it could be proved that:

$$E[X] = g(\theta), \tag{3.74}$$

$$\begin{aligned} E\left[(X - g(\theta))^2\right] &= g'_{\lambda_1}(\theta)^2 E\left[(\lambda_1 - \theta_{\lambda_1})^2\right] \\ &+ g'_{\lambda_K}(\theta)^2 E\left[(\lambda_K - \theta_{\lambda_K})^2\right] \\ &+ 2g'_{\lambda_1}(\theta) g'_{\lambda_K}(\theta) E\left[(\lambda_1 - \theta_{\lambda_1})(\lambda_K - \theta_{\lambda_K})\right], \end{aligned} \tag{3.75}$$

$$\begin{aligned} E\left[(X - g(\theta))^3\right] =& g'_{\lambda_1}(\theta)^3 E\left[(\lambda_1 - \theta_{\lambda_1})^3\right] \\ &+ g'_{\lambda_K}(\theta)^3 E\left[(\lambda_K - \theta_{\lambda_K})^3\right] \\ &+ 3g'_{\lambda_1}(\theta)^2 g'_{\lambda_K}(\theta) E\left[(\lambda_1 - \theta_{\lambda_1})^2 (\lambda_K - \theta_{\lambda_K})\right] \\ &+ 3g'_{\lambda_1}(\theta) g'_{\lambda_K}(\theta)^2 E\left[(\lambda_1 - \theta_{\lambda_1})(\lambda_K - \theta_{\lambda_K})^2\right], \end{aligned} \tag{3.76}$$

Accordingly, we give the following theorems that formulate a simple approximation for the central moments of the SCN.

Theorem 3.7. *Let X be the SCN of $\boldsymbol{W} \sim \mathcal{CW}_K(N, \sigma_\eta^2 \boldsymbol{I}_K)$. The mean, the variance and the skewness of X, as AC is satisfied, can be tightly approximated using the mean, the variance and the skewness of the $\lambda_1^{\mathcal{H}_0}$ and $\lambda_K^{\mathcal{H}_0}$ as follows:*

$$\mu_X = \frac{\mu_{\lambda_1^{\mathcal{H}_0}}}{\mu_{\lambda_K^{\mathcal{H}_0}}} \tag{3.77}$$

$$\sigma_X^2 = \frac{\sigma^2_{\lambda_1^{\mathcal{H}_0}}}{\mu^2_{\lambda_K^{\mathcal{H}_0}}} + \frac{\mu^2_{\lambda_1^{\mathcal{H}_0}} \sigma^2_{\lambda_K^{\mathcal{H}_0}}}{\mu^4_{\lambda_K^{\mathcal{H}_0}}} \tag{3.78}$$

$$\mathcal{S}_X = \frac{1}{\sqrt{\sigma_X^3}} \cdot \left[\frac{\sqrt{\sigma^3_{\lambda_1^{\mathcal{H}_0}}} \mathcal{S}_{\lambda_1^{\mathcal{H}_0}}}{\mu^3_{\lambda_K^{\mathcal{H}_0}}} - \frac{\sqrt{\sigma^3_{\lambda_K^{\mathcal{H}_0}}} \mu^3_{\lambda_1^{\mathcal{H}_0}} \mathcal{S}_{\lambda_K^{\mathcal{H}_0}}}{\mu^6_{\lambda_K^{\mathcal{H}_0}}} \right] \tag{3.79}$$

Proof. The result follows (3.74), (3.75) and (3.76) while considering $\lambda_1^{\mathcal{H}_0}$ and $\lambda_K^{\mathcal{H}_0}$ asymptotically independent [197]. The mean, the variance and the skewness of $\lambda_1^{\mathcal{H}_0}$ and $\lambda_K^{\mathcal{H}_0}$ are given in Section 3.4.1. □

Theorem 3.8. *Let X be the SCN of $\boldsymbol{W} \sim \mathcal{CW}_K(N, \boldsymbol{\Sigma})$ where $\boldsymbol{\Sigma}$ has only one non-unit eigenvalue. The mean, the variance and the skewness of X, as the AC and CC are satisfied, can be tightly approximated using the mean, the variance and the skewness of $\lambda_1^{\mathcal{H}_1}$ and $\lambda_K^{\mathcal{H}_1}$ as follows:*

$$\mu_X = \frac{\mu_{\lambda_1^{\mathcal{H}_1}}}{\mu_{\lambda_K^{\mathcal{H}_1}}} \tag{3.80}$$

$$\sigma_X^2 = \frac{\sigma^2_{\lambda_1^{\mathcal{H}_1}}}{\mu^2_{\lambda_K^{\mathcal{H}_1}}} + \frac{\mu^2_{\lambda_1^{\mathcal{H}_1}} \sigma^2_{\lambda_K^{\mathcal{H}_1}}}{\mu^4_{\lambda_K^{\mathcal{H}_1}}} \tag{3.81}$$

$$\mathcal{S}_X = -\frac{\sqrt{\sigma^3_{\lambda_K^{\mathcal{H}_1}}} \mu^3_{\lambda_1^{\mathcal{H}_1}} \mathcal{S}_{\lambda_K^{\mathcal{H}_1}}}{\sqrt{\sigma_X^3} \cdot \mu^6_{\lambda_K^{\mathcal{H}_1}}} \tag{3.82}$$

Proof. The result follows (3.74), (3.75) and (3.76) while considering $\lambda_1^{\mathcal{H}_1}$ and $\lambda_K^{\mathcal{H}_1}$ asymptotically independent [198]. The mean, the variance and the skewness of $\lambda_1^{\mathcal{H}_1}$ and $\lambda_K^{\mathcal{H}_1}$ are given in Section 3.4.1 □

3.4.3 Approximating the SCN using GEV

Following the footsteps of Sec. 3.3.3, the following two propositions provides an approximate for the distribution of the SCN under $\mathcal{H}_0$ and $\mathcal{H}_1$ hypotheses respectively.

Proposition 3.2. *Let X be the SCN of $\boldsymbol{W} \sim \mathcal{CW}_K(N, \sigma_\eta^2 \boldsymbol{I}_K)$. If AC is satisfied, then the CDF and PDF of X can be asymptotically and tightly approximated respectively by:*

$$F(x; \theta_0, \beta_0, \xi_0) = e^{-(1+(\frac{x-\theta_0}{\beta_0})\xi_0)^{-1/\xi_0}} \tag{3.83}$$

$$f(x; \theta_0, \beta_0, \xi_0) = \frac{1}{\beta_0}(1 + (\frac{x-\theta_0}{\beta_0})\xi_0)^{\frac{-1}{\xi_0}-1} e^{-(1+(\frac{x-\theta_0}{\beta_0})\xi_0)^{-1/\xi_0}} \tag{3.84}$$

where ξ_0, β_0 and θ_0 are defined respectively by:

$$\xi_0 = -0.06393\mathcal{S}_{X_{SCN}}^2 + 0.3173\mathcal{S}_{X_{SCN}} - 0.2771 \tag{3.85}$$

$$\beta_0 = \sqrt{\frac{\sigma_{X_{SCN}}^2 \xi^2}{g_2 - g_1^2}} \tag{3.86}$$

$$\theta_0 = \mu_{X_{SCN}} - \frac{(g_1 - 1)\beta}{\xi} \tag{3.87}$$

where $\mu_{X_{SCN}}$, $\sigma_{X_{SCN}}^2$ and $\mathcal{S}_{X_{SCN}}$ are defined in Theorem 3.7 and $g_i = \Gamma(1 - i\xi)$.

Proof. The result comes after using Lemma C.1 in Appendix C. □

Proposition 3.3. *Let X_{SCN} be the SCN of $\boldsymbol{W} \sim \mathcal{CW}_K(N, \boldsymbol{\Sigma})$ with $\boldsymbol{\Sigma}$ has only one non-unit eigenvalue. If AC and CC are satisfied, then the CDF and PDF of X_{SCN} can be asymptotically and tightly approximated by:*

$$F(x; \theta_1, \beta_1, \xi_1) = e^{-(1+(\frac{x-\theta_1}{\beta_1})\xi_1)^{-1/\xi_1}} \tag{3.88}$$

$$f(x; \theta_1, \beta_1, \xi_1) = \frac{1}{\beta_1}(1 + (\frac{x - \theta_1}{\beta_1})\xi_1)^{\frac{-1}{\xi_1}-1} e^{-(1+(\frac{x-\theta_1}{\beta_1})\xi_1)^{-1/\xi_1}} \tag{3.89}$$

where ξ_1, β_1 and θ_1 are defined respectively by:

$$\xi_1 = -0.06393\mathcal{S}_{X_{SCN}}^2 + 0.3173\mathcal{S}_{X_{SCN}} - 0.2771 \tag{3.90}$$

$$\beta_1 = \sqrt{\frac{\sigma_{X_{SCN}}^2 \xi^2}{g_2 - g_1^2}} \tag{3.91}$$

$$\theta_1 = \mu_{X_{SCN}} - \frac{(g_1 - 1)\beta}{\xi} \tag{3.92}$$

where $\mu_{X_{SCN}}$, $\sigma_{X_{SCN}}^2$ and $\mathcal{S}_{X_{SCN}}$ are defined in Theorem 3.8 and $g_i = \Gamma(1 - i\xi)$.

Proof. The result comes after using Lemma C.1 in Appendix C. □

3.4.4 Performance Probabilities and Decission Threshold

Based on Propositions 3.2 and 3.3, and using (2.6), (2.7) and (2.8), the P_{fa} and P_d are respectively expressed as:

$$P_{fa} = 1 - e^{-(1+(\frac{\lambda_{SCN}-\theta_0}{\beta_0})\xi_0)^{-1/\xi_0}}, \tag{3.93}$$

$$P_{md} = 1 - P_d = e^{-(1+(\frac{\lambda_{SCN}-\theta_1}{\beta_1})\xi_1)^{-1/\xi_1}}. \tag{3.94}$$

The threshold could be computed using (3.93) and (3.94) according to a required error constraint. For example, for a target false alarm probability, the threshold is given by:

$$\hat{\lambda}_{SCN} = \theta_0 + \frac{\beta_0}{\xi_0}\Big(-1 + \big[-\ln(1-P_{fa})\big]^{-\xi_0}\Big). \tag{3.95}$$

3.4.5 Numerical Results and Discussion

In this section, we verify the analytical derivation results through Monte-Carlo simulations. We validate the theoretical analysis presented in sections 3.4.1, 3.4.2, 3.4.3 and 3.4.4.

Table 3.2 shows the accuracy of the analytical approximation of the mean, the variance and the skewness of the SCN provided by Theorems 3.7 and 3.8. It can be easily seen that these Theorems provide a good approximation for the statistics of the SCN, however, it could be noticed that the skewness is not perfectly approximated. In fact, the skewness is affected by the slow convergence of the skewness of λ_K that must converge to $-\mathcal{S}_{TW2}$ (i.e. -0.2241) as AC is satisfied. For example, for $K = 50$, the empirical skewness increases from $\mathcal{S}_{\lambda_K} = -0.1504$ to $\mathcal{S}_{\lambda_K} = -0.1819$ as the number of samples increases from $N = 500$ to $N = 1000$. Comparing these results with SCN results in Table 3.2, one can notice that the empirical and approximated SCN skewness become closer as λ_K skewness converges to that of TW2. Accordingly, Theorems 3.7 and 3.8 are good approximations for the mean, the variance and the skewness of the SCN under both hypotheses. It is worth noting that one could approximate the SCN moments using second order bi-variate Taylor series to get a slightly higher accuracy, however, this will cost higher complexity and it is not necessary as shown in Table 3.2 and the rest of this section.

Table 3.2: Empirical mean, variance and skewness of the SCN under $\mathcal{H}_0$ and $\mathcal{H}_1$ hypotheses and it corresponding proposed analytical approximation using Theorems 3.7 and 3.8 respectively.

	$K \times N$	Empirical			Proposed App.		
		mean	variance	skewness	mean	variance	skewness
$\mathcal{H}_0$	50×500	3.3946	0.0117	0.2639	3.3975	0.0114	0.1652
$\mathcal{H}_1$		12.3363	0.4006	0.1710	12.3139	0.3906	0.0291
$\mathcal{H}_0$	100×500	6.3076	0.0386	0.2992	6.3126	0.0367	0.1740
$\mathcal{H}_1$		34.6345	3.2246	0.1618	34.5387	3.1154	0.0306
$\mathcal{H}_0$	50×1000	2.3386	0.0026	0.2339	2.3396	0.0026	0.1619
$\mathcal{H}_1$		9.6702	0.1205	0.1177	9.6612	0.1184	0.024

Figure 3.11 shows the empirical CDF of the SCN and its corresponding GEV approximation given by Proposition 3.2. The results are shown for $K = \{10, 20, 50, 100\}$ antennas and $N = \{500, 1000\}$ samples per antenna. Results show a perfect match between the empirical results and our proposed approximation. Also, it could be noticed that the convergence of the skewness does not affect the approximation and thus the skewness in Theorem 3.7 holds for this approximation even though the convergence of the skewness of λ_K is slow.

Figure 3.12 shows the empirical CDF of the SCN and its corresponding GEV approximation given by Proposition 3.3. The results are shown for $K = \{20, 50\}$ antennas and $N = \{500, 1000\}$ samples per antenna and $\rho = -10dB$. Results show high accuracy in approximating the empirical CDF. Also, the difference in the skewness shown in Table 3.2 does not affect the approximation.

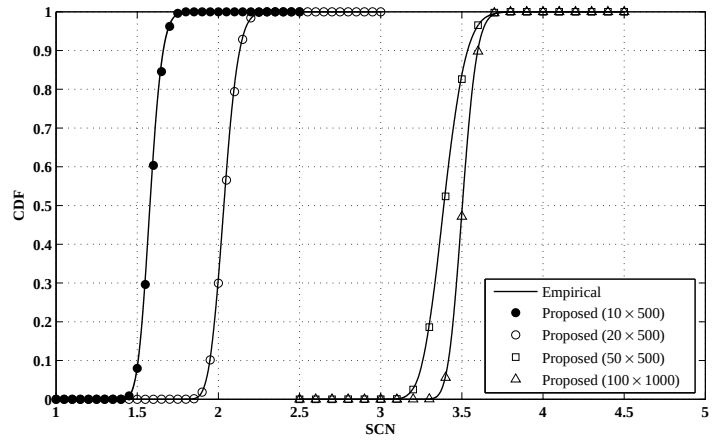

Figure 3.11: Empirical CDF of the SCN and its corresponding proposed GEV approximation for different values of K and N under $\mathcal{H}_0$ hypothesis.

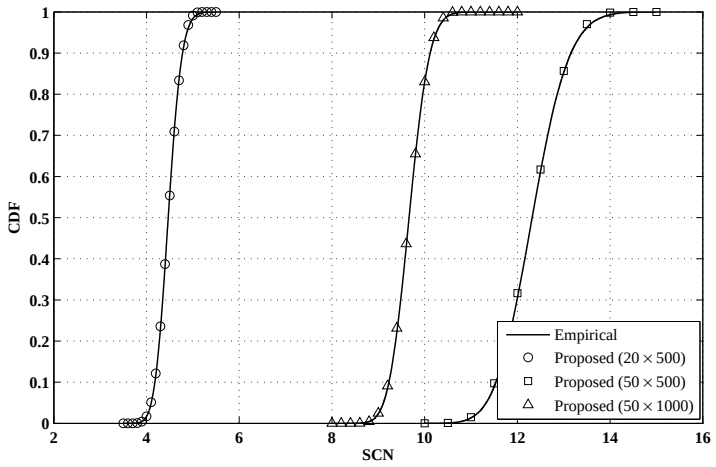

Figure 3.12: Empirical CDF of the SCN and its corresponding proposed GEV approximation for different values of K and N under $\mathcal{H}_1$ hypothesis with $\rho = -10dB$.

Figure 3.13 shows the empirical Receiver Operating Characteristic (ROC) of the SCN detector and its corresponding proposed approximation. The results are shown for $K = \{20, 25, 50\}$ antennas and $N = 500$ samples per antenna for $SNR = -18dB$. Results show that the proposed approximation

matches the empirical results with high accuracy. In addition, Fig. 3.13 shows the gain in the performance as the number of antenna increases.

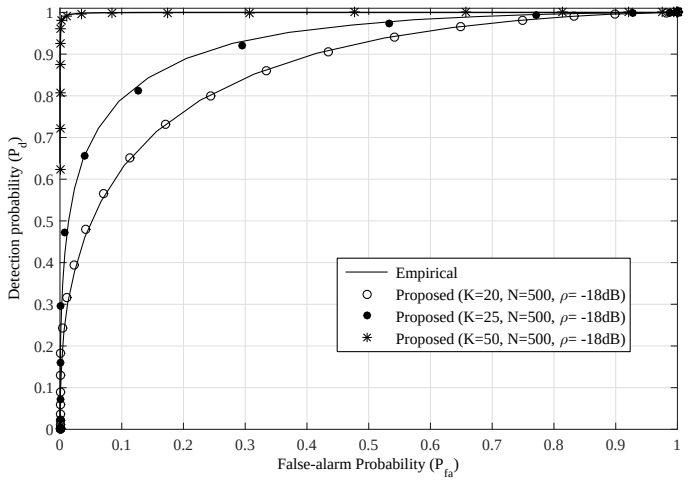

Figure 3.13: Empirical ROC of the SCN detector and its corresponding proposed approximation for different values of K with $N = 500$ and $\rho = -18dB$.

Figure 3.14 plots the empirical P_d versus SNR (ρ) and its corresponding proposed analytical approximation. P_{fa} is fixed to 0.001 and the threshold is calculated using (3.95) for different values of $K = \{20, 25, 30\}$ and $N = \{300, 400, 500\}$. Results show the accuracy of the approximation as a function of the SNR for different K and N values. Figure 3.14(a) shows how the P_d is improved as N increases while Figure 3.14(b) shows the P_d improvement as K increases. Both Figures show a high P_d when using large number of antennas and relatively large number of samples.

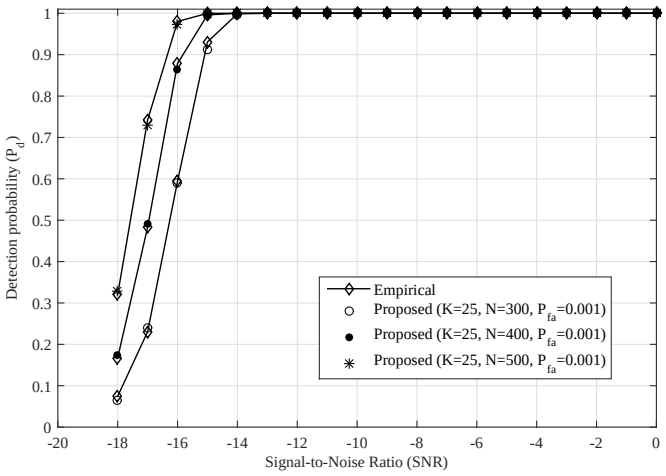

(a) P_d versus ρ for $K = 25$ and N varies

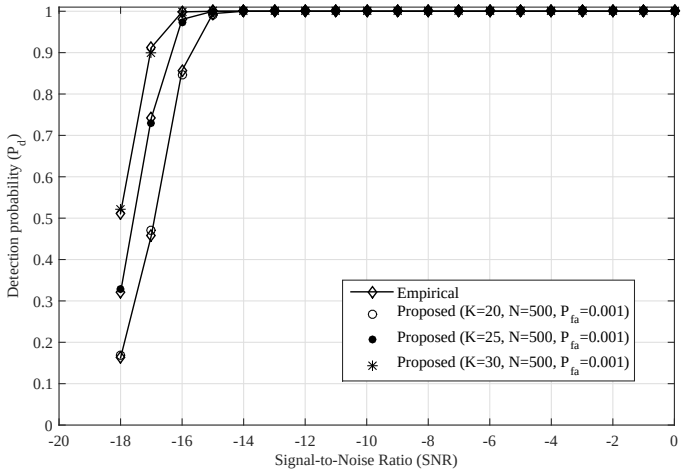

(b) P_d versus ρ for $N = 500$ and K varies

Figure 3.14: Empirical P_d of the SCN detector as a function of SNR and its corresponding proposed approximation for different values of N and K with $P_{fa} = 0.001$.

It is worth mentioning that Figures 3.13 and 3.14 show high improvement in the system performance by a simple increase of the number of antennas or number of samples used in the sensing process. Accordingly, it is very important to have a simple form for the performance probabilities and thus for the decision threshold so a CR system with large number of antennas can

dynamically adapt its threshold according to pre-defined error constraints and channel conditions.

3.4.6 Section Conclusion

In this section, we have considered the asymptotic case of the SCN detector. We have derived the asymptotic mean, the asymptotic variance and the asymptotic skewness of the SCN using those of the extreme eigenvalues of the sample covariance matrix by means of bi-variate Taylor expansion. GEV approximation for the distribution of the SCN under $\mathcal{H}_0$ and $\mathcal{H}_1$ hypotheses were proposed. Consequently, simple forms for the false-alarm probability, detection probability and the decision threshold are derived for real-time computations such that a CR system with large number of antennas can dynamically adapt its threshold according to pre-defined error constraints and channel conditions. In addition to their simple forms, simulation results show high accuracy of the proposed approximation for different number of antennas and different number of samples on various SNR values.

3.5 Performance Comparison between SCN detector and ED

This section provides an empirical performance comparison between the SCN discussed through this chapter and the ED discussed in Sec. 2.4.2. This is illustrated in Figures 3.15 and 3.16. In this case, we set $K = 3$, $N = 500$ and $P_{fa} = 0.1$ with $0.1dB$ noise uncertainty. Fig. 3.15 shows the P_d as a function of SNR while Fig. 3.16 shows the ROC of both detectors. Results show that the SCN detector outperforms the ED as noise uncertainty is considered.

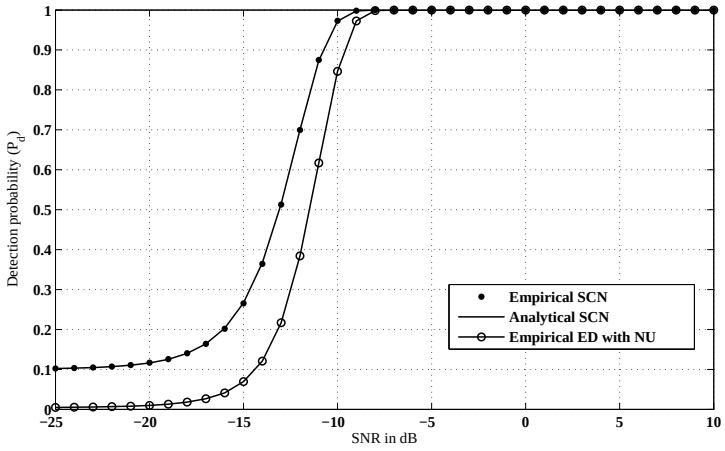

Figure 3.15: P_d of the SCN detector and the ED with $0.1dB$ noise uncertainty as a function of SNR for $K = 3$, $N = 500$, and $P_{fa} = 0.1$.

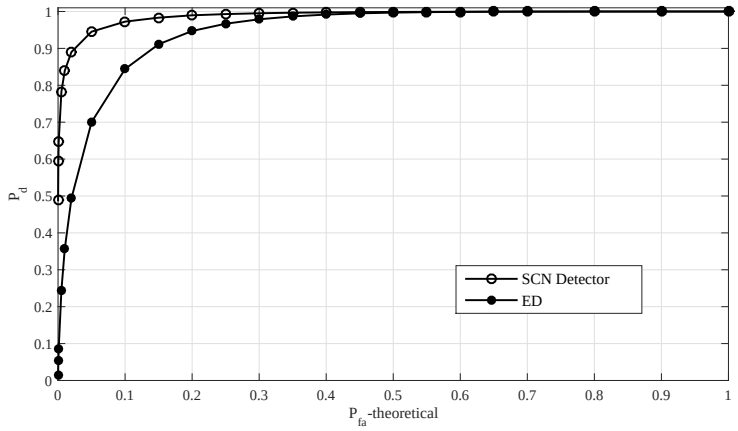

Figure 3.16: ROC of the SCN Detector vs. ROC of the ED for $K = 3$, $N = 500$, $SNR = -10dB$ and $0.1dB$ noise uncertainty.

3.6 Chapter Conclusion

This chapter discusses the SCN statistics, performance and threshold. We have first considered the joint distribution of the ordered eigenvalue of different Wishart matrices and derived the expression of the joint PDF of the ordered eigenvalues of the central semi-correlated complex Wishart matrices

when the correlation matrix exhibit equal eigenvalues. The non-central/central approximation is empirically studied and results show that it has perfect accuracy in low SNR regions and could be considered as a good fit for P_d for sufficiently large values of N when the SNR is high. Moreover, in the finite case, We have derived the exact distribution of the SCN of the central uncorrelated, central semi-correlated and non-central uncorrelated Wishart matrices. In addition, the p-th moment of the SCN is considered as we derived the exact form for the pre-mentioned Wishart matrices. To overcome the computational complexity of the exact SCN distribution, we have proposed to approximate it using the GEV distribution based on moment matching criteria. Accordingly, an approximation for the performance probabilities of the SCN detector and its decision threshold are given through simple expressions. Moreover, and using the non-central/central approximation we have proposed a 2-step approximation for the detection probability of the SCN detector which provides analogous accuracy with simpler moment complexity. Finally, in the asymptotic case, We have derived the asymptotic mean, the asymptotic variance and the asymptotic skewness of the SCN using those of the extreme eigenvalues of the sample covariance matrix by means of bi-variate Taylor expansion. GEV approximation for the distribution of the SCN under $\mathcal{H}_0$ and $\mathcal{H}_1$ hypotheses were proposed. Consequently, simple forms for the false-alarm probability, detection probability and the decision threshold are derived for real-time computations such that a CR system with large number of antennas can dynamically adapt its threshold according to pre-defined error constraints and channel conditions. The analytical results are validated through extensive Monte-Carlo simulations with different system parameters. Results show high accuracy of the proposed approximation for different number of antennas and different number of samples on various SNR values.

Chapter 4

Scaled largest Eigenvalue Detector: A Simple Formulation Approach

This chapter considers the performance probabilities and the decision threshold of the SLE detector. Consequently, it discusses the statistical distribution of the SLE decision metric of the SLE detector. First, the distribution of the largest eigenvalue and the trace of the Wishart matrix are considered and our contributions are presented in Sec. 4.2. Subsequently, the distribution of the SLE decision metric is derived in Sec. 4.3. The performance probabilities and the decision threshold are also considered. The correlation between the largest eigenvalue and the trace is then considered in Sec. 4.4. Finally, all our contributions are validated in Sec. 4.5 using numerical simulations.

4.1 Scaled Largest Eigenvalue

In the literature, several eigenvalue ratios have been considered as discussed in Sec. 2.5. The SCN ratio has been extensively studied and has many applications mainly in the context of MIMO systems and SS as mentioned in Ch. 3. On the other hand, Scaled Largest Eigenvalue detector (SLE) is another eigenvalue ratio measure that recently received an important attention. SLE detector is an efficient technique that is proved to be the optimal detector under the Generalized Likelihood Ratio (GLR) criterion and noise

uncertainty environments [40, 41]. Indeed, it is a practical scenario since in practical systems the noise power may not be perfectly known. Moreover, since Spectrum Sensing (SS) is the task of obtaining awareness about the spectrum usage, as presented in Chapter 2, then it mainly concerns two scenarios of detection: (i) detecting the absence of the Primary User (PU) in a licensed spectrum in order for the Secondary User (SU) to use it and (ii) detecting the presence of the PU so the SU avoid the channel, stop transmission or switch to another channel to avoid any interference to the Primary Receiver (PR). Hence, SS plays a major role in the performance of the CR as well as in the performance of the PU network. In this context, an extreme importance for a CR network is to have an optimal SS technique with high accuracy in uncertain environments.

Recall the SLE decision metric from (2.26):

$$X_{SLE} = \frac{\lambda_1}{\frac{1}{K}\sum_{i=1}^{K}\lambda_i} \tag{4.1}$$

Before it was introduced to CR [199], the SLE previously appeared in signal processing [200] and statistics literature [201, 202]. SLE detector is a totally-blind detector, which is not effected by noise power uncertainty and which stands out as the optimal single-PU detector as mentioned. For a given decision threshold, $\hat{\lambda}_{SLE}$, the SLE detector algorithm could be done by using one of Algorithms 4.1 and 4.2 given below.

Algorithm 4.1: SLE Detector using EVD

Input: $\boldsymbol{Y}$, $\hat{\lambda}_{SLE}$
Output: D_{SLE}
1 compute $\boldsymbol{W} = \boldsymbol{Y}\boldsymbol{Y}^{\dagger}$;
2 get $\lambda_{1\leq i\leq K}$ of $\boldsymbol{W}$ in descending order;
3 evaluate $X_{SLE} = \frac{\lambda_1}{\frac{1}{K}\sum\lambda_i}$;
4 decide $D_{SLE} = X_{SLE} \underset{\mathcal{H}_0}{\overset{\mathcal{H}_1}{\gtrless}} \hat{\lambda}_{SLE}$;

The results on the statistics of the SLE, in the literature, are relatively limited. They are based on tools from Random Matrix Theory (RMT) [40, 203, 204] and Mellin transform [204–206]. SLE was considered, asymptotically, to follow the LE distribution (i.e. TW distribution) [40]. However,

Algorithm 4.2: SLE Detector using Power method

Input: $\boldsymbol{Y}$, $\hat{\lambda}_{SLE}$
Output: D_{SLE}
compute $\boldsymbol{W} = \boldsymbol{Y}\boldsymbol{Y}^{\dagger}$;
compute $tr(\boldsymbol{W})$;
get λ_1 of $\boldsymbol{W}$ using Power method;
evaluate $X_{SLE} = \frac{\lambda_1}{\frac{1}{K}tr(\boldsymbol{W})}$;
decide $D_{SLE} = X_{SLE} \underset{\mathcal{H}_0}{\overset{\mathcal{H}_1}{\gtrless}} \hat{\lambda}_{SLE}$;

a non-negligible error still exists and a new form was derived based on the TW distribution and its second derivative [203]. Using Mellin transform, The distribution of the SLE was derived by the exploitation of the distribution of LE and the distribution of the trace [204–206]. However, all the findings on SLE are too complex to be considered in real-environments and hence are not easily scalable. This is due to either a complexity in the original distributions used to model the SLE (e.g. the TW distribution) or in the methods used to derive the thresholds. Hence, there is a necessity to propose novel yet simple forms in both SS cases (presence and absence of PU activity).

In this chapter, we tackle this problem by considering simple solution deduced from the properties of the LE and trace of the Wishart matrices. In this regard, we start by considering the LE of the Wishart matrices under $\mathcal{H}_0$ and $\mathcal{H}_1$ hypothesis. After that the distribution of the trace is considered to end up with a new form distribution of the SLE decision metric.

4.2 LE and Trace Distributions

This section considers the distributions of the LE and of the trace under $\mathcal{H}_0$ and $\mathcal{H}_1$ hypothesis. We prove that the LE and the trace follow Gaussian distributions for which the means and variances are formulated. Since the SLE does not depend on the noise power, we suppose, in this section, that $\sigma_\eta^2 = 1$. Based on the results of this section, we derive the distribution of the SLE in the next section.

4.2.1 Largest Eigenvalue Distribution

It has been shown that, for a fixed K and as $N \to \infty$, $\lambda_1^{\mathcal{H}_0}$ follows a normal distribution under $\mathcal{H}_0$ hypothesis [150, 207]. The mean and the variance of $\lambda_1^{\mathcal{H}_0}$ could be approximated using TW2 and they are, respectively, given by :

$$\mu_{\lambda_1^{\mathcal{H}_0}} = b_1(K,N)\mu_{TW2} + a_1(K,N), \tag{4.2}$$

$$\sigma^2{}_{\lambda_1^{\mathcal{H}_0}} = b_1^2(K,N)\sigma_{TW2}^2, \tag{4.3}$$

where $\mu_{TW2} = -1.7710868074$ and $\sigma_{TW2}^2 = 0.8131947928$ are, respectively, the mean and variance of TW2 distribution; $a_1(K,N)$ and $b_1(K,N)$ are respectively given by (3.52) and (3.53) as follows:

$$a_1(K,N) = (\sqrt{K} + \sqrt{N})^2, \tag{4.4}$$

$$b_1(K,N) = (\sqrt{K} + \sqrt{N})(K^{-1/2} + N^{-1/2})^{\frac{1}{3}}. \tag{4.5}$$

This approximation is very efficient and it achieves high accuracy for K as small as 2 [150].

On the other hand, Recall that the Asymptotic Condition (AC) and the Critical Condition (CC) are defined as follows:

$$\textbf{AC}: \qquad (K,N) \to \infty \text{ with } K/N \to c \in (0,1), \tag{4.6}$$

$$\textbf{CC}: \qquad \rho > \rho_c = \frac{1}{\sqrt{KN}}, \tag{4.7}$$

then as mentioned in Sec. 3.4.1, as AC and CC are satisfied, $\lambda_1^{\mathcal{H}_1}$ follows a normal distribution under $\mathcal{H}_1$ hypothesis [194]. The mean and the variance of $\lambda_1^{\mathcal{H}_1}$ are due to (3.64) and (3.65) given respectively by:

$$\mu_{\lambda_1^{\mathcal{H}_1}} = \sigma_1(N + \frac{K}{\sigma_1 - 1}), \tag{4.8}$$

$$\sigma^2{}_{\lambda_1^{\mathcal{H}_1}} = \sigma_1^2(N - \frac{K}{(\sigma_1 - 1)^2}). \tag{4.9}$$

4.2.2 Distribution of the Trace

As shown earlier, the distributions of $\lambda_1^{\mathcal{H}_0}$ and $\lambda_1^{\mathcal{H}_1}$ converge to Gaussian distribution. On the other hand, let $T = \sum \lambda_i$ be the trace of the Wishart matrix $\boldsymbol{W}$ then the following theorem holds:

Theorem 4.1. *Let T be the trace of central semi-correlated complex Wishart matrix $\boldsymbol{W} \sim \mathcal{CW}_K(N, \boldsymbol{\Sigma})$ where the vector of eigenvalues of $\boldsymbol{\Sigma}$, not necessary equal, is given by $[\sigma_1, \sigma_2, \cdots, \sigma_K]$. Then, as $N \to \infty$, T follows a Gaussian distribution as follows:*

$$P(\frac{T - N\sum_{i=1}^{K}\sigma_i}{\sqrt{N\sum_{i=1}^{K}\sigma_i^2}} \leq x) = \frac{1}{\sqrt{2\pi}}\int_{-\infty}^{x} e^{-\frac{u^2}{2}}du, \tag{4.10}$$

Proof. Let $\boldsymbol{D}$ be an orthogonal matrix that diagonalizes $\boldsymbol{\Sigma}$, then we write:

$$\begin{aligned} T &= tr(\boldsymbol{YY}^\dagger) = tr(\boldsymbol{DD}^T\boldsymbol{YY}^\dagger) = tr(\boldsymbol{D}^T\boldsymbol{YY}^\dagger\boldsymbol{D}) \\ &= tr(\boldsymbol{ZZ}^\dagger) = \sum_{i=1}^{K}\left[\sum_{j=1}^{N}|z_{i,j}|^2\right] \end{aligned} \tag{4.11}$$

with $z_{i,j}$ is the (i,j)-th element of matrix $\boldsymbol{Z} = \boldsymbol{D}^T\boldsymbol{Y}$. Let $\boldsymbol{Z} = [\boldsymbol{z}_1\ \boldsymbol{z}_2 \cdots \boldsymbol{z}_N]$ with $\boldsymbol{z}_j = [z_{1j}\ z_{2j} \cdots z_{Kj}]^T$. Since the vectors $\boldsymbol{z}_1, \boldsymbol{z}_2, \cdots \boldsymbol{z}_N$ are independent and $\boldsymbol{z}_j \sim \mathcal{CN}_K(\boldsymbol{0}, \boldsymbol{D}^T\boldsymbol{\Sigma}\boldsymbol{D})$ then the elements z_{ij} are independent and form a circularly symmetric complex normal random variable ($z_{i,j} \sim \mathcal{CN}(0, \sigma_i)$). Accordingly, the square of the norm, $|z_{i,j}|^2$, is exponentially distributed with parameter σ_i^{-1} and hence, the mean and variance are σ_i and σ_i^2 respectively.

According to CLT, as $N \to \infty$ the term in the square bracket of (4.11) follows the Gaussian distribution with mean and variance given by $N\sigma_i$ and $N\sigma_i^2$ respectively. □

To the best of our knowledge, the result in Theorem 4.1 is new. The distribution of the trace T of $\boldsymbol{W}$ under $\mathcal{H}_0$ is given by the following Corollary:

Corollary 4.1. *Let T be the trace of central uncorrelated complex Wishart matrix $\boldsymbol{W} \sim \mathcal{CW}_K(N, \sigma_\eta^2\boldsymbol{I}_K)$. Then, as $N \to \infty$, T follows Gaussian distribution as follows:*

$$P(\frac{T - NK\sigma_\eta^2}{\sqrt{NK\sigma_\eta^4}} \leq x) = \frac{1}{\sqrt{2\pi}}\int_{-\infty}^{x} e^{-\frac{u^2}{2}}du, \tag{4.12}$$

Proof. It follows from Theorem 4.1. □

Under $\mathcal{H}_1$ hypothesis, after using the non-central/central approximation in Lemma 3.3, the distribution of the trace T of $\boldsymbol{W}$ is given by the following Corollary:

Corollary 4.2. *Let T be the trace of central semi-correlated Wishart matrix $\boldsymbol{W} \sim \mathcal{CW}_K(N, \boldsymbol{\Sigma})$ where the eigenvalues of $\boldsymbol{\Sigma}$ are given by $\sigma_1 > \sigma_2 = \cdots = \sigma_K$. Then, as $N \to \infty$, T follows Gaussian distribution as follows:*

$$P(\frac{T - N(\sigma_1 + (K-1)\sigma_2)}{\sqrt{N(\sigma_1^2 + (K-1)\sigma_2^2)}} \leq x) = \frac{1}{\sqrt{2\pi}} \int_{-\infty}^{x} e^{-\frac{u^2}{2}} du, \tag{4.13}$$

Proof. All the eigenvalues of $\boldsymbol{\Sigma}$ are equal except σ_1. Then, the result follows from Theorem 4.1. □

4.2.3 Normalized Trace

Let $T_n = \frac{1}{K}T$ be the normalized trace. Then T_n, following Theorem 4.1, is normally distributed.

Denote the normalized trace of $\boldsymbol{W}$ under $\mathcal{H}_0$ hypothesis by $T_n^{\mathcal{H}_0}$, then, following Corollary 4.1, $T_n^{\mathcal{H}_0}$ is normally distributed with mean and variance given respectively, when $\sigma_\eta^2 = 1$, by

$$\mu_{T_n^{\mathcal{H}_0}} = N, \tag{4.14}$$

$$\sigma^2{}_{T_n^{\mathcal{H}_0}} = N/K, \tag{4.15}$$

Denote the normalized trace of $\boldsymbol{W}$ under $\mathcal{H}_1$ hypothesis by $T_n^{\mathcal{H}_1}$, then, following Corollary 4.2, $T_n^{\mathcal{H}_1}$ is normally distributed with mean and variance given respectively, when $\sigma_\eta^2 = 1$, by:

$$\mu_{T_n^{\mathcal{H}_1}} = \frac{N}{K}(\sigma_1 + K - 1), \tag{4.16}$$

$$\sigma^2{}_{T_n^{\mathcal{H}_1}} = \frac{N}{K^2}(\sigma_1^2 + K - 1), \tag{4.17}$$

4.3 Scaled Largest Eigenvalue Detector

This section provides a new formulation for the SLE distribution for $\mathcal{H}_0$ and $\mathcal{H}_1$ hypotheses as follows:

4.3.1 $\mathcal{H}_0$ Hypothesis

Under $\mathcal{H}_0$ hypothesis, both the largest eigenvalue and the normalized trace follow the Gaussian distribution as $N \to \infty$ which is realistic in practical

spectrum sensing scenarios. Herein, we show that the SLE could be formulated using standard Gaussian function as stated by the following theorem:

Theorem 4.2. *Let X_{SLE} be the SLE of central uncorrelated complex Wishart matrix $\boldsymbol{W} \sim \mathcal{CW}_K(N, \sigma_\eta^2 \boldsymbol{I}_K)$. Then, for a fixed K and as $N \to \infty$, the CDF and the PDF of X_{SLE} are, respectively, given by:*

$$F_i(x) = \Phi\left(\frac{x\mu_{T_n^{\mathcal{H}_i}} - \mu_{\lambda_1^{\mathcal{H}_i}}}{\sqrt{\sigma^2{}_{\lambda_1^{\mathcal{H}_i}} - 2xc_i + x^2\sigma^2{}_{T_n^{\mathcal{H}_i}}}}\right) \tag{4.18}$$

$$\begin{aligned} f_i(x) =& \frac{\mu_{T_n^{\mathcal{H}_i}}\sigma^2{}_{\lambda_1^{\mathcal{H}_i}} - c_i\mu_{\lambda_1^{\mathcal{H}_i}} + (\mu_{\lambda_1^{\mathcal{H}_i}}\sigma^2{}_{T_n^{\mathcal{H}_i}} - c_i\mu_{T_n^{\mathcal{H}_i}})x}{(\sigma^2{}_{\lambda_1^{\mathcal{H}_i}} - 2xc_i + x^2\sigma^2{}_{T_n^{\mathcal{H}_i}})^{\frac{3}{2}}} \\ & \times \ \phi\left(\frac{x\mu_{T_n^{\mathcal{H}_i}} - \mu_{\lambda_1^{\mathcal{H}_i}}}{\sqrt{\sigma^2{}_{\lambda_1^{\mathcal{H}_i}} - 2xc_i + x^2\sigma^2{}_{T_n^{\mathcal{H}_i}}}}\right) \end{aligned} \tag{4.19}$$

with

$$\Phi(v) = \int_{-\infty}^{v} \phi(u)du \quad \textbf{\textit{and}} \quad \phi(u) = \frac{1}{\sqrt{2\pi}} e^{-\frac{u^2}{2}} \tag{4.20}$$

where $i = 0$ denoting the $\mathcal{H}_0$ hypothesis; thus, $\mu_{\lambda_1^{\mathcal{H}_0}}$, $\mu_{T_n^{\mathcal{H}_0}}$ and $\sigma^2{}_{\lambda_1^{\mathcal{H}_0}}$, $\sigma^2{}_{T_n^{\mathcal{H}_0}}$ are, respectively, the means and the variances of $\lambda_1^{\mathcal{H}_0}$ and $T_n^{\mathcal{H}_0}$ given by (4.2), (4.14) and (4.3), (4.15) respectively. The parameter c_0 is given by $c_0 = \sigma_{\lambda_1^{\mathcal{H}_0}}\sigma_{T_n^{\mathcal{H}_0}} r_0$ where r_0 is the correlation coefficient between $\lambda_1^{\mathcal{H}_0}$ and $T_n^{\mathcal{H}_0}$.

Proof. Let λ_1 and T_n be two normally distributed random variables with means μ_{λ_1}, μ_{T_n}, and variances $\sigma^2{}_{\lambda_1}$ and $\sigma^2{}_{T_n}$ receptively and let ϱ be their correlation coefficient. Since $\boldsymbol{W}$ is positive definite then $Pr(T_n > 0) = 1$ and the CDF of X could be written as:

$$F_X(x) = Pr(\lambda/t < x) = Pr(\lambda_1 - xt < 0) \tag{4.21}$$

Accordingly, its CDF is given by (4.18) and the PDF is its derivative in (4.19) [208]. □

4.3.2 $\mathcal{H}_1$ Hypothesis

Under $\mathcal{H}_1$ hypothesis, both the largest eigenvalue and the normalized trace follow the Gaussian distribution as AC and CC are satisfied. Accordingly, the distribution of the SLE is given by the following Theorem:

Theorem 4.3. *Let X_{SLE} be the SLE of central semi-correlated complex Wishart matrix $\boldsymbol{W} \sim \mathcal{CW}_K(N, \boldsymbol{\Sigma})$. Then, as AC and CC satisfied, the CDF and PDF of X_{SLE} are, respectively, given by (4.18) and (4.19) where $i = 1$ denoting the $\mathcal{H}_1$ hypothesis; thus, $\mu_{\lambda_1^{\mathcal{H}_1}}$, $\mu_{T_n^{\mathcal{H}_1}}$ and ${\sigma^2}_{\lambda_1^{\mathcal{H}_1}}$, ${\sigma^2}_{T_n^{\mathcal{H}_1}}$ are, respectively, the means and the variances of $\lambda_1^{\mathcal{H}_1}$ and $T_n^{\mathcal{H}_1}$ given by (4.8), (4.16) and (4.9), (4.17) respectively. The parameter c_1 is defined by $c_1 = \sigma_{\lambda_1^{\mathcal{H}_1}} \sigma_{T_n^{\mathcal{H}_1}} r_1$ where r_1 is the correlation coefficient between $\lambda_1^{\mathcal{H}_1}$ and $T_n^{\mathcal{H}_1}$.*

Proof. Same as the proof of Theorem 4.2. □

4.3.3 Performance Probabilities and Threshold

Using (2.6) and (4.18), then P_{fa} is given by:

$$P_{fa}(\lambda_{SLE}) = Q\left(\frac{\lambda_{SLE}\mu_{T_n^{\mathcal{H}_0}} - \mu_{\lambda_1^{\mathcal{H}_0}}}{\sqrt{{\sigma^2}_{\lambda_1^{\mathcal{H}_0}} - 2\lambda_{SLE}c_0 + \lambda_{SLE}{\sigma^2}_{T_n^{\mathcal{H}_0}}}}\right) \tag{4.22}$$

where $Q(.)$ is the Q-function. P_d can be derived the same way using $\mathcal{H}_1$ hypothesis.

Using P_{fa} and P_d, the threshold could be set according to a required error constraint. For example, and based on (4.22), we can derive a simple and accurate form for the threshold as a function of the means and variances of the λ_1 and T_n and the correlation coefficient between them as well as the false alarm probability. That is, for a CFAR, the equation of the threshold of the SLE detector will be:

$$\lambda_{SLE} = \frac{\mu_{12}^{\mathcal{H}_0} - \Delta^2 r_0 \sigma_{12}^{\mathcal{H}_0} + \Delta\sqrt{m_v^{\mathcal{H}_0} - 2r_0\mu_{12}^{\mathcal{H}_0}\sigma_{12}^{\mathcal{H}_0} + \Delta^2[\sigma_{12}^{\mathcal{H}_0}]^2(r_0^2 - 1)}}{\mu^2_{T_n^{\mathcal{H}_0}} - \Delta^2\sigma^2_{T_n^{\mathcal{H}_0}}} \tag{4.23}$$

where $\mu_{12}^{\mathcal{H}_0} = \mu_{\lambda_1^{\mathcal{H}_0}}\mu_{T_n^{\mathcal{H}_0}}$, $\sigma_{12}^{\mathcal{H}_0} = \sigma_{\lambda_1^{\mathcal{H}_0}}\sigma_{T_n^{\mathcal{H}_0}}$, $m_v^{\mathcal{H}_0} = \mu^2_{T_n^{\mathcal{H}_0}}\sigma^2_{\lambda_1^{\mathcal{H}_0}} + \mu^2_{\lambda_1^{\mathcal{H}_0}}\sigma^2_{T_n^{\mathcal{H}_0}}$ and $\Delta = Q^{-1}(P_{fa})$ with $Q^{-1}(.)$ is the inverse Q-function.

4.4 Correlation Coefficients r_i

Theorems 4.2 and 4.3 give the form of the distribution of the SLE as a function of the mean and the variance of $\lambda_1^{\mathcal{H}_i}$ and $T_n^{\mathcal{H}_i}$ as well as the correlation

coefficient between them (r_i). Consequently, P_{fa}, P_d, P_{md} and the threshold are functions of these same parameters.

The mean and the variance of λ_1 and T_n are provided in Sections 4.2.1 and 4.2.3. In this section, we will give a simple analytical form to calculate the correlation coefficient r_i between the largest eigenvalue and the trace of Wishart matrix based on the mean of the SLE. In the following, we calculate the mean of SLE in two different ways such that a simple form for r_i could be derived.

4.4.1 Mean of SLE using λ_1 and T_n

Under both hypotheses ($\mathcal{H}_0$ and $\mathcal{H}_1$), the mean of the SLE could be computed using the means of λ_1 and T_n as follows:

$\mathcal{H}_0$ case: using independent property

Under $\mathcal{H}_0$, the SLE and the trace of central uncorrelated Wishart matrices are proved to be independent [200]. Accordingly, and using (2.26), the mean of $\lambda_1^{\mathcal{H}_0}$ could be written as:

$$E[\lambda_1^{\mathcal{H}_0}] = E\big[X_{SLE}^{\mathcal{H}_0} \times T_n^{\mathcal{H}_0}\big] = E[X_{SLE}^{\mathcal{H}_0}] \cdot E[T_n^{\mathcal{H}_0}] \tag{4.24}$$

Recall that the mean of $\lambda_1^{\mathcal{H}_0}$ and the mean of $T_n^{\mathcal{H}_0}$ are given respectively by (4.2) and (4.14), then based on (4.24), the mean of the SLE is given by:

$$\mu_{X_{SLE}^{\mathcal{H}_0}} = \frac{\mu_{\lambda_1^{\mathcal{H}_0}}}{\mu_{T_n^{\mathcal{H}_0}}} = \frac{b_1(K,N) \cdot \mu_{TW2} + a_1(K,N)}{N} \tag{4.25}$$

$\mathcal{H}_1$ case: using Taylor series

Using Taylor series, discussed in Sec. 3.4.2, then the mean of the SLE under $\mathcal{H}_1$ hypothesis could be approximated by:

$$\mu_{X_{SLE}^{\mathcal{H}_1}} = \frac{\mu_{\lambda_1^{\mathcal{H}_1}}}{\mu_{T_n^{\mathcal{H}_1}}} = \frac{\sigma_1(N + \frac{K}{\sigma_1 - 1})}{\frac{N}{K}(\sigma_1 + K - 1)}, \tag{4.26}$$

It is worth mentioning that it is more accurate to use higher order Taylor series. However, this will increase the complexity for a slightly more accurate values which is not necessary.

4.4.2 Mean of SLE using variable transformation

Using SLE distribution, it is difficult to find numerically the mean of the SLE, however, it turns out that a simple and accurate approximation could be found.

An approximation of the mean of the ratio $(u + Z_1)/(v + Z_2)$ could be found when u and v are positive constants and Z_1 and Z_2 are two independent standard normal random variables. It is based on approximating formula for $E[1/(v + Z_2)]$ when $v + Z_2$ is normal variate conditioned by $Z_2 > -4$ and $v + Z_2$ is not expected to approach zero as follows [208]:

$$E\left[\frac{1}{v + Z_2}\right] = \frac{1}{1.01v - 0.2713} \tag{4.27}$$

By using the transformation of the general ratio of two jointly normal random variable λ_1/T_n into the ratio $(u + Z_1)/(v + Z_2)$, which has the same distribution, we have:

$$\frac{\lambda_1}{T_n} \sim \frac{1}{q}\left(\frac{u + Z_1}{v + Z_2}\right) + s \tag{4.28}$$

with $s = r\frac{\sigma_{\lambda_1}}{\sigma_{T_n}}$, $v = \frac{\mu_{T_n}}{\sigma_{T_n}}$ and

$$u = \frac{\mu_{\lambda_1} - \varrho\frac{\mu_{T_n} \cdot \sigma_{\lambda_1}}{\sigma_{T_n}}}{(\pm\sigma_{\lambda_1}\sqrt{1 - \varrho^2})} \tag{4.29}$$

$$q = \frac{\sigma_{T_n}}{(\pm\sigma_{\lambda_1}\sqrt{1 - \varrho^2})} \tag{4.30}$$

where the $\pm$ sign (in both u and q) are chosen such that u and v have the same sign (i.e. positive). As the left-side and the right-side of (4.28) must have the same mean, we can write:

$$E[\frac{\lambda_1}{T_n}] = \frac{u}{q}E[\frac{1}{v + Z_2}] + s \tag{4.31}$$

therefore the mean of the SLE could be approximated as follows:

$$\mu_{X_{SLE}^{\mathcal{H}_i}} = \frac{\mu_{\lambda_1^{\mathcal{H}_i}} - s_i\ \mu_{T_n^{\mathcal{H}_i}}}{\theta_i} + s_i \tag{4.32}$$

with $\theta_i = 1.01\mu_{T_n^{\mathcal{H}_i}} - 0.2713\sigma_{T_n^{\mathcal{H}_i}}$ and $s_i = r_i\frac{\sigma_{\lambda_1^{\mathcal{H}_i}}}{\sigma_{T_n^{\mathcal{H}_i}}}$.

This practical approximation shows high accuracy; however, it could be noticed from (4.31) that as the factor u increases the error due to this approximation increases.

4.4.3 Deduction of the Correlation coefficients r_i

Based on these results, the correlation coefficient under $\mathcal{H}_0$ and $\mathcal{H}_1$ hypotheses is considered as follows:

$\mathcal{H}_0$ case

Using (4.32), then r_0, after some algebraic manipulation, is given by:

$$r_0 = \frac{\sigma_{T_n^{\mathcal{H}_0}}}{\sigma_{\lambda_1^{\mathcal{H}_0}}} \cdot \frac{\theta_0 \ \mu_{X^{\mathcal{H}_0}} - \mu_{\lambda_1^{\mathcal{H}_0}}}{\theta_0 - \mu_{T_n^{\mathcal{H}_0}}} \tag{4.33}$$

where $\mu_{\lambda_1^{\mathcal{H}_0}}$, $\mu_{T_n^{\mathcal{H}_0}}$ and $\mu_{X^{\mathcal{H}_0}}$ are respectively the means of the $\lambda_1^{\mathcal{H}_0}$, the normalized trace and the SLE given by (4.2), (4.14) and (4.25) respectively. $\sigma_{\lambda_1^{\mathcal{H}_0}}$ and $\sigma_{T_n^{\mathcal{H}_0}}$ are respectively the standard deviations of the $\lambda_1^{\mathcal{H}_0}$ and the normalized trace and are the square root of (4.3) and (4.15) respectively.

$\mathcal{H}_1$ case

Under $\mathcal{H}_1$ hypothesis, results show the u increases as K or N increases because of the high correlation between $\lambda_1^{\mathcal{H}_1}$ and $T_n^{\mathcal{H}_1}$. Accordingly, results show a small error in the value of the mean of SLE with respect to the true value. Consequently, and using (4.32), then r_1 is given by:

$$r_1 = \frac{\sigma_{T_n^{\mathcal{H}_1}}}{\sigma_{\lambda_1^{\mathcal{H}_1}}} \cdot \frac{\theta_1 \ (\mu_X^{\mathcal{H}_1} + \epsilon) - \mu_{\lambda_1^{\mathcal{H}_1}}}{\theta_1 - \mu_{T_n^{\mathcal{H}_1}}} \tag{4.34}$$

where $\mu_{\lambda_1^{\mathcal{H}_1}}$, $\mu_{T_n^{\mathcal{H}_1}}$ and $\mu_{X^{\mathcal{H}_1}}$ are respectively the means of the $\lambda_1^{\mathcal{H}_1}$, the normalized trace and the SLE given by (4.8), (4.16) and (4.26) respectively. $\sigma_{\lambda_1^{\mathcal{H}_1}}$ and $\sigma_{T_n^{\mathcal{H}_1}}$ are respectively the standard deviations of the $\lambda_1^{\mathcal{H}_1}$ and the normalized trace and are the square root of (4.9) and (4.17) respectively. Finally, ϵ is a variable used to model the mean error.

4.5 Numerical Results and Discussion

In this section, we discuss the analytical results through Monte-Carlo simulations. We validate the theoretical analysis presented in sections 4.2, 4.3

Table 4.1: The Empirical and Approximated value of the correlation coefficient r_0 under $\mathcal{H}_0$ hypothesis for different values of $\{K, N\}$.

$K \times N$	2×500	4×500	2×1000	4×1000	50×1000
r_0-Emp.	0.849	0.6974	0.839	0.6915	0.3353
r_0-Ana.	0.8548	0.6957	0.8623	0.6967	0.3356

and 4.4. The simulation results are obtained by generating 10^5 random realizations of $\boldsymbol{Y}$.

Table 4.1 shows the accuracy of the analytical approximation of the correlation coefficient (r_0) of the SLE under the $\mathcal{H}_0$ hypothesis in (4.33). The results are shown for $K = \{2, 4, 50\}$ antennas and $N = \{500, 1000\}$ samples per antenna. Table 4.1 shows that the accuracy of this approximation is higher as the number of antennas increases, however, we can also notice that we have very high accuracy even when $K = 2$ antennas. Also, as expected, it is easy to notice that the correlation between the largest eigenvalue and the trace decreases as the number of antenna increases, however, this correlation could not be ignored even if the number of antennas is large.

For the $\mathcal{H}_1$ hypothesis, Fig. 4.1 shows the accuracy of the mean of the SLE as well as the correlation coefficient between the largest eigenvalue and the trace. The results are shown for different values of K where $N = 500$ and $\rho = -10dB$. Figure 4.1(a) plots the empirical mean and its corresponding Taylor series approximation in (4.26). In addition, the figure shows the mean error (ϵ) between the Taylor approximation and the mean expression provided using variable transformation in (4.32). the results show a high accuracy in the approximation of the mean using Taylor series, however, it also shows a small error, ϵ, that increases as K increases. Another important point here concerns the error value ϵ. Indeed, one can easily observe the ϵ is small however its effect on correlation coefficient r_1 is relatively high as shown in Fig. 4.1(b) , hence corrective action should be taken to yield correct results. The corrected version is considered (i.e. Fig. 4.1(a)) then the results show high accuracy. We should mention that modeling the mean error is out of the scope of this work but it is worth mentioning it for future research.

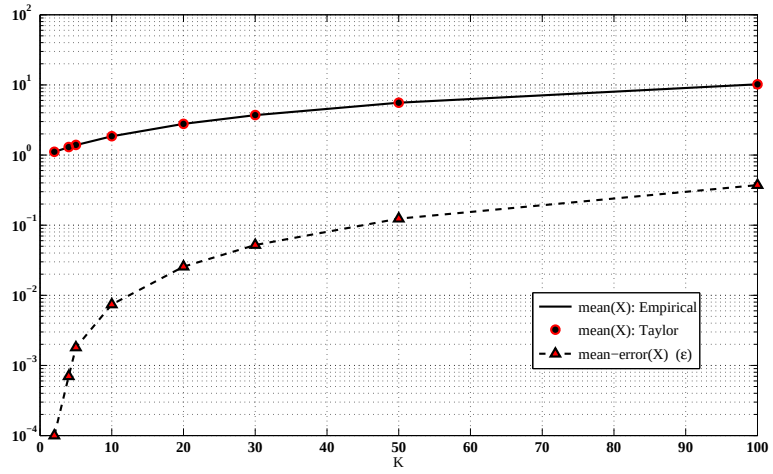

(a) Mean of SLE μ_X with the corresponding error (ϵ)

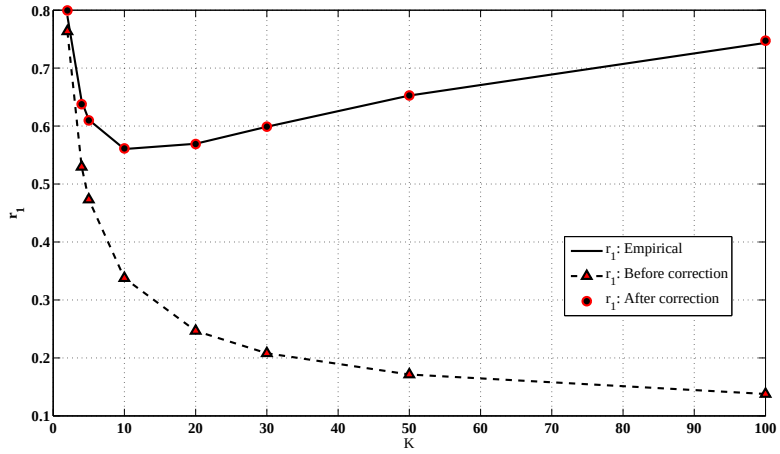

(b) Correlation coefficient r_1 between $\lambda_1^{\mathcal{H}_1}$ and $T_n^{\mathcal{H}_1}$ before and after mean error correction w.r.t. (a)

Figure 4.1: Empirical and analytical results under $\mathcal{H}_1$ hypothesis for different values of K where $N = 500$ sample and $\rho = -10dB$.

Figure 4.2 shows the empirical CDF of the SLE and its corresponding approximation under $\mathcal{H}_0$ hypothesis given by Theorem 4.2. The results are shown for $K = \{2, 4, 10, 20\}$ antennas and $N = 1000$ samples per antenna. Results show a perfect match between the empirical results and our Gaussian formulation.

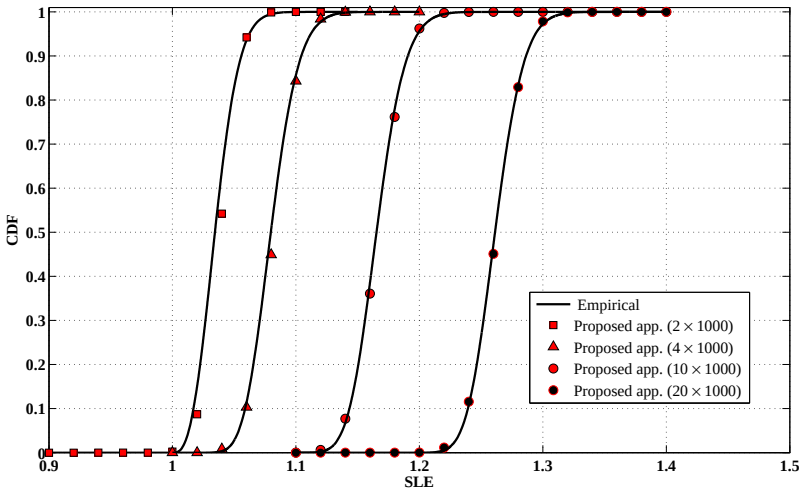

Figure 4.2: Empirical CDF of the SLE under $\mathcal{H}_0$ hypothesis and its corresponding Gaussian approximation for different values of K with $N = 1000$.

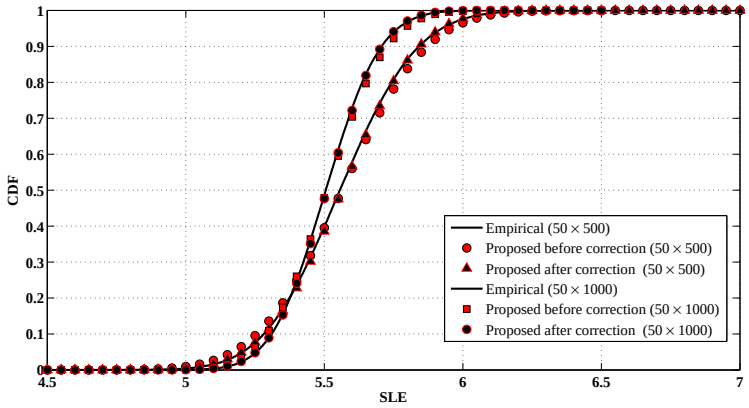

Figure 4.3: Empirical CDF of the SLE under $\mathcal{H}_1$ hypothesis and its corresponding proposed approximation for $K = 50$ with $N = \{500, 100\}$ and $\rho = -10dB$.

Figure 4.3 shows the empirical CDF of the SLE and its corresponding approximation (before and after mean correction) given by Theorem 4.3. The results are shown for $K = 50$ antennas, $N = \{500, 1000\}$ samples per antenna and $\rho = -10dB$. Again, the results show a perfect match between the empirical results and the proposed approximation after the mean correction

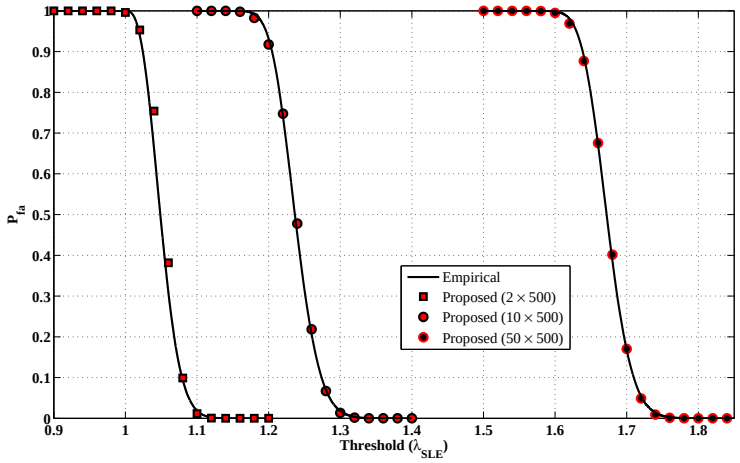

Figure 4.4: Empirical P_{fa} for the SLE detector and its corresponding proposed form in (4.22) for different values of K with $N = 500$ samples.

in (4.34). However if the we consider $\epsilon = 0$, results show a slight difference between empirical and the proposed distributions in comparison with the big error in r_1 (see Fig. 4.1(b) when $K = 50$ and $N = 500$).

Figure 4.4 shows the accuracy of the proposed false alarm form in (4.22). Here, we have considered multi-antenna CR with different number of antennas and $N = 500$ samples. The considered number of antennas is as small as $K = 2$ and as large as $K = 50$. Simulation results show a high accuracy in our proposed form which increases as K increases. It is worth reminding the reader, that in addition to the accuracy, the form given in (4.22) is a simple Q-function equation.

The empirical and analytical P_d is illustrated in Fig. 4.5 for different number of antennas, $N = 500$ samples and $\rho = -10dB$. The analytical P_d is considered before and after mean error correction. Results show perfect match between the empirical results and its corresponding analytical expressions after mean error correction and as K increases. The small difference between the empirical and analytical results when K is very small, such as $K = 2$ in the figure, is due to the AC that must be satisfied for the largest eigenvalue to converge to Gaussian distribution. On the other hand, the effect of the mean error could be noticed as K increases. In this regard, modelling the mean error is very important to achieve high accuracy for large K values.

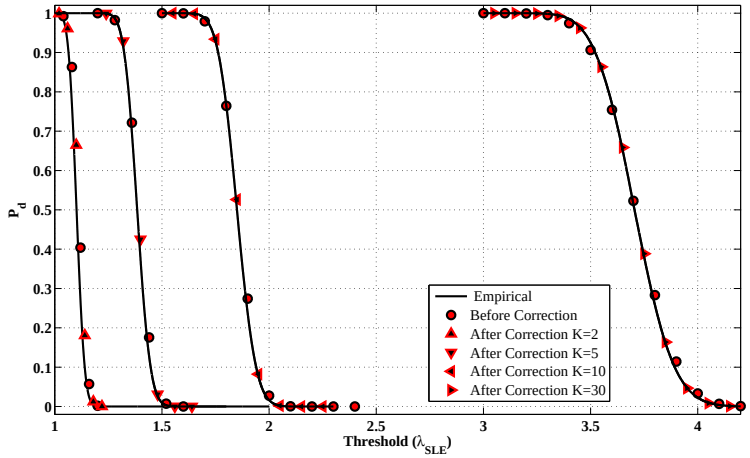

Figure 4.5: Empirical P_d for the SLE detector and its corresponding proposed form for different values of K with $N = 500$ samples and $\rho = -10dB$ before and after mean error correction.

4.6 Conclusion

SLE detector is the optimal single-PU detector in noise uncertain environments. In this chapter, we have considered the SLE detector and its statistical distribution. We proved that the SLE could be modelled using standard Gaussian function and we have derived its CDF and PDF. The false alarm probability, the detection probability and the threshold were also considered as we derived new simple and accurate forms. These forms are simple functions of the means and variances of the largest eigenvalue and of the trace as well as the correlation coefficient between them. The correlation between the largest eigenvalue and the trace is studied and simple expressions are provided. Simulation results have shown that the proposed expressions achieve high accuracy. Further, the approximation of the correlation coefficient under $\mathcal{H}_0$ shows high accuracy while under $\mathcal{H}_1$ hypothesis, small mean error correction must be applied in order to achieve high accuracy. In addition, results have shown that the correlation between the largest eigenvalue and the trace, under $\mathcal{H}_0$, decreases as the number of antenna increases but it could not be ignored even for large number of antennas.

Chapter 5

Multi-Antenna Based Spectrum Sensing: Approaching Massive MIMOs

This chapter considers a cognitive radio (CR) equipped with massive MIMO technology that uses the EBD for SS. Sec. 5.1 introduces the problem and discusses the different scenarios and cases considered in this chapter. The LE detector in the finite case is considered in Sec. 5.2 where we derive exact expressions and approximated ones. The full exploitation of the antennas are discussed in 5.3 and the partial exploitation is discussed in 5.4 for LE, SCN and SLE detectors. Finally, the conclusion is derived in Sec. 5.6.

5.1 Introduction

The fifth generation (5G) of mobile network is expected to be deployed by 2020. As 5G has to accommodate new demands and high data-rates growing at an unprecedented pace, a large amount of radio frequency resources is still under-utilized. For instance, by exploiting the spatial domain, massive MIMO is introduced to increase the network capacity for the next generation wireless systems [209–211]. A massive MIMO system uses up to few hundred of antennas to gain all the benefits of the conventional MIMO but on a much larger scale. As such, CR could be combined with massive MIMO through the additional degree of freedom offered by the large number of antennas

to identify the unused channels while achieving a significant increase in the performance of the SS detector. In this regard, it is very likely to consider the EBD to detect the spectrum holes in CR with massive MIMO technology.

In fact, a CR system with massive MIMO technology could use all antennas for the SS and achieve an enormous performance enhancement. However it might be enough to use a fewer number of antennas for the sensing process and thus define a more efficient way for antenna exploitation. In this regard, two scenarios could be considered:

1. Full antenna exploitation scenario: Therein, the CR module may use all of its antennas in the SS and hence may reduce the number of samples required for SS.

2. Partial antenna exploitation scenario: In this scenario, the CR may fix certain number of antennas to a given SS process and use the others for other purposes (such as transmission) or it may dynamically change the number of antennas K and/or the number of samples N according to predefined performance and also use the rest for other purposes.

In this chapter, the EBD is used due to its importance in multi-antenna SS. Specifically, we will consider the LE detector which is proved to be the optimal if noise power is perfectly known. Accordingly, we suppose that the noise power is perfectly known. Moreover, LE detector could be evaluated without the need of the EVD and thus avoid some computational complexity by using the power method. From here, let us differentiate between the following cases:

Case 1: Finite K and finite N: In this case, the CR module utilizes a small finite number of antennas K and a relatively small finite number of samples N for partial exploitation.

Case 2: Finite K and asymptotic N: Here, the CR module utilizes a finite number of antennas K and a relatively large number of samples N for partial exploitation.

Case 3: Asymptotic K and asymptotic N: In this case, the CR uses a Large number of antennas K and a large number of samples N such that $N > K$ for full antenna exploitation.

It is worth mentioning that in case 1, the performance analysis and the decision threshold selection could not rely on any asymptotic approximations.

Indeed, the use of finite RMT analysis to study the statistics of the LE detector is the best solution. On the other hand, in cases 2 and 3 the use of approximations related to large number of antenna and/or large number of samples are extremely beneficial.

On the other hand, when noise power is not perfectly known then the SCN and SLE detectors discussed in previous chapters could be considered. Accordingly, an extension to the SCN and SLE detectors is done by using the results derived in Chapters 3 and 4. The dynamic antenna exploitation case is considered for the mentioned three detectors (i.e. LE, SCN and SLE detectors) and the minimum requirements needed to achieve a target performance is considered. Accordingly, a comparison between these detectors is provided in terms of sensing performance and minimum requirements.

5.2 LE Detector in Finite Case: Small number of antennas and samples

In this section, we will consider the LE detector in the finite case (i.e. Case 1). The CDF of the LE decision metric is considered since it is directly related to the performance probabilities as provided by (2.6), (2.7) and (2.8). Consequently, we show that the computational complexity of these expressions increases as K or N increases. Moreover, it is difficult to derive a threshold using such expressions. Accordingly and since we are dealing with the extreme eigenvalue, we propose to approximate the distribution of the LE decision metric using the GEV approximation described in Appendix C. Based on this approximation, a simple expression of the decision threshold is provided by which a CR system using small number of antennas and relatively small number of samples for SS can compute the threshold value online.

5.2.1 LE Detector in Finite Case

The Largest eigenvalue detector is a semi-blind detector since it requires the knowledge of noise power, however, if perfect knowledge is available then LE is the optimal detector [42]. LE is the largest eigenvalue of the sample covariance matrix and its exact distribution is derived in literature (see, for instance, [178, 212]) in the form of matrix determinant whose complexity increases as the number of antenna increases. Asymptotically, LE is proved

to follow a Tracy-Widom (TW) distribution for central uncorrelated Wishart matrices and a Gaussian distribution for sample covariance matrices of spiked population model [192, 195]. Moreover, as mentioned in Ch. 4, for a fixed K and as $N \to \infty$ then the LE converges to a Gaussian distribution [150, 207]. For a given decision threshold $\hat{\lambda}_{LE}$, the LE detector algorithm is given as follows:

Algorithm 5.1: LE Detector using Power method

Input: $\boldsymbol{Y}$, σ_η^2, $\hat{\lambda}_{LE}$
Output: D_{LE}
1 compute $\boldsymbol{W} = \boldsymbol{Y}\boldsymbol{Y}^\dagger$;
2 get λ_1 of $\boldsymbol{W}$ using EVD or Power method;
3 evaluate $X_{LE} = \frac{\lambda_1}{\sigma_\eta^2}$;
4 decide $D_{LE} = X_{LE} \underset{\mathcal{H}_0}{\overset{\mathcal{H}_1}{\gtrless}} \hat{\lambda}_{LE}$;

According to the LE algorithm, the problem is to find the threshold. To do so, it is then required to have the CDF of the LE decision metric. In this regard, the exact CDF of the LE metric under $\mathcal{H}_0$ hypothesis is given by [212]:

$$F_0(x) = \mathcal{K}_{cu} |\boldsymbol{\Upsilon}^{cu}|. \tag{5.1}$$

where $\boldsymbol{\Upsilon}^{cu}$ is a $K \times K$ matrix with entries $\Upsilon_{i,j}^{cu} = \gamma(i+j+N-K-1, x)$ and $\mathcal{K}_{cu}$ is given by (3.3). $\gamma(.,.)$ is the lower incomplete gamma function [179, Eq.(8.350.1)].

Under $\mathcal{H}_1$ hypothesis, the exact CDF of the LE metric (as shown in Lemma 3.3) could be approximated by the CDF of the LE metric of central semi-correlated complex Wishart matrix with correlation matrix of eigenvalues $\sigma_1 > \sigma_2 = \cdots = \sigma_K$. In this regard, we provide the following Theorem:

Theorem 5.1. *Let $\boldsymbol{W} \sim \mathcal{CW}_K(N, \boldsymbol{\Sigma})$ be a central semi-correlated complex Wishart matrix with N DoF ($N > K$) and correlation matrix $\boldsymbol{\Sigma}$ with eigenvalues $\sigma_1 > \sigma_2 = \cdots = \sigma_K$. Then, the CDF of λ_1 of $\boldsymbol{W}$ is given by:*

$$F_1(x) = \mathcal{K}_{cc} |\boldsymbol{\Upsilon}^{cc}| \tag{5.2}$$

where $\mathcal{K}_{cc}$ is given by (A.7) and $\boldsymbol{\Upsilon}^{cc}$ is $K \times K$ matrix with entries:

$$\Upsilon_{i,j}^{cc} = \begin{cases} \sigma_j^{N+i-K} \gamma(N+i-K, x/\sigma_1) & j = 1 \\ (-1)^{K-j} \sigma_j^{N+i-j} \gamma(N+i-j, x/\sigma_2) & j > 1 \end{cases} \tag{5.3}$$

Proof. Starting from the joint distribution in (A.5), the CDF of the largest eigenvalue, using [176, Corollary 2], is given by:

$$F_1(x) = \int_0^x \cdots \int_0^x f(\boldsymbol{\lambda}) d\boldsymbol{\lambda} \tag{5.4}$$

$$= \mathcal{K}_{cc} \left| \int_0^x \mathrm{v}_i(u) \mathrm{e}_j(u) u^{N-K} du \right|_{i,j=1,\cdots,K}, \tag{5.5}$$

then, the integral of (5.5) is evaluated using [179, Eq. 3.351.1]. □

Note that $\gamma(n,x) = (n-1)!e^{-x}\sum_{m=0}^{n-1}\frac{x^m}{m!}$ [179], then the evaluation of these exact CDFs is more complicated as K or N increases. However, the target is to find a simple threshold form which is not straightforward since it requires the inverse of the CDF function. Next, we show that the LE distribution could be perfectly approximated using the GEV distribution and thus a simple threshold form could be derived.

5.2.2 Approximating LE

Herein, the approximation of the LE distribution is considered. First, the moments of the LE are derived and then an approximation of the LE distribution with the GEV distribution will follow using Lemma C.1. We should mention that this approximation is feasible if the moments are derived. Thus, the exact form of the p-th moment of the LE under hypothesis $\mathcal{H}_0$ is provided by the following Theorem.

Theorem 5.2. *Let $\boldsymbol{W} \sim \mathcal{CW}_K(N, \sigma_\eta^2 \boldsymbol{I}_K)$ be a central uncorrelated complex Wishart matrix with N DoF and correlation matrix $\sigma_\eta^2 \boldsymbol{I}_K$. Then, the p-th moment of the LE of $\boldsymbol{W}$ is given by:*

$$M(p) = p\mathcal{K}_{cu} \sum_{\delta \in \mathbb{P}_0} sgn(\delta) \prod_{i=1}^{K} (\delta(i) + i + N - K - 2)!$$
$$\times \sum_{\boldsymbol{s} \in \mathbb{S}_0^*} \frac{(-1)^{|\boldsymbol{s}|+1} (\Sigma \boldsymbol{s} + p - 1)!}{\Pi \boldsymbol{s}! \cdot |\boldsymbol{s}|^{\Sigma \boldsymbol{s} + p}} \tag{5.6}$$

with $\mathbb{P}_0$ is the set of all possible permutations of the vector $[1, \cdots, K]$ and the sum is taken over all possible permutations. $sgn(\delta)$ is the permutation sign of the permuted vector δ. $\mathbb{S}_0^*$ is the set of all subsets of the vector $[l_1, \cdots, l_K]$

and the sum is taken over all possible subsets except the null subset such that $\sum_{\boldsymbol{s}\in\mathbb{S}_0^*} = \sum_{l_1}^{L_1}\cdots\sum_{l_{|\boldsymbol{s}|}}^{L_{|\boldsymbol{s}|}}$ *with* $|\boldsymbol{s}|$ *is the cardinality of the subset* $\boldsymbol{s}$ *and* $L_j = \delta(j) + j + N - K - 2$.

Proof. See App. A.5. □

Under $\mathcal{H}_1$ hypothesis and following the results in Ch. 3, the use of the moments of the central semi-correlated Wishart matrices provide good approximation for the LE. Hence, the exact form of the p-th moment of the largest eigenvalue of the central semi-correlated Wishart matrices of spiked population is provided by the following Theorem:

Theorem 5.3. *Let* $\boldsymbol{W} \sim \mathcal{CW}_K(N, \boldsymbol{\Sigma})$ *be a central semi-correlated complex Wishart matrix with* N *DoF* ($N > K$) *and correlation matrix* $\boldsymbol{\Sigma}$ *with eigenvalues* $\sigma_1 > \sigma_2 = \cdots = \sigma_K$. *Then, the p-th moment of* λ_1 *of* $\boldsymbol{W}$ *is given by:*

$$M(p) = p\mathcal{K}'_{cu}\sum_{\delta\in\mathbb{P}_0} sgn(\delta)\prod_{i=1}^{K}\frac{(N+\delta(i)-b_{i,K}-1)!}{\sigma_i^{b_{i,K}-\delta(i)-N}} \times \sum_{\boldsymbol{s}\in\mathbb{S}_0^*}\frac{(-1)^{|\boldsymbol{s}|+1}(\Sigma\boldsymbol{s}+p-1)!}{\Pi\boldsymbol{s}!\cdot\ \Pi\sigma_s^s\cdot|\Sigma\frac{1}{\sigma_s}|^{\Sigma\boldsymbol{s}+p}}, \tag{5.7}$$

with $\mathcal{K}'_{cu}$ *is a modified normalization constant as follows:*

$$\mathcal{K}'_{cc} = \frac{(-1)^{\frac{(K-1)(K-2)}{2}}\sigma_1^{K-N-1}\ \sigma_2^{(N-1)(1-K)}}{\Gamma_K(N)\Gamma_{K-1}(K-1)(\sigma_2-\sigma_1)^{K-1}}, \tag{5.8}$$

and we define $b_{n,m}$ *as:*

$$b_{n,m} = \begin{cases} m & n = 1 \\ n & n \neq 1 \end{cases} \tag{5.9}$$

Proof. See App. A.5. □

Same as for the CDF case, the p-th moment of the LE metric is provided by (5.7) after the normalization of $\boldsymbol{W}$ by σ_η^2. Now by exploiting the moments of the LE given by Theorems 5.2 and 5.3, we can approximate the LE distribution by the GEV distribution as given by the following proposition.

Proposition 5.1. *The CDF and PDF of the LE, under hypotheses $\mathcal{H}_0$ and $\mathcal{H}_1$, can be accurately approximated by:*

$$F(x;\theta,\beta,\xi) = e^{-(1+(\frac{x-\theta}{\beta})\xi)^{-1/\xi}} \tag{5.10}$$

$$f(x;\theta,\beta,\xi) = \frac{1}{\beta}(1+(\frac{x-\theta}{\beta})\xi)^{\frac{-1}{\xi}-1} e^{-(1+(\frac{x-\theta}{\beta})\xi)^{-1/\xi}} \tag{5.11}$$

where the shape, scale and location parameters are defined by (3.43), (3.44) and (3.45) with the mean, variance and skewness of LE given by:

$$\mu_{LE} = M(1) \tag{5.12}$$

$$\sigma^2_{LE} = M(2) - \mu^2_{LE} \tag{5.13}$$

$$\mathcal{S}_{LE} = \frac{M(3) - 3M(2)\mu_{LE} + 2\mu^3_{LE}}{\sigma^{3/2}_{LE}} \tag{5.14}$$

with $M_(p)$ is the p-th moments of the LE given by Theorems 5.2 and 5.3 for $\mathcal{H}_0$ and $\mathcal{H}_1$ cases respectively.

Using (5.10), the performance probabilities and the decision threshold could be derived as in Sec. 3.3.4. It should be noted that the computational complexity of the moments of the LE in (5.6) and (5.7) is higher than that of the CDF in (5.1) and (5.2). This is obvious since the determinant could be calculated using LU decomposition algorithm ($O(K^3)$) and we use the Leibniz formula which requires $n!n$ operations. However, as mentioned in Ch. 3, this approximation only requires the values of the location, scale and shape parameters of the GEV distribution that could be computed off-line.

We should here mention that the approximation of the LE using GEV is for any K and N (i.e. finite and asymptotic). However, in the particular case when K is finite and N asymptotic, the LE could be modelled as a Gaussian RV, as mentioned in Ch. 4, which is simple and useful as discussed later in this chapter.

5.3 LE Detector with Asymptotic Regime: Full antenna exploitation

In this scenario, the CR will use all of its antennas for the SS process. Accordingly, recall the asymptotic and critical conditions as follows:

$$\textbf{AC}: \qquad (K,N) \to \infty \text{ with } K/N \to c \in (0,1), \tag{5.15}$$

$$\textbf{CC}: \qquad \rho > \rho_c = \frac{1}{\sqrt{KN}}, \tag{5.16}$$

Again, in asymptotic regime, the problem turns out to find the distribution and the threshold. By considering the AC, then under $\mathcal{H}_0$ hypothesis, LE, properly centered and scaled, follows a TW distribution of order 2 (TW2) as follows [192]:

$$LE' = \frac{LE - a_1(K,N)}{b_1(K,N)} \sim TW2, \tag{5.17}$$

where $a_1(K,N)$ and $b_1(K,N)$ are respectively the centering and scaling coefficients defined by (3.52) and (3.53).

The CDF of the TW2, first considered in [186], is given by (5.18) where $q(x)$ is the solution to the Painlevé II differential equation $q''(x) = xq(x) + 2q^3(x)$ satisfying the boundary condition $q(x) \sim Ai(x)$ as $x \to \infty$ where $Ai(x)$ is the Airy function.

$$F_{TW2}(y) = e^{-\int_y^\infty (x-y)q^2(x)dx}. \tag{5.18}$$

On the other hand, if both AC and CC are met then LE under $\mathcal{H}_1$ hypothesis and using Lemma 3.3 follows a normal distribution as follows [195]:

$$P\left(\frac{LE - a_3(K,N,\boldsymbol{\sigma})}{\sqrt{b_3(K,N,\boldsymbol{\sigma})}} \leq x\right) = \frac{1}{\sqrt{2\pi}} \int_{-\infty}^{x} e^{-\frac{u^2}{2}} du, \tag{5.19}$$

with $a_3(K,N,\boldsymbol{\sigma})$ and $b_3(K,N,\boldsymbol{\sigma})$ are defined in (3.64) and (3.65) respectively with $\sigma_\eta^2 = 1$.

It is worth mentioning that the TW2 distribution could not be evaluated numerically online. In fact, the cognitive radio system needs to evaluate the threshold which requires the inverse of the CDF. In the next subsection, we approximate the LE distribution with the GEV distribution in the asymptotic regime.

5.3.1 Approximating LE in asymptotic regime

Under $\mathcal{H}_0$ hypothesis and when AC is satisfied, the distribution of the LE metric could be approximated through GEV using the mean, the variance and the skewness provided in (3.57), (3.58) and (3.59) respectively. Accordingly, we give the following proposition:

Proposition 5.2. *Let N and K obey AC in (5.15), then the CDF and PDF of the LE under $\mathcal{H}_0$ hypothesis can be accurately approximated by (5.10) and (5.11) respectively. The shape, scale and location parameters are defined by (3.43), (3.44) and (3.45) where the mean, the variance and the skewness of LE are given by (3.57), (3.58) and (3.59) respectively.*

It follows from Proposition 5.2 that the GEV approximation could also be used to approximate the TW2 distribution by considering the mean, the variance and the skewness of TW2 given by $\mu_{TW2} = -1.7710868074$, $\sigma^2_{TW2} = 0.8131947928$ and $\mathcal{S}_{TW2} = 0.2240842036$ respectively.

Based on Proposition 5.2, the threshold expression is simple and have the same form of (3.95) for CFAR. On the other hand under $\mathcal{H}_1$ hypothesis, the distribution is Gaussian and it is indeed simple and any approximation in this case is useless.

5.4 Partial Exploitation of Massive MIMO antennas

This scenario could be decomposed into two different options; The first is the fixed number of antenna approach where the CR will fix a predefined number of antennas for the SS and thus uses the rest for other purposes as it will be discussed in this section. The other approach is the dynamic approach in which the CR does not fix a predefined number of antennas but it dynamically allocates a certain number of antennas for SS according to certain constraints such as a target performance. The rest of the antennas is used for other purposes.

The division in this case into approaches could be simply justified by the simple fact that a tradeoff between SS performance and exploitation of available of antennas for other use could exist. This depends on the different metrics and outcomes expected in this case. For instance, fixing predefined number of antennas for the SS or knowing the minimum number of antennas

necessary to reach a prescribed performance within a given time has many advantages such as:

- Sensing multi-channels simultaneously: in this case, the antennas are clustered and each cluster of antennas is ordered to sense certain channel and/or certain direction. Accordingly, several spectrum holes could be found at the same time which results in a more efficient utilization of the spectrum bands. Moreover, several techniques have been proposed in literature to sense a wide-band channel such as the filter-bank, compressive sensing, wavelet decomposition as mentioned in Ch. 2. Alternatively, massive MIMO could be used to sense a wide-band channel by dedicating the clusters to sense several narrow-band channels simultaneously.

- Sense and transmit simultaneously: conventional SS could be either done in a periodic sensing approach or in a simultaneous sensing and transmission approach. In periodic sensing, the CR operates in a time-slots model where it senses for a short time duration and transmits data in the remaining time of total frame duration [213]. On the other hand, simultaneous sensing and transmission approach could be considered as a full duplex approach in which two RF chains are required at the CR receiver [214]. Likewise, the CR could maintain a set antennas for SS and the others for the transmission in a full duplex scenario.

- Green radio: green radio concept has received a great attention in recent years. It is one of the most important considerations in the present scenario of global warming. From an energy efficiency perspective, it makes sense to put inactive antenna elements into sleep mode and thus reduce energy consumption [215].

- Reduce the sensing time: sensing time is the time required for the CR to make a decision. It indeed includes the required sampling duration and the time the sensing algorithm needs to make a decision. Accordingly, the full antenna exploitation scenario may not be the optimal for sensing time reduction. Indeed, if a trade-off between the complexity of the algorithm and the required number of samples to make a decision is done this may decrease the total sensing time.

- Increase system throughput: In general, using some or all of these methods, i.e. sense multi-channels simultaneously, sense and transmit

simultaneously and reducing the sensing time, would increase the total system throughput.

Consequently, the use of a fixed number or dynamic number of antennas for SS is extremely important for CR with massive MIMO technology. In fixed number case, the CR may define any number of antenna K and samples N for SS. Accordingly, and based on our derivations for LE, SLE and SCN detector through this thesis, the threshold could be computed according to maintain a CFAR or an optimized threshold could be used as to minimize the total error probabilities. The threshold optimization criteria is considered for the LE detector in Sec. 5.4.2. On the other hand, the minimum number of antennas and/or the minimum number of samples required to reach a target performance is very important for the dynamic approach. These values are directly related to the statistics of the SS decision metric being used and the environmental information. This is considered in Sec. 5.4.3 while using the LE detector and in Sec. 5.4.4 for the SCN and SLE detectors.

5.4.1 Performance Probabilities

To model the system, we should first define the performance probabilities of the detector used. In the partial antenna exploitation scenario, we consider the following:

- Fixed number of antenna approach: in this case, the CR will use certain fixed number K and $N > K$. If K is large, then N is obviously large and hence the results of asymptotic regime, in previous section, could be applied. On the other hand, if K is small, then N may be relatively small and hence the results of finite case in Sec. 5.2 are applied. However, it is more likely that N will be relatively large.

- Dynamic number of antenna approach: here, the CR will use dynamic number of antenna K and $N > K$. If K is large, then N is obviously large and the asymptotic results are applied. Also, if K is small and N is relatively small then the results of finite case are applied. However, it is more likely to have certain number K and relatively large N.

Consequently, we will consider the case in which K is finite and N is relatively large which is more practical. Hence the LE metric could be modeled as Gaussian RV under $\mathcal{H}_0$ hypothesis. Under $\mathcal{H}_1$ hypothesis, results

in [150] shows that LE metric could be approximated by Gaussian even if K is small and N is relatively large and CC is satisfied. Accordingly, if we denote the decision threshold of the LE detector by λ_{LE}, then P_{fa}, P_d and P_{md} are expressed as follows:

$$P_{fa} = 1 - \Phi(\frac{\lambda_{LE} - \mu_0}{\sigma_0}) \tag{5.20}$$

$$P_{md} = 1 - P_d = \Phi(\frac{\lambda_{LE} - \mu_1}{\sigma_1}) \tag{5.21}$$

where $\Phi(.)$ is the CDF of the standard normal distribution; μ_0, σ_0 are the mean and the standard deviation of the LE metric under $\mathcal{H}_0$ hypothesis and are given by (5.22) and (5.23) (recalled from Ch. 3); μ_1, σ_1 are the mean and the standard deviation of the LE metric under $\mathcal{H}_1$ hypothesis and are given by (5.24) and (5.25) (recalled from Ch. 3).

$$\mu_0 = b_1(K,N)\mu_{TW2} + a_1(K,N), \tag{5.22}$$

$$\sigma_0^2 = b_1^2(K,N)\sigma_{TW2}^2, \tag{5.23}$$

$$\mu_1 = \sigma_1(N + \frac{K}{\sigma_1 - 1}), \tag{5.24}$$

$$\sigma_1^2 = \sigma_1^2(N - \frac{K}{(\sigma_1 - 1)^2}), \tag{5.25}$$

where $\mu_{TW2} = -1.7710868074$, $\sigma_{TW2}^2 = 0.8131947928$ and

$$a_1(K,N) = (\sqrt{K} + \sqrt{N})^2, \tag{5.26}$$

$$b_1(K,N) = (\sqrt{K} + \sqrt{N})(K^{-1/2} + N^{-1/2})^{\frac{1}{3}}. \tag{5.27}$$

5.4.2 Optimal Threshold

The performance probabilities depend on the decision threshold (λ_{LE}), and hence it is necessary to choose an appropriate value based on system requirements. The typical approach for setting the threshold is given by the CFAR strategy in which the threshold is chosen in order to guarantee a target false-alarm rate ($\hat{P}_{fa}$). Hence, for finite K and relatively large N and based on the CFAR scenario, the decision threshold is expressed using the inverse of P_{fa} as follows:

$$\hat{\lambda}_{LE} = \mu_0 + \sigma_0 \Phi^{-1}(1 - \hat{P}_{fa}) \tag{5.28}$$

It is worth mentioning that the threshold for other cases (i.e. asymptotic and finite) is previously derived and given by (3.95). Another threshold optimization approach would be to minimize the total error probability of the system. Accordingly, the optimized threshold could be expressed as follows:

$$\hat{\lambda}_{LE} = \underset{\lambda_{LE}}{\operatorname{argmin}}(p_0 P_{fa} + p_1 P_{md}) \tag{5.29}$$

where p_0 and p_1 are weighting coefficients that are chosen according to system priority. To solve this minimization problem, one can simply take the derivative equals to zero and the second derivative positive (i.e. concave). One can choose $p_0 = 0$ or $p_1 = 0$ to minimize one of the error probabilities. However, it is typical to choose $p_0 = p_1 = 0.5$ to minimize the sum of the error probabilities. Then λ_{LE} should be selected such that it minimizes $P_{fa} + P_{md}$, i.e. its derivative equal to zero such that:

$$(\frac{1}{2\sigma_0^2} - \frac{1}{2\sigma_1^2})\lambda_{LE}^2 + (\frac{\mu_1}{\sigma_1^2} - \frac{\mu_0}{\sigma_0^2})\lambda_{LE} + (\frac{\mu_0^2}{2\sigma_0^2} - \frac{\mu_1^2}{2\sigma_1^2} - ln(\frac{\sigma_1}{\sigma_0})) = 0 \tag{5.30}$$

and finally the optimal threshold is given by:

$$\hat{\lambda}_{LE} = \frac{\mu_1\sigma_0^2 - \mu_0\sigma_1^2 + \sqrt{\sigma_0^2\sigma_1^2\left((\mu_0 - \mu_1)^2 - 2(\sigma_0^2 - \sigma_1^2)ln(\frac{\sigma_1}{\sigma_0})\right)}}{\sigma_0^2 - \sigma_1^2} \tag{5.31}$$

The same derivation procedure could be done for any value p_0 and p_1. The optimal threshold in (5.31) requires the knowledge of the SNR value. It could be used in any of the scenarios to minimize the error probabilities. However, in the dynamic case, i.e. when K and/or N are to be selected dynamically, the designer should set up the target P_{fa} and P_{md} to be obtained while the optimization will consist in finding the minimal K and N. Accordingly, we choose a fixed $(\hat{P}_{fa}, \hat{P}_d)$ performance to evaluate the required K and N to achieve this performance. This will be discussed next.

5.4.3 Minimum Requirements

For a target $(\hat{P}_{fa}, \hat{P}_d)$ and at a given SNR, the CR system should optimize certain number of antennas for a certain number of samples. By eliminating λ_{LE} from P_{fa} and P_d in (5.20) and (5.21) respectively, one can solve for K (or N) the following equation:

$$\sigma_0\Phi^{-1}(1 - \hat{P}_{fa}) - \sigma_1\Phi^{-1}(1 - \hat{P}_d) + \mu_0 - \mu_1 = 0 \tag{5.32}$$

Now, let us substitute μ_0, μ_1, σ_0 and σ_1 to get a single equation involving the parameters: K, N, $\hat{P}_{fa}$, $\hat{P}_d$ and ρ. Hence, at a certain SNR value and for a target detection performance $(\hat{P}_{fa}, \hat{P}_d)$ the system can dynamically choose the couple (K, N) that most enhances its global performance (i.e. throughput, power saving etc.). In is worth mentioning that finding a general solution for (5.32) is not straightforward and thus we solve for numerical values. Consider the following example:

Example 1: Consider the following example, $\hat{P}_{fa} = 0.1$, $\hat{P}_d = 0.9$ and $\rho = -15dB$, then we get Tables 5.1 and 5.2.

Table 5.1: Required K for a given N in Example 1.

N	200	300	350	400	450	500	600	1000
K	14	10	8	8	7	6	5	4

Table 5.2: Required N for a given K in Example 1.

K	20	18	15	10	8
N	132	147	177	273	349

Table 5.1 shows different values of N and its corresponding required number of antennas K that should be involved in the sensing process to achieve the performance illustrated in Example 1. On the other hand, Table 5.2 shows different values of K and its corresponding required number of samples N that should be acquired by each antenna in the sensing process to achieve the considered performance. It is worth mentioning that the values of K and N evaluated using (5.32) are real valued numbers and thus are rounded to $+\infty$. Consequently, for a target performance as illustrated in Example 1 it is enough for a CR to use $K = 8$ and $N = 350$. However, using a greater number of antennas is inefficient and a waste of resources.

The system may also be expected to have dynamic behaviour in case of the change of the SNR values. This could be also achieved using (5.32). This kind of dynamical behaviour is extremely important to any multi-antenna system. This will be considered in the simulations.

5.4.4 Extension to SCN and SLE

In this subsection, we use the results provided in Chapters 3 and 4 to extend this work for both SCN and SLE detectors. Let us consider the SCN detector and by eliminating λ_{SCN} from both (3.93) and (3.94) we get:

$$\theta_0 - \frac{\beta_0}{\xi_0} - \theta_1 + \frac{\beta_1}{\xi_1} + \frac{\beta_0}{\xi_0}\big[-\ln(1-\hat{P}_{fa})\big]^{-\xi_0} - \frac{\beta_1}{\xi_1}\big[-\ln(1-\hat{P}_{d})\big]^{-\xi_1} = 0 \quad (5.33)$$

where $\hat{P}_{fa}$ and $\hat{P}_d$ are target false-alarm and detection probabilities; θ_i, β_i and ξ_i are the location, scale and shape parameters of the GEV distribution where $i = 0$ refers to $\mathcal{H}_0$ hypothesis and $i = 1$ refers to $\mathcal{H}_1$ hypothesis. Their expressions are provided by Theorems 3.2 and 3.3.

For the SLE detector, the probability of detection could be derived in a similar manner used for the derivation of P_{fa} in Sec. 4.3.3. Accordingly, by eliminating λ_{SLE} from the performance probabilities we get:

$$\frac{\mu_{12}^{\mathcal{H}_0} - \Delta^2 r_0 \sigma_{12}^{\mathcal{H}_0}}{\mu^2_{T_n^{\mathcal{H}_0}} - \Delta^2 \sigma^2_{T_n^{\mathcal{H}_0}}} - \frac{\mu_{12}^{\mathcal{H}_1} - \Lambda^2 r_1 \sigma_{12}^{\mathcal{H}_1}}{\mu^2_{T_n^{\mathcal{H}_1}} - \Lambda^2 \sigma^2_{T_n^{\mathcal{H}_1}}} + \frac{\Delta\sqrt{m_v^{\mathcal{H}_0} - 2r_0\mu_{12}^{\mathcal{H}_0}\sigma_{12}^{\mathcal{H}_0} + \Delta^2[\sigma_{12}^{\mathcal{H}_0}]^2(r_0^2-1)}}{\mu^2_{T_n^{\mathcal{H}_0}} - \Delta^2 \sigma^2_{T_n^{\mathcal{H}_0}}}$$
$$- \frac{\Lambda\sqrt{m_v^{\mathcal{H}_1} - 2r_1\mu_{12}^{\mathcal{H}_1}\sigma_{12}^{\mathcal{H}_1} + \Lambda^2[\sigma_{12}^{\mathcal{H}_1}]^2(r_1^2-1)}}{\mu^2_{T_n^{\mathcal{H}_1}} - \Lambda^2 \sigma^2_{T_n^{\mathcal{H}_1}}} = 0 \quad (5.34)$$

where $\Delta = Q^{-1}(\hat{P}_{fa})$ and $\Lambda = Q^{-1}(\hat{P}_d)$; the expressions of the parameters in (5.34) are provided in Ch. 4.

Similar to the LE detector case, using (5.33) and (5.34) we can determine the minimum requirements of the system that could be used to achieve target performance.

5.5 Simulation and Discussion

In this section, we verify the analytical derivation results through Monte-Carlo simulations. We validate the theoretical analysis presented in sections 5.2, 5.3 and 5.4. The simulation results are obtained by generating 10^5 random realizations of $\boldsymbol{Y}$. In addition, we compare the results of different scenarios of antenna exploitation for different considered detectors. Moreover, a comparison between the LE, SCN and SLE detectors is considered from the performance perspective and the minimum requirements needed to achieve target performance.

5.5.1 Validation of Analytical Results

Figure 5.1 shows the CDF expression derived in Theorem 5.1 and its use in approximating the $\mathcal{H}_1$ hypothesis. Different small number of antennas K and different relatively small values of N are considered with $\rho = -10dB$. Simulation results show perfect match with the analytical expressions. Moreover, empirical results of non-central uncorrelated Wishart ($\mathcal{H}_1$ hypothesis) present show perfect match with the provided expressions.

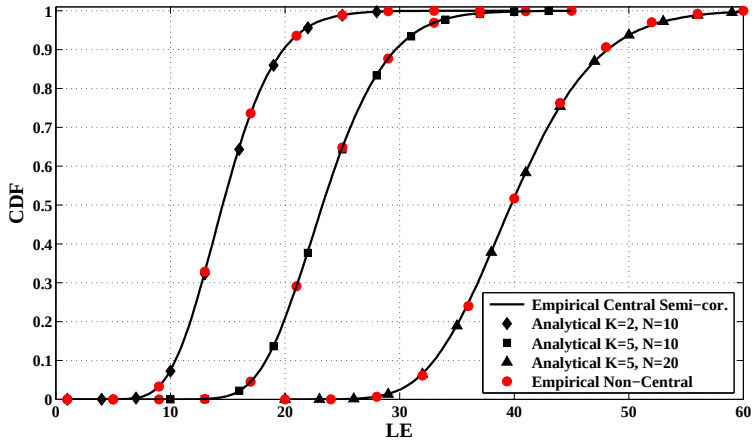

Figure 5.1: Empirical CDF of LE metric of central semi-correlated Wishart matrix and its corresponding Analytical expression and the empirical CDF of LE metric of non-central uncorrelated Wishart matrix under $\mathcal{H}_1$ hypothesis for different values of K and N.

The analytical expressions of the p-th moments in Theorems 5.2 and 5.3 are validated in Table 5.3 by considering the first moment. Table 5.3 provides the empirical and corresponding analytical mean of central uncorrelated Wishart ($\mathcal{H}_0$ hypothesis) and central semi-correlated Wishart (approximation of $\mathcal{H}_1$ hypothesis). Results show perfect match with the values evaluated using the derived expressions.

Figure 5.2 plots the empirical P_{fa} and P_d of the LE detector in the finite case and its corresponding analytical values using GEV approximation provided by Proposition 5.1, (2.6) and (2.7). The results are taken for different values of K and N and $\rho = -10dB$. Results show perfect match between the empirical results and the proposed approximation under both hypothesis.

Asymptotic approximation provided by Proposition 5.2 is validated in

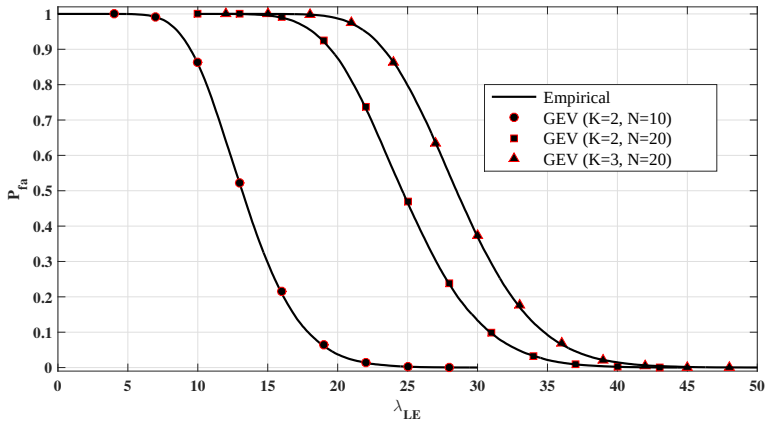

(a) P_{fa}

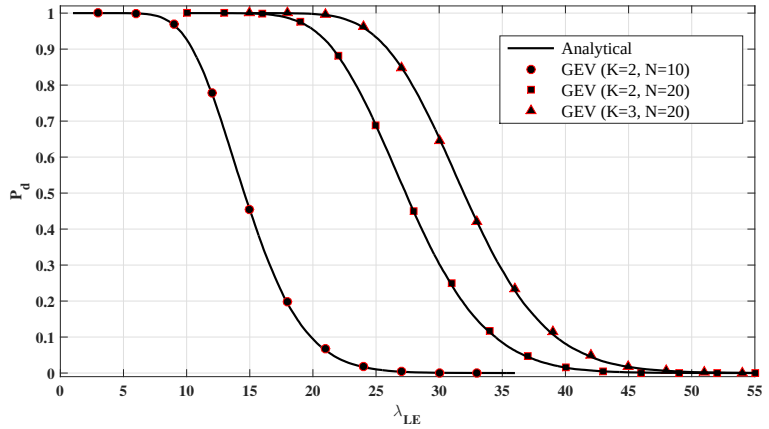

(b) P_d

Figure 5.2: Empirical P_{fa} and P_d of the LE detector and its corresponding GEV approximation for different values of K and N with fixed $\rho = -10dB$.

Table 5.3: Empirical and Analytical Mean of the LE metric of central uncorrelated and semi-correlated Wishart matrices.

	N	10		20	
	K	2	3	2	3
Central Uncorr.	Empirical	13.5195	16.3636	25.0133	28.8718
	Analytical	13.5239	16.3287	25.0148	28.8535
Central Semi-corr.	Empirical	14.9668	18.2241	27.8013	32.4138
	Analytical	14.9718	18.19	27.8008	32.3977

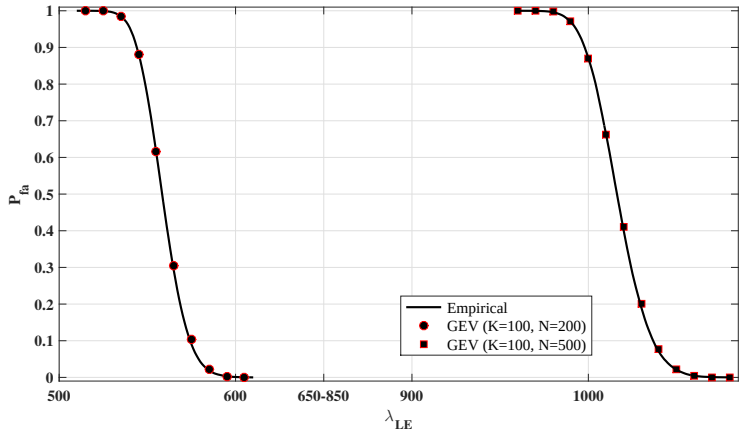

Figure 5.3: Empirical P_{fa} of the LE detector in the asymptotic case and its corresponding GEV approximation for $K = 100$ and different values of N.

Fig. 5.3. The results are taken for different values of N while fixing $K = 100$ and $\rho = -10dB$. Results show perfect match between empirical results and the proposed approximation.

5.5.2 Full and Partial antenna exploitation scenarios

Figure 5.4 shows the empirical P_{fa} and P_d of the LE detector and its corresponding target values ($\hat{P}_{fa} = 0.01, \hat{P}_d = 0.9$) while changing the other parameters. In Fig. 5.4(a) we set the SNR $\rho = -20dB$ and we consider a variable N while in Fig. 5.4(b) we set $N = 500$ and we consider a variable ρ, as summarized by Algorithm 5.2. Simulation results show high accuracy

of the analytical results evaluated using (5.32). The empirical P_{fa} is indeed 0.01 while the accuracy of the P_d increases as K increases which reflects the effect of AC under $\mathcal{H}_1$ hypothesis. However, one can use the proposed GEV approximation instead of the Gaussian which may result in better accuracy for small K values. In addition, this small difference between the empirical and the target P_d is also due to the rounding of K to $+\infty$. The effect of rounding of K could be clearly noticed in Fig. 5.4(b) when $\rho = -12dB$ where the exact value is $K = 3.3$ and the rounded value will be $K = 4$. Moreover, the results also show that as N increases or ρ decreases the number of antennas required to achieve the target performance decreases and hence these antennas could be exploited for other use. This is the main idea behind this dynamic use, for example if the CR is monitoring a good environmental condition then it can easily lower the number of antennas used to sense the channel and vice versa.

Algorithm 5.2: Dynamic K simulation algorithm for LE detector

Input: $\boldsymbol{Y}$, σ_η^2, $(\hat{P}_{fa}0.01, \hat{P}_d = 0.9)$, ρ, N
Output: (P_{fa}, P_d)
1 evaluate K w.r.t. ρ or N;
2 compute $\hat{\lambda}_{LE}$ w.r.t. K and N ;
3 generate $(K \times N)$ matrix $\boldsymbol{Y}$ for $\mathcal{H}_0$ and $\mathcal{H}_1$;
4 get λ_1 of $\boldsymbol{W} = \boldsymbol{Y}\boldsymbol{Y}^\dagger$ for $\mathcal{H}_0$ and $\mathcal{H}_1$;
5 evaluate $X_{LE_i} = \frac{\lambda_1}{\sigma_\eta^2}$ for $\mathcal{H}_0$ and $\mathcal{H}_1$;
6 if $X_{LE_0} > \hat{\lambda}_{LE} \rightarrow P_{fa}$;
7 if $X_{LE_1} > \hat{\lambda}_{LE} \rightarrow P_d$;
8 repeat;

Figure 5.5 shows a comparison between different scenarios, full use, dynamic use and fixed use. We suppose that the CR is equipped with 200 antennas where they are all used in the full exploitation scenario and only 5 antennas are used in the fixed exploitation scenario and the choice of K for the dynamic scenario depends on the SNR value and calculated using (5.32). It is obvious that the full exploitation of the antenna scenario achieves the best performance, however it is exploiting all the antennas all the time even if it not necessary. In this case, the threshold is calculated using the GEV approximation in Sec. 5.3. Using fixed number of antennas will lead to a worst

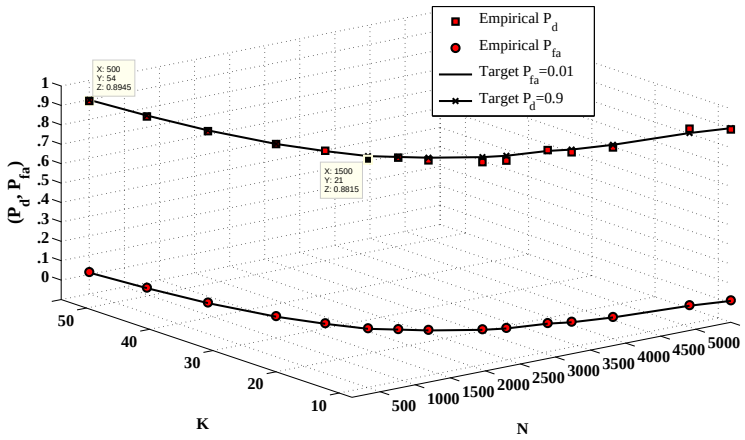

(a) Fixed $\rho = -20dB$ and variable N

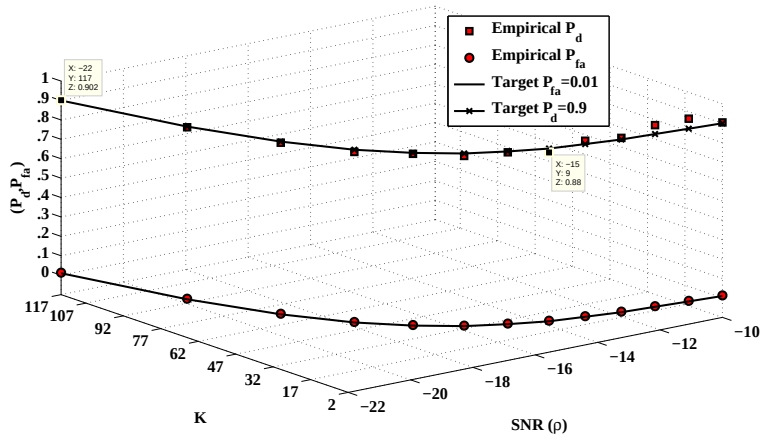

(b) Fixed $N = 500$ and variable ρ

Figure 5.4: Empirical P_{fa} and P_d of the LE detector and its corresponding target values by using dynamic method.

performance as the environmental conditions gets worst. On the other hand, if the system performance is well defined then we can achieve the desired performance all the time while efficiently exploiting all the antennas and/or relaxing the system. From the figure, results show high decrease in the value of K as SNR increases with approximately stable $P_d = 0.9$. Using dynamic exploitation scenario, CR system will gain around 115 antennas that could be used for other purposes. In addition, the computational complexity of the sample covariance matrix and the eigenvalues in the detection algorithm will be decreased since the received matrix size, $(K \times N)$, is decreased. Moreover, results show that it is enough to use $K = 2$ for $N = 500$ starting from $\rho = -10dB$. Indeed, since $K = 2$ is the smallest value for the EBD then, for $\rho \leq -10dB$, the designer can fix $K = 2$ and starts to minimize N accordingly. In this case, as N decreases the threshold could be computed using the GEV approximation in the finite case.

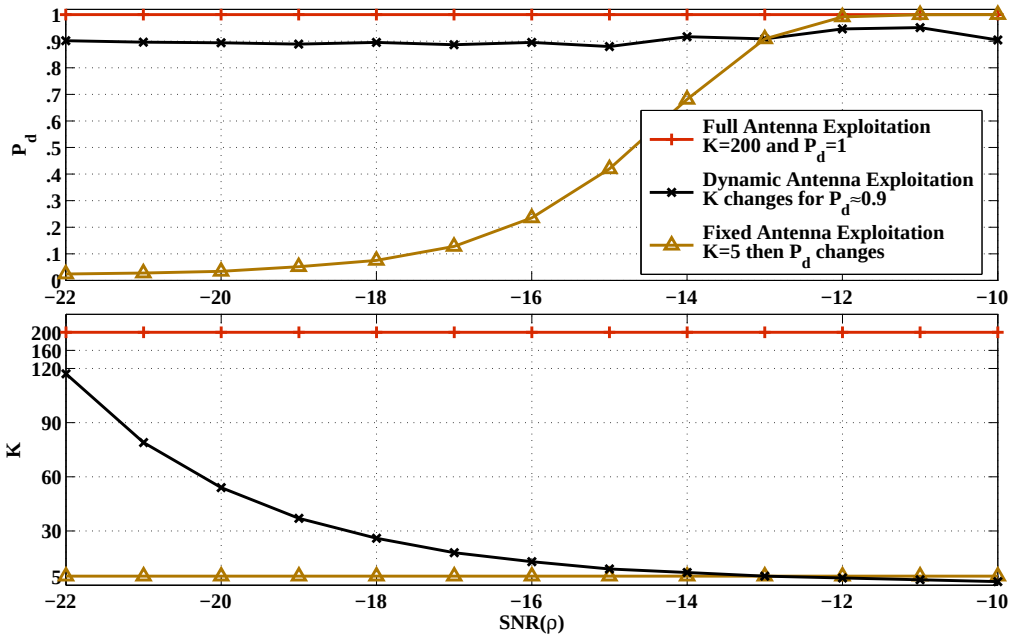

Figure 5.5: Empirical P_d of the LE detector and the corresponding number of antennas, K, used for sensing in Full, Dynamic and Fixed methods w.r.t ρ and fixing $N = 500$.

The SCN and SLE detector are considered next and an algorithm similar

to Algorithm 5.2 is applied. The results are shown in Figures 5.6, 5.7, 5.8 and 5.9. Figures 5.6 and 5.8 show the P_d and P_{fa} of the SCN and SLE detectors respectively for different values of K which is changed according to the target ($\hat{P}_{fa} = 0.01, \hat{P}_d = 0.9$) and the variation of SNR or N. Figures 5.7 and 5.9 show the variation of P_d with respect to SNR and K in the aforementioned scenarios for SCN and SLE detectors respectively. In the SLE detector case, we suppose that the mean error $\epsilon = 0$. Results show high accuracy of the analytical results evaluated using (5.33) and (5.34). Like the LE case, when K takes small values, the difference between the empirical and target P_d is due to both the AC and the rounding of K. Moreover, it could be noticed from Fig. 5.7 that at $\rho = -22dB$ and using $N = 500$ then the required value of K is 203. In this case and since the CR is equipped with 200 antennas, then the designer must fix $K = 200$ and starts to increase N accordingly to achieve the target performance. Finally, these expressions are very useful and accurate to make a dynamic system in which the antennas are efficiently utilized.

5.5.3 LE, SCN and SLE comparison

In this section, we provide a comparison between the considered detectors. For the LE detector, the noise power is supposed to be perfectly known while SCN and SLE detectors are totally-blind and do not require this knowledge. Figure 5.10 plots the ROC of these detectors for $N = 500$, $K = 5$ and $\rho = -15dB$. Simulation results show that the LE detector outperforms the SLE detector and the SLE detector in turn outperforms the SCN detector. However, if noise power is not perfectly known, the performance of the LE detector will degrades and it might be worst than the performance of SLE and SCN detectors as shown in Fig. 5.10 where $0.2dB$ noise uncertainty is considered. These results are expected as discussed through this thesis.

Figures 5.11 and 5.12 show the minimum required number of antenna K for the LE, SCN and SLE detectors to achieve a target ($\hat{P}_{fa} = 0.01, \hat{P}_d = 0.9$) when changing ρ and N respectively. As expected, due to the superior performance of the LE detector followed by the SLE detector and the SCN detector, the required K to acheive the target performance for LE detector is smaller than that for the SLE detector which in turn is also smaller than that for the SCN detectors. In addition, it is also noticeable that the difference in K for LE and SLE are close whereas K required of the SCN detector is larger. Indeed, LE and SLE detectors are optimal when the noise power is perfectly

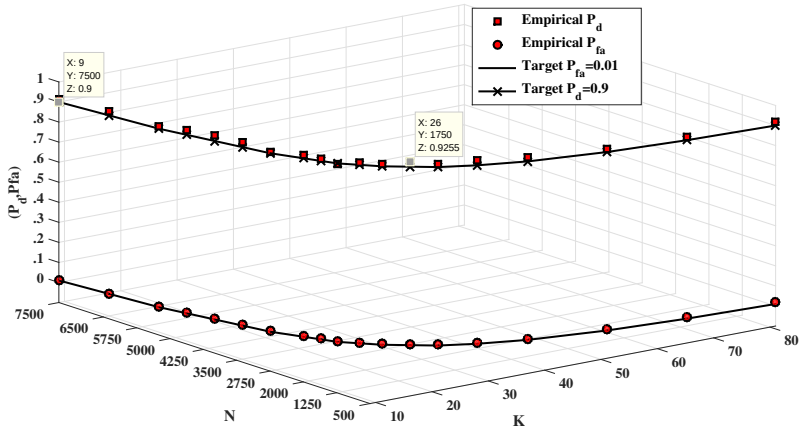

(a) Fixed $\rho = -20dB$ and variable N

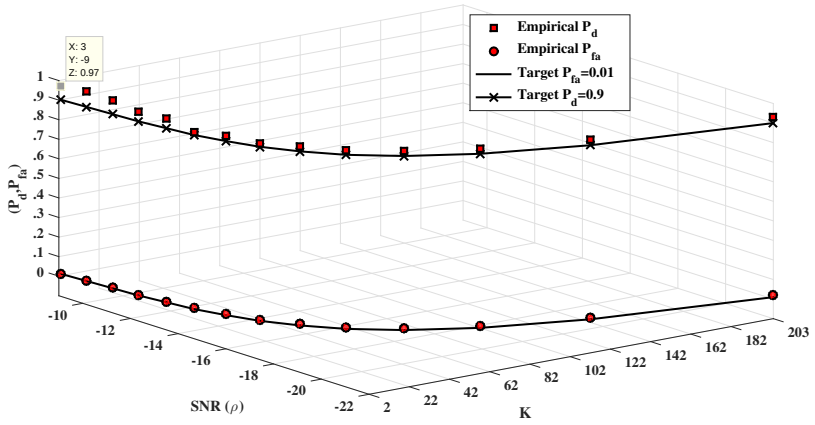

(b) Fixed $N = 500$ and variable ρ

Figure 5.6: Empirical P_{fa} and P_d of the SCN detector and its corresponding target values by using dynamic method.

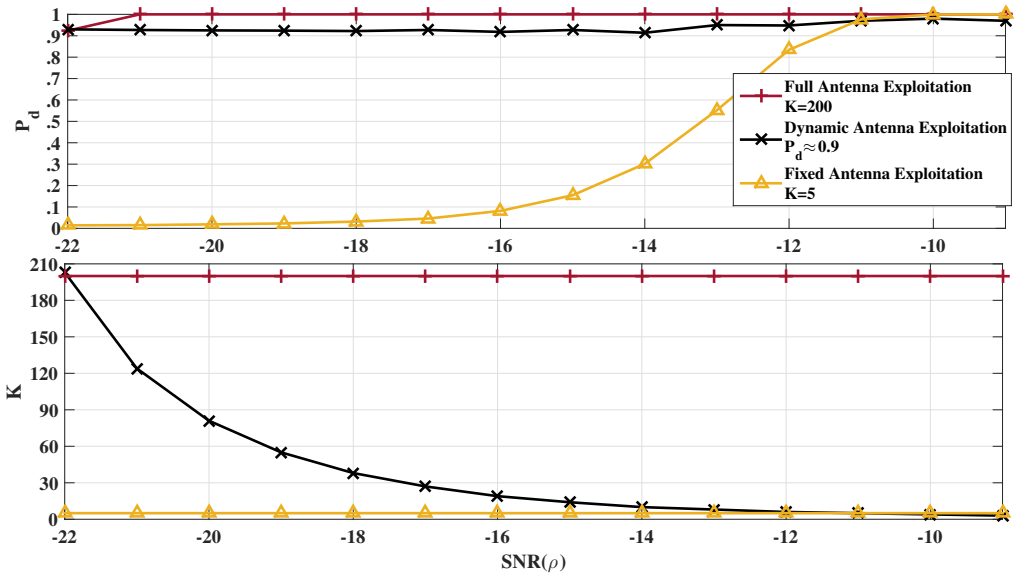

Figure 5.7: Empirical P_d of the SCN detector and the corresponding number of antennas, K, used for sensing in Full, Dynamic and Fixed methods w.r.t ρ and fixing $N = 500$.

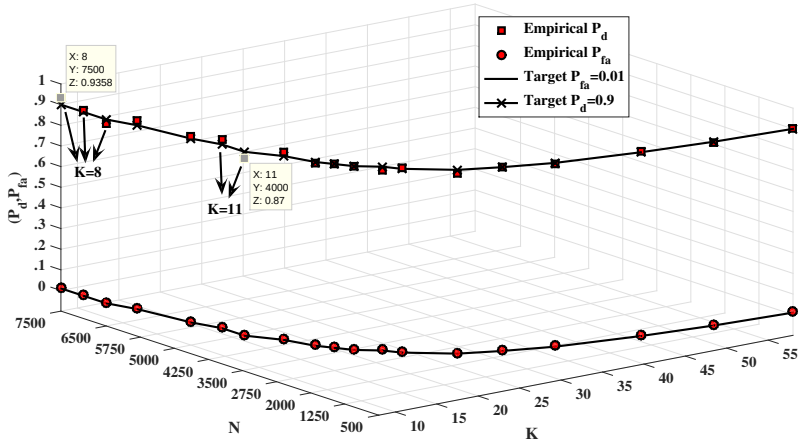

(a) Fixed $\rho = -20dB$ and variable N

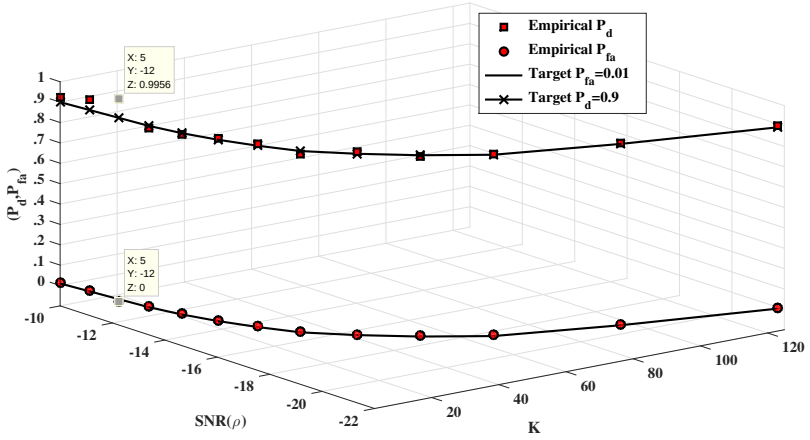

(b) Fixed $N = 500$ and variable ρ

Figure 5.8: Empirical P_{fa} and P_d of the SLE detector and its corresponding target values by using dynamic method.

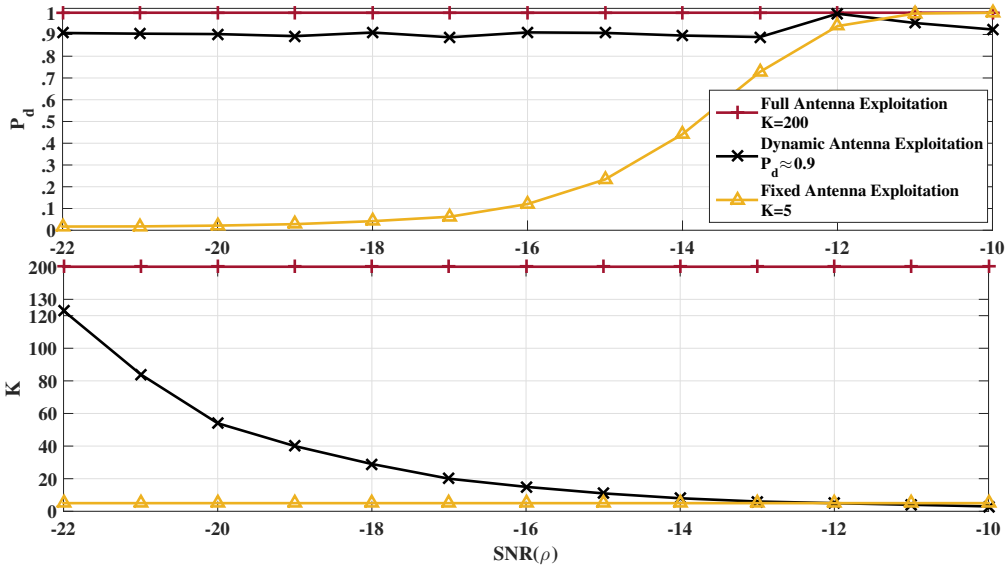

Figure 5.9: Empirical P_d of the SLE detector and the corresponding number of antennas, K, used for sensing in Full, Dynamic and Fixed methods w.r.t ρ and fixing $N = 500$.

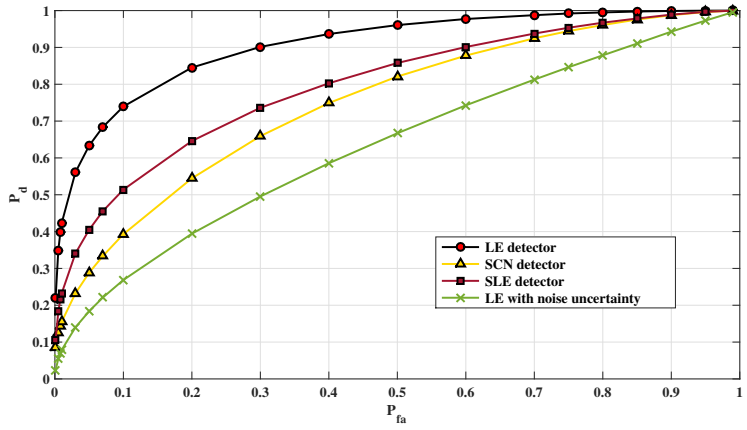

Figure 5.10: ROC of the LE, SCN and SLE detectors when $k = 5$, $N = 500$ and $\rho = -15dB$.

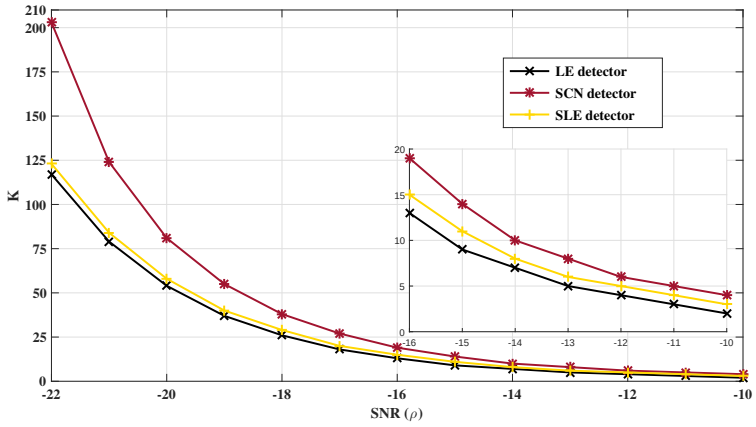

Figure 5.11: Required K of the LE, SCN and SLE detectors for dynamic antenna exploitation w.r.t ρ and fixing $N = 500$, $P_d = 0.9$ and $P_{fa} = 0.01$.

known and noise power uncertain environments respectively. In this regard, it is worth mentioning that by considering LE detector with noise uncertain environment the performance of the LE detector will degrade and thus the number of required K will increase. This case is considered in the future recommendations.

5.6 Conclusion

CR equipped with massive MIMO technology will achieve a significant increase in the performance of the multi-antenna SS detector. However, it might be enough to use a much fewer number of antennas for the sensing process and achieve a desired performance. We considered the LE, SCN and SLE detectors with two exploitation scenarios: (i) Full exploitation of the antennas and (ii) Partial exploitation of the antenna. The latter is further decomposed into two options: (i) Fixed use and (ii) Dynamic use. We derived the exact CDF of LE metric and its moments then we approximate this distribution using GEV distribution for both finite and asymptotic cases to get a simple form for the decision threshold. An optimized decision threshold is derived for the fixed use approach that minimizes the error probabilities of the LE detector. Finally, we illustrated a way to compute the minimum requirements of the CR system to achieve the desired performance in the

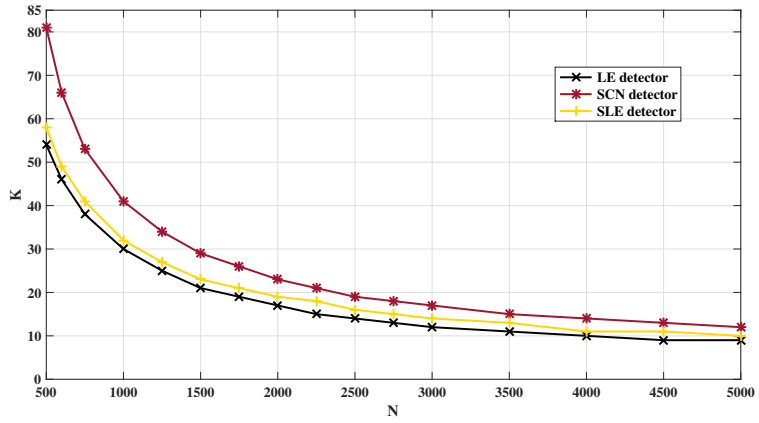

Figure 5.12: Required K of the LE, SCN and SLE detectors for dynamic antenna exploitation w.r.t N and fixing $\rho = -20dB$, $P_d = 0.9$ and $P_{fa} = 0.01$.

dynamic use approach for the LE, SCN and SLE detectors. Simulation tests have been done to validate the derived expressions and to study the different approaches. It has been shown that using the dynamic approach is the best solution for an efficient antenna exploitation. In addition, comparison between LE, SCN and SLE detectors is illustrated in terms of detector performance and minimum requirements.

Chapter 6

Conclusions and Future Recommendations

In this thesis, we have considered the EBD in a multiple-antenna CR systems. EBD is usually a blind detector that overcomes noise uncertainty problems and is efficient in low SNR environments. Moreover, the use of multi-antenna technology in CR further extends the detection of spectrum holes from the conventional frequency-time-space dimensions to a wider space that includes the angle-of-arrival dimension. However, the main disadvantage of the EBD is the complexity of its performance probabilities and the threshold which cannot be evaluated on the fly. Moreover, the concept of massive MIMO in SS and CRs still needs to be explored. There are various contributions in the areas presented in this thesis and detailed in [J1-J5, C1-C3] and summarized as follows:

In Chapter 3, we considered the SCN detector and discussed the complexity of its decision metric distribution expressions, i.e. PDF and CDF. This would result in complicated forms for the probability and the decision threshold which could not be computed online. In this regard, we have started by deriving the analytical expression of the joint distribution of the ordered eigenvalues of the central semi-correlated Wishart matrices when the some of the eigenvalues of the correlation matrix are equal. We studied the non-central/central approximation empirically and showed that it has perfect accuracy for low SNR values and could be considered as a good fit for P_d for sufficiently large values of N when the SNR is high. The finite case of the SCN detector is considered next. We derived the exact distribution of

the SCN of the central uncorrelated, central semi-correlated and non-central uncorrelated Wishart matrices. In addition, the p-th moment of the SCN is considered as we derived the exact form for the pre-mentioned Wishart matrices. To overcome the computational complexity of the exact SCN distribution, we proposed to approximate it using the GEV distribution based on moment matching criteria. Accordingly, an approximation for the performance probabilities of the SCN detector and its decision threshold are given through simple expressions. Moreover, and using the non-central/central approximation we have proposed a 2-step approximation for the detection probability of the SCN detector which provides similar accuracy with simpler moment complexity. Finally, in the asymptotic case, We derived the asymptotic mean, the asymptotic variance and the asymptotic skewness of the SCN using those of the extreme eigenvalues of the sample covariance matrix by means of bi-variate Taylor expansion. GEV approximation for the distribution of the SCN under $\mathcal{H}_0$ and $\mathcal{H}_1$ hypotheses were proposed. Consequently, simple forms for the false-alarm probability, detection probability and the decision threshold are derived for real-time computations such that a CR system with large number of antennas can dynamically adapt its threshold according to pre-defined error constraints and channel conditions.

In Chapter 4, we considered the SLE detector which is an optimal detector for detecting a single-PU in uncertain noise environments. We discussed the complexity of its decision metric distribution expressions in literature that are based on TW2 distribution or derived using Mellin transform. We proved that the SLE could be modeled using standard Gaussian function under some constraints. We showed that the trace is a Gaussian RV using the CLT. We derived the CDF and the PDF of the SLE based on the distributions of the largest eigenvalue and the trace. The false alarm probability, the detection probability and the decision threshold were also considered as we derived new simple and accurate forms. These forms are simple functions of the means and variances of the largest eigenvalue and the trace as well as the correlation coefficient between them. The correlation between the largest eigenvalue and the trace is studied and simple expressions are provided.

In Chapter 5, we considered a CR equipped with massive MIMO technology. We discussed different scenarios for SS using these large number of antennas. In the first scenario, we considered that the CR will use all these antennas for SS and thus we approximate the LE using the GEV approximation under $\mathcal{H}_0$ hypothesis while keeping the Gaussian approximation under $\mathcal{H}_1$ hypothesis. Accordingly, the threshold could be set. In the second

scenario, we considered two approaches: (i) fixed resource and (ii) dynamic resources. For this scenario, an optimal threshold for the LE detector was derived and the minimum required resources are discussed for the LE detector if noise power is perfectly known and for SCN and SLE detectors when noise uncertainty exists. we showed that the dynamic approach is the best solution for an efficient antenna exploitation while maintaining on a target performance. We showed the importance of this scenario from different aspects.

Finally, we present open research problems and future recommendations related to the topics discussed in this thesis:

1. Noise power uncertainty: In practical scenarios, the cognitive receiver is affected by several factors such as interference, noise uncertainty, channel uncertainty etc.. It is still an open challenge to model the LE detector in noise uncertain environments.

2. Noise correlation: In practice, the noise is never white and noise correlation is indeed a big challenge for EBD. Modelling the noise correlation and studying their effect on different decision metrics of the EBD is highly recommended for future work.

3. Hardware implementation and real scenario comparison: As mentioned, several factors will affect the detection performance for any detector in practical scenarios. Hence, it would be interesting to implement the mentioned detectors using USRPs and study their performances in real scenario. Moreover, performance comparison of these detectors and others, like ED and CFD, in real environments is very important for future use of any of the mentioned detectors.

4. Massive MIMO:

   – Antenna Selection: as discussed in Ch. 5, dynamic antenna exploitation is very important for an efficient exploitation of the huge number of antenna that a CR is equipped with. Thus, the antenna selection criteria is worth considered in future work. Moreover, the exploitation of beam-forming for detecting the angle-of-arrival of the signal must be considered in the antenna clustering or selection criteria.

5. Hybrid Cooperative Detectors: As discussed in Ch. 2, cooperative spectrum sensing has several benefits such as avoiding HNP and increasing the sensing performance. On the other hand, different devices may have different capabilities and may face different environmental conditions. Here, according to device capability, to the amount of knowledge and environmental conditions, the SU may use different detector for spectrum sensing. For example, if the SU device is equipped with single antenna then it may use ED whereas a multi-antenna device with perfect noise power knowledge may use LE detector and so on. Then, the cooperation between different SUs using different detectors is worth considered and modeled.

Appendix A

Proofs

A.1 Proof of Theorem 3.1

Before we start the proof, it is required to give the following Lemma presenting the n^{th} derivative of any function of the form $e^{-\frac{a}{x}}$ with respect to the variable x.

Lemma A.1. *let us define the function $f(x) = e^{-\frac{a}{x}}$, then the n^{th} derivative of $f(x)$ is given by:*

$$f^{(n)}(x) = \frac{a}{x^{2n}} \cdot e^{-\frac{a}{x}} \cdot \left[\sum_{k=1}^{n} (-1)^{k+n} \mathcal{L}(n,k) x^{n-k} a^{k-1} \right] \tag{A.1}$$

where the Lah number defined by $\mathcal{L}(n,k) = \binom{n}{k}\binom{n-1}{k-1}(n-k)!$.

Proof. It should be noted that, for any value of n, the n^{th} derivative of $e^{-\frac{a}{x}}$ will result into the function $e^{-\frac{a}{x}}$ multiplied by sum of (a/x) with different powers for a and x. Regardless of the sign, it is found that the number multiplied by each component of this sum is exactly equals to the Lah number.

Following the pattern seen by calculating the derivative of $f(x)$ for small values of n, and matching the numbers at each derivative level, "n", with the Lah number $\mathcal{L}(n,k)$, it can be proved, by recurrence, that the n^{th} derivative of the function $f(x)$ of the form $e^{-\frac{a}{x}}$ is given by (A.1). □

Now, we proceed in proving theorem A.2. If we have L equal eigenvalues ($\sigma_p = \cdots = \sigma_q$), we must generalize the result of central semi-correlated

Wishart with distinct correlation eigenvalues for arbitrary number of coincident eigenvalues by taking the limit of joint distribution given by [157, Eq. 6] as follows:

$$\lim_{\sigma_{p,q}\to\sigma_p} f(\boldsymbol{\lambda}) = |\boldsymbol{\Phi}(\boldsymbol{\lambda})| \prod_{i=1}^{K} \xi(\lambda_i) \lim_{\sigma_{p,q}\to\sigma_p} (C \times |\mathbf{E}(\boldsymbol{\lambda}, \boldsymbol{\sigma})|) \tag{A.2}$$

$$= |\boldsymbol{\Phi}(\boldsymbol{\lambda})| \prod_{i=1}^{K} \xi(\lambda_i) \lim_{\sigma_{p,q}\to\sigma_p} \left(\frac{\prod_{i<j}^{K} \sigma_i \sigma_j}{\prod_{i=1}^{K} \sigma_i^N (N-i)!} \cdot \frac{|\mathbf{E}(\boldsymbol{\lambda}, \boldsymbol{\sigma})|}{\prod_{i<j}^{K} \sigma_j - \sigma_i} \right)$$

with $\sigma_{p,q} = [\sigma_p, \cdots, \sigma_q]$, and C the normalization constant, $\boldsymbol{\Phi}(\boldsymbol{\lambda})$ is a Vandermonde matrix of entries λ_j^{i-1}, $\boldsymbol{E}(\boldsymbol{\lambda}, \boldsymbol{\sigma})$ is matrix of entries $e^{-\lambda_j/\sigma_i}$, and $\xi(\lambda_i) = \lambda_i^{N-K}$ [157, Table I]. To evaluate the limit in (A.2) we apply lemma 2 from [216] to obtain:

$$\lim_{\sigma_{p,q}\to\sigma_p} \frac{|\mathbf{E}(\boldsymbol{\lambda}, \boldsymbol{\sigma})|}{\prod_{i<j}^{K} \sigma_j - \sigma_i} = \frac{\begin{vmatrix} e(\lambda_1, \sigma_1) & \cdots & \cdots & e(\lambda_K, \sigma_1) \\ \vdots & \ddots & \ddots & \vdots \\ e(\lambda_1, \sigma_{p-1}) & \cdots & \cdots & e(\lambda_K, \sigma_{p-1}) \\ e^{(L-1)}(\lambda_1, \sigma_p) & \cdots & \cdots & e^{(L-1)}(\lambda_K, \sigma_p) \\ \vdots & \ddots & \ddots & \vdots \\ e^{(0)}(\lambda_1, \sigma_p) & \cdots & \cdots & e^{(0)}(\lambda_K, \sigma_p) \\ e(\lambda_1, \sigma_{q+1}) & \cdots & \cdots & e(\lambda_K, \sigma_{q+1}) \\ \vdots & \ddots & \ddots & \vdots \\ e(\lambda_1, \sigma_K) & \cdots & \cdots & e(\lambda_K, \sigma_K) \end{vmatrix}}{\prod_{\substack{i<j \\ \sigma_i \neq \sigma_j}}^{K} (\sigma_j - \sigma_i) \cdot \Gamma_L(L)} \tag{A.3}$$

with $e(\lambda_i, \sigma_j) = e^{-\frac{\lambda_i}{\sigma_j}}$, the required derivatives are evaluated using (A.1) and $\Gamma_s(l) = \prod_{i=1}^{s}(l-i)!$. Then, the result is obtained by substituting (A.1) and (A.3) into (A.2) and simplifying.

In the case we have several coincidence (eg. $\sigma_{p,q} = \sigma_p$, $\sigma_{t,s} = \sigma_s$, etc.), the same analysis could be applied and the limit must be taken over all coincidence cases.

A.2 Proof of Equations 3.16-3.17, 3.22-3.23, 3.29-3.30.

Consider the equations (3.14), (3.19) and (3.26) and apply Laplace expansion followed by Leibniz formula of the determinant [217] we get:

$$F(x) = \mathcal{K}_{\{.\}} \sum_{n,m=1}^{K} (-1)^{n+m} \sum_{\delta \in \mathbb{P}_1} sgn(\delta) \int_0^{\infty} \Upsilon_{n,m}^{\{.\}}(\lambda_K) \prod_{i=1}^{K-1} \int_{\lambda_K}^{x\lambda_K} \Upsilon_{r_{\delta_i,n},r_{i,m}}^{\{.\}}(u) du \, d\lambda_K \tag{A.4}$$

where $\{.\}$ refers to one of these cases (cu: central uncorrelated, nu: non-central uncorrelated, or cc: central semi-correlated).

Knowing that $\gamma(n,\lambda) = (n-1)!\left(1 - e^{-\lambda}\sum_{l=0}^{n-1}\frac{\lambda^l}{l!}\right)$ and ${}_0F_1(n,\lambda) = \sum_{l=0}^{\infty}\frac{\lambda^l}{(n)_l l!}$, then (3.16), (3.22) and (3.29) are derived as follows:

- substitute (3.15), (3.20) or (3.27) in (A.4) for (3.16), (3.22) and (3.29) respectively.
- algebraic manipulation and integrate.

Equations (3.17), (3.23) and (3.30) are, respectively, the derivatives of (3.16), (3.22) and (3.29).

A.3 Proof of Theorems 3.2 and 3.3

Starting by particularizing the joint distribution of the ordered eigenvalues of the central semi-correlated Wishart matrices when the correlation matrix has $K-1$ equal eigenvalues, then we have the following Lemma:

Lemma A.2. *Let $\boldsymbol{W} \sim \mathcal{CW}_K(N, \boldsymbol{\Sigma})$ be a central semi-correlated complex Wishart matrix with correlation matrix $\boldsymbol{\Sigma}$ of eigenvalues $\sigma_1 > \sigma_2 = \cdots = \sigma_K$. Then, the joint distribution of the ordered eigenvalues of $\boldsymbol{W}$ is given by:*

$$f(\boldsymbol{\lambda}) = \mathcal{K}_{cc} |\boldsymbol{V}(\boldsymbol{\lambda})| |\boldsymbol{E}(\boldsymbol{\lambda}, \boldsymbol{\sigma})| \prod_{l=1}^{K} \lambda_l^{N-K}, \tag{A.5}$$

with (i,j)-th entries of $\boldsymbol{E}(\boldsymbol{\lambda}, \boldsymbol{\sigma})$ and $\mathcal{K}_{cc}$ are given respectively by:

$$e_i(\lambda_j) = \begin{cases} e^{-\frac{\lambda_j}{\sigma_1}} & i = 1 \\ (-\lambda_j)^{K-i} e^{-\frac{\lambda_j}{\sigma_2}} & 1 < i \leq K \end{cases} \tag{A.6}$$

$$\mathcal{K}_{cc} = \frac{\sigma_1^{K-N-1}\ \sigma_2^{(N-1)(1-K)}}{\Gamma_K(N)\Gamma_{K-1}(K-1)(\sigma_2-\sigma_1)^{K-1}} \tag{A.7}$$

Now, Using joint distribution in (3.4) and (A.5), then the result in (3.19) and (3.26) follows the analytical derivation of (3.14) while considering the different cases of $f_i(\lambda_j)$ and $\mathrm{e}_i(\lambda_j)$. Finally, substitute the hypergeometric function for the non-central case and integrate using [179, Eq.(3.351.1)].

A.4 Proof of Theorems 3.4, 3.5 and 3.6.

The p^{th} moment of the SCN is given by:

$$M(p) = \int_0^\infty \int_{\lambda_K}^\infty \cdots \int_{\lambda_2}^\infty (\frac{\lambda_1}{\lambda_K})^p \cdot f(\boldsymbol{\lambda})\ d\lambda_1 \cdots d\lambda_K \tag{A.8}$$

then the result is derived as follows:

- substitute the joint distribution of the ordered eigenvalues for the central uncorrelated, non-central uncorrelated, and central semi-correlated Wishart cases.
- apply Laplace expansion.
- apply Leibniz formula
- algebraic manipulation to transform the product into sum then collect common terms
- integrate using [179, Eq.(3.351.2)] and [179, Eq.(3.351.3)] and watch the recurrence.

A.5 Proof of Theorems 5.2 and 5.3.

Using integration by parts, the p-th moment of the LE could be written as follows:

$$\begin{aligned} M_p^{LE} &= \int_0^{+\infty} x^p d(F_{LE}(x)) \\ &= x^p F_{LE}(x)\Big|_0^{+\infty} - \int_0^{+\infty} p x^{p-1} F_{LE}(x) dx, \end{aligned} \tag{A.9}$$

now, using the alternative sum of determinant (Leibniz formula) [217] and the definition of lower incomplete gamma function [179, Eq. 8.352.1], then $F_{LE}(x)$ of central uncorrelated and central semi-correlated Wishart matrices, after some algebraic manipulation, could be written, respectively, as follows:

$$\begin{aligned} F_{\lambda_1}^{cu}(x) =& \mathcal{K}_{cu} \sum_{\delta \in \mathbb{P}_0} sgn(\delta) \prod_{i=1}^{K} (\delta(i) + i + N - K - 2)! \\ & \times \sum_{s \in \mathbb{S}_0} \frac{(-1)^{|s|} e^{-|s|x} x^{\Sigma l_s}}{\Pi l_s!} \end{aligned} \tag{A.10}$$

$$\begin{aligned} F_{\lambda_1}^{cc}(x) =& \mathcal{K}'_{cc} \sum_{\delta \in \mathbb{P}_0} sgn(\delta) \prod_{i=1}^{K} \frac{(N + \delta(i) - b_{i,K} - 1)!}{\sigma_i^{b_{i,K} - \delta(i) - N}} \\ & \times \sum_{s \in \mathbb{S}_0} \frac{(-1)^{|\boldsymbol{s}|} e^{-\Sigma \frac{1}{\sigma_{\boldsymbol{s}}} x} x^{\Sigma \boldsymbol{s}}}{\Pi \boldsymbol{s}! \ \cdot \ \Pi \sigma_{\boldsymbol{s}}^{\boldsymbol{s}}} \end{aligned} \tag{A.11}$$

Finally, equations (5.6) and (5.7) results after substituting (A.10) and (A.11), respectively, in (A.9) and integrate using [179, Eq. 3.351.3].

Appendix B

SCN Distribution for SU equipped with 3 antennas

Consider a SU equipped with only 3 antennas, then the CDF formulas of the SCN for this particular case under the hypotheses $\mathcal{H}_0$ and $\mathcal{H}_1$ are provided by the following theorems. In Theorem B.1, we derive the exact CDF expression for the SCN under $\mathcal{H}_0$ hypothesis. In Theorem B.2, we derive the approximation of the CDF for the SCN under $\mathcal{H}_1$ hypothesis using non-central/central approximation in Lemma 3.3.

Theorem B.1.

$$\begin{aligned} F_0(x) = K_{un}[&\delta_1(x, N-1, N+1, N-3) - \delta_1(x, N, N, N-3) + \\ &\delta_1(x, N-3, N-1, N+1) - \delta_1(x, N-2, N-2, N+1) - \\ &2\delta_1(x, N-2, N+1, N-2) + 2\delta_1(x, N-1, N, N-2) + \\ &2\delta_1(x, N-2, N, N-1) - 3\delta_1(x, N-1, N-1, N-1) + \\ &\delta_1(x, N-3, N+1, N-1) - 2\delta_1(x, N-3, N, N) + \\ &2\delta_1(x, N-1, N-2, N)] \end{aligned} \tag{B.1}$$

where K_{uc} and $\delta_1(x, L, M, P)$ are respectively given by:

$$K_{uc} = \frac{1}{2(N-1)!(N-2)!(N-3)!} \tag{B.2}$$

$$\delta_1(x, L, M, P) = L!M! \sum_{l=0}^{L} \sum_{m=0}^{M} [\frac{(\alpha-1)!}{l!m!}(\frac{1}{3^\alpha} - \frac{x^l + x^m}{(x+2)^\alpha} + \frac{x^{l+m}}{(2x+1)^\alpha})] \tag{B.3}$$

where $\alpha = l + m + P + 1$.

Proof. The proof could be summarized as follows:

1. Considering (3.14) and setting $K = 3$.
2. Expanding the summation and using (3.15).
3. Expanding the determinant and integrating using [179, Eqs. (3.351.1) and (3.351.3)].

Then the result comes after simplification. □

Theorem B.2. *The CDF of the SCN of a* 3×3 *central semi-correlated Wishart matrix* $\mathbf{W} \sim \mathcal{CW}_K(N, \mathbf{\Sigma}_3)$ *whose* $\mathbf{\Sigma}_3$ *has* 2 *equal eigenvalues* ($\sigma_1 > \sigma_2 = \sigma_3$) *is given by:*

$$F_1(x) = C_{sc}[R_1(N, x) - G_1(N, x)] \tag{B.4}$$

where $R_1(N, x)$ *is defined in (B.5),* $G_1(N, x)$ *in (B.6),* $S_1(r, s, t, \mu, \nu, x)$ *in (B.7),* $\Delta_1(r, s, t, \mu, \nu, \varepsilon, x)$ *in (B.8) and* C_{sc} *in (B.9).*

$$\begin{aligned} R_i(N, x) =& S_i(N-3, N, N-2, \sigma_1^{-1}, \sigma_2^{-1}, x) + S_i(N-2, N-2, N-1, \sigma_1^{-1}, \sigma_2^{-1}, x) \\ &+ S_i(N-1, N-1, N-3, \sigma_1^{-1}, \sigma_2^{-1}, x), \quad i = 1, 2 \end{aligned} \tag{B.5}$$

$$\begin{aligned} G_i(N, x) =& \Delta_i(N-2, N-1, N-2, \sigma_2^{-1}, \sigma_2^{-1}, \sigma_1^{-1}, x) \\ &+ \Delta_i(N-2, N, N-3, \sigma_2^{-1}, \sigma_2^{-1}, \sigma_1^{-1}, x) \\ &+ \Delta_i(N-3, N-1, N-1, \sigma_2^{-1}, \sigma_2^{-1}, \sigma_1^{-1}, x), \quad i = 1, 2 \end{aligned} \tag{B.6}$$

$$\begin{aligned} S_i(r, s, t, \mu, \nu, x) =& \Delta_i(r, s, t, \nu, \nu, \mu, x) + \Delta_i(t, r, s, \nu, \mu, \nu, x) - \Delta_i(r, t, s, \nu, \mu, \nu, x) \\ &- \Delta_i(r, s, t, \nu, \mu, \nu, x) + \Delta_i(t, s, r, \nu, \mu, \nu, x), \quad i = 1, 2 \end{aligned} \tag{B.7}$$

$$\Delta_1(r, s, t, \mu, \nu, \varepsilon, x) = -\mu^2 \Delta_3(r, s, t, \nu, \varepsilon, \mu, x) \tag{B.8}$$

$$C_{sc} = \frac{(\sigma_2 - \sigma_1)^{-2}}{(N-1)!(N-2)!(N-3)!\sigma_1^{N-2}\sigma_2^{2(N-2)}} \tag{B.9}$$

where Δ_3 *defined by:*

$$\begin{aligned} \Delta_3(r, s, t, \mu, \nu, \varepsilon, x) =& \left(\frac{r!s!}{\mu^{r+1}\varepsilon^{s+1}}\right) \sum_{k=0}^{r} \sum_{u=0}^{s} \left[\frac{(k+u+t)!}{k!u!\mu^{-k}\varepsilon^{-u}} \cdot \left(\frac{1}{(\mu+\varepsilon+\nu)^{k+u+t+1}}\right.\right. \\ &\left.\left. - \frac{x^u}{(\mu+\varepsilon x+\nu)^{k+u+t+1}} - \frac{x^k}{(\mu x+\varepsilon+\nu)^{k+u+t+1}} + \frac{x^{k+u}}{(\mu x+\varepsilon x+\nu)^{k+u+t+1}}\right)\right] \end{aligned} \tag{B.10}$$

Proof. The proof could be summarized as follows:

1. Considering (3.26) and setting $K = 3$.
2. Substituting the parameters from Lemma A.2.
3. Expanding the summation and using (3.28).
4. Expanding the determinant and integrating using [179, Eqs. (3.351.1) and (3.351.3)].

Then the result comes after simplification. □

It is worth mentionning that the PDF expressions are the derivative of the CDF expressions w.r.t x.

Appendix C

Generalized Extreme Value Distribution

Generalized Extreme Value (GEV) is a flexible 3-parameter distribution used to model the extreme events of a sequence of i.i.d random variables. The GEV parameters are the location parameter ($\mu \, \epsilon \, \mathbb{R}$), the scale parameter ($\sigma > 0$), and the shape parameter ($\xi \, \epsilon \, \mathbb{R}$). Various values of the shape parameter yield to a type of the extreme value distributions [218].

Let X be a GEV distributed random variable, then the CDF and the PDF of X are given by [218]:

$$F(x; \mu, \sigma, \xi) = e^{-t(x)}, \tag{C.1}$$

$$f(x; \mu, \sigma, \xi) = \frac{1}{\sigma} t(x)^{\xi+1} e^{-t(x)}, \tag{C.2}$$

with $t(x)$ given by (C.3).

$$t(x) = \begin{cases} e^{-\frac{x-\mu}{\sigma}} & \xi = 0 \\ (1 + (\frac{x-\mu}{\sigma})\xi)^{-1/\xi} & \xi \neq 0 \end{cases}. \tag{C.3}$$

The mean, variance and skewness of the X are given in Table C.1 where $g_k = \Gamma(1 - k\xi)$, γ is Euler's constant, and $\zeta(.)$ is the Riemann zeta function, with $\Gamma(.)$ is the gamma function [219].

Finding the inverse function of the skewness in Table C.1 is not straightforward, thus, applying non-linear least squares change this inversion into

Table C.1: Mean, Variance and Skewness for GEV

ξ	Mean (μ)	Variance (σ^2)	Skewness ($\mathcal{S}$)
< 0	$\delta - (1 - g_1)\frac{\beta}{\xi}$	$(g_2 - g_1^2)\frac{\beta^2}{\xi^2}$	$-\frac{g_3 - 3g_1g_2 + 2g_1^3}{(g_2 - g_1^2)^{3/2}}$
$= 0$	$\delta + \beta\gamma$	$\beta^2\frac{\pi^2}{6}$	$\frac{12\sqrt{6}\zeta(3)}{\pi^3}$
$]0, \frac{1}{2}[$	$\delta - (1 - g_1)\frac{\beta}{\xi}$	$(g_2 - g_1^2)\frac{\beta^2}{\xi^2}$	$\frac{g_3 - 3g_1g_2 + 2g_1^3}{(g_2 - g_1^2)^{3/2}}$
$[\frac{1}{2}, 1[$	$\delta - (1 - g_1)\frac{\beta}{\xi}$	∞	$\frac{g_3 - 3g_1g_2 + 2g_1^3}{(g_2 - g_1^2)^{3/2}}$
≥ 1	∞	∞	$\frac{g_3 - 3g_1g_2 + 2g_1^3}{(g_2 - g_1^2)^{3/2}}$

squared error minimization problem as follows:

$$\hat{\boldsymbol{\theta}} = \min_{\boldsymbol{\theta}} \sum_{i=1}^{d} (\xi_i - f(\mathcal{S}_{X,i}, \boldsymbol{\theta}))^2, \tag{C.4}$$

where $f(\mathcal{S}_{X,i}, \boldsymbol{\theta})$ is a pre-chosen inverse function and $\boldsymbol{\theta}$ is a vector of p parameters to be estimated. $(\mathcal{S}_{X,i}, \xi_i)$ are d data points calculated using the skewness in Table C.1.

Defining a proper inverse function and refining $\boldsymbol{\theta}$ iteratively for each interval[1], then the inverse of the skewness is given by (C.5). Accordingly, the inverse of the mean and variance are straightforward as provided by the following Lemma:

Lemma C.1. *Let X be a GEV random variable with mean, variance and skewness given by μ_X, σ_X^2 and $\mathcal{S}_X$ respectively. Then, the shape, scale and*

[1]We decompose ξ axis as follows: $\xi < -0.5$, $\xi \in [-0.5, 0[$, $\xi = 0$, and $\xi \in]0, \frac{1}{3}[$ and the resulting RMSE is of order 10^{-5}. However, for the interval $\xi < -0.5$, the error increases as ξ decreases.

location of X are given, respectively, by:

$$\xi = \begin{cases} a_1 \ln(b_1 \mathcal{S}_X^2 + c_1 \mathcal{S}_X + d_1) & \mathcal{S}_X < -0.63 \\ a_2 \mathcal{S}_X^2 + b_2 \mathcal{S}_X + c_2 & -0.63 \leq \mathcal{S}_X < 1.14 \\ 0 & \mathcal{S}_X = 1.14 \\ \frac{a_3 \mathcal{S}_X^2 + b_3 \mathcal{S}_X + c_3}{\mathcal{S}_X^2 + d_3 \mathcal{S}_X + e_3} & \mathcal{S}_X > 1.14 \end{cases} \tag{C.5}$$

$$\beta = \begin{cases} \sqrt{\frac{\sigma_X^2 \xi^2}{g_2 - g_1^2}} & \mathcal{S}_X \neq 1.14 \\ \frac{\sqrt{6\sigma_X^2}}{\pi} & \mathcal{S}_X = 1.14 \end{cases} \tag{C.6}$$

$$\delta = \begin{cases} \mu_X - \frac{(g_1 - 1)\sigma}{\xi} & \mathcal{S}_X \neq 1.14 \\ \mu_X - \sigma\gamma & \mathcal{S}_X = 1.14 \end{cases} \tag{C.7}$$

where the constants in (C.5) are given in Table C.2.

Table C.2: Constants of Eq. (C.5), Lemma C.1

i	a_i	b_i	c_i	d_i	e_i
1	−0.43544	2.3227	−0.97563	1.3781	–
2	−0.06393	0.3173	−0.2771	–	–
3	0.333	−0.09862	−0.3195	0.9553	1.599

Bibliography

[1] K. Patil, R. Prasad, and K. Skouby, "A survey of worldwide spectrum occupancy measurement campaigns for cognitive radio," in *Devices and Communications (ICDeCom), 2011 International Conference on*, pp. 1–5, Feb 2011.

[2] D. Datla, A. M. Wyglinski, and G. J. Minden, "A spectrum surveying framework for dynamic spectrum access networks," *IEEE Transactions on Vehicular Technology*, vol. 58, pp. 4158–4168, Oct 2009.

[3] K. Patil, K. E. Skouby, and R. Prasad, "Spectrum measurement and analysis of tv band support of cognitive radio operation in india," in *Wireless Communications, Vehicular Technology, Information Theory and Aerospace Electronic Systems (VITAE), 2013 3rd International Conference on*, pp. 1–5, June 2013.

[4] D. Das and S. Das, "A survey on spectrum occupancy measurement for cognitive radio," *Wireless Personal Communications*, vol. 85, no. 4, pp. 2581–2598, 2015.

[5] FCC, "Et docket no 02-135: spectrum policy task force report," Nov. 2002.

[6] FCC, "Et docket no. 03-108: Facilitating opportunities for flexible, efficient, and reliable spectrum use employing cognitive radio technologies," March 2005.

[7] L. Berlemann and S. Mangold, *Cognitive Radio and Dynamic Spectrum Access*. WILEY, 1st ed., 2009.

[8] Q. Zhao and B. M. Sadler, "A survey of dynamic spectrum access," *IEEE Signal Processing Magazine*, vol. 24, pp. 79–89, May 2007.

[9] J. Mitola and G. Q. Maguire, "Cognitive radio: making software radios more personal," *IEEE Personal Communications*, vol. 6, pp. 13–18, Aug 1999.

[10] B. Wang and K. J. R. Liu, "Advances in cognitive radio networks: A survey," *IEEE Journal of Selected Topics in Signal Processing*, vol. 5, pp. 5–23, Feb 2011.

[11] C. R. Stevenson, G. Chouinard, Z. Lei, W. Hu, S. J. Shellhammer, and W. Caldwell, "Ieee 802.22: The first cognitive radio wireless regional area network standard," *IEEE Communications Magazine*, vol. 47, pp. 130–138, January 2009.

[12] "Standard for cognitive wireless regional area networks (ran) for operation in tv bands," July 2011.

[13] ETSI-RRS, "Mobile broadband services in the 23002400 mhz frequency band under licensed shared access regime," tr 103.113, ETSI, 2013.

[14] ETSI-RRS, "System reference document; mobile broadband services in the 2300 mhz 2400 mhz frequency band under licensed shared access regime," ts 103.154, ETSI, 2014.

[15] ETSI-RRS, "System architecture and high level procedures for operation of licensed shared access (lsa) in the 2300 mhz-2400 mhz band," ts 103.235, ETSI, 2015.

[16] FCC, "Third memorandum opinion and order," *FCC 12-36*, April 2012.

[17] OFCOM, "Regulatory requirements for white space device in the uhf tv band," tech. rep., OFCOM, July 2012.

[18] C. S. Sum, G. P. Villardi, M. A. Rahman, T. Baykas, H. N. Tran, Z. Lan, C. Sun, Y. Alemseged, J. Wang, C. Song, C. W. Pyo, S. Filin, and H. Harada, "Cognitive communication in tv white spaces: An overview of regulations, standards, and technology [accepted from open call]," *IEEE Communications Magazine*, vol. 51, pp. 138–145, July 2013.

[19] M. Nekovee, "Cognitive radio access to tv white spaces: Spectrum opportunities, commercial applications and remaining technology challenges," in *New Frontiers in Dynamic Spectrum, 2010 IEEE Symposium on*, pp. 1–10, April 2010.

[20] T. Yucek and H. Arslan, "A survey of spectrum sensing algorithms for cognitive radio applications," *IEEE Communications Surveys Tutorials,*, vol. 11, no. 1, pp. 116–130, 2009.

[21] D. Cabric, A. Tkachenko, and R. W. Brodersen, "Spectrum sensing measurements of pilot, energy, and collaborative detection," in *MILCOM 2006 - 2006 IEEE Military Communications conference*, pp. 1–7, Oct 2006.

[22] S. P. Herath, N. Rajatheva, and C. Tellambura, "Energy detection of unknown signals in fading and diversity reception," *IEEE Transactions on Communications*, vol. 59, pp. 2443–2453, September 2011.

[23] C. H. Lim, "Adaptive energy detection for spectrum sensing in unknown white gaussian noise," *IET Communications*, vol. 6, pp. 1884–1889, Sept 2012.

[24] M. Gautier, V. Berg, and D. Noguet, "Wideband frequency domain detection using Teager-Kaiser energy operator," in *IEEE 5th International Conference on Cognitive Radio Oriented Wireless Networks and Communications (Crowncom'12)*, (Stockholm, Sweden), June 2012.

[25] J. Palicot and C. Roland, "A new concept for wireless reconfigurable receivers," *IEEE Communications Magazine*, vol. 41, pp. 124–132, July 2003.

[26] R. Chen and J. M. Park, "Ensuring trustworthy spectrum sensing in cognitive radio networks," in *Networking Technologies for Software Defined Radio Networks, 2006. SDR '06.1st IEEE Workshop on*, pp. 110–119, Sept 2006.

[27] Z. Khalaf, A. Nafkha, and J. Palicot, "Blind cyclostationary feature detector based on sparsity hypotheses for cognitive radio equipment," in *2011 IEEE 54th International Midwest Symposium on Circuits and Systems (MWSCAS)*, pp. 1–4, Aug 2011.

[28] Z. Khalaf, J. Palicot, A. Nafkha, and H. Zhang, "Blind free band detector based on the sparsity of the cyclic autocorrelation function," in *EUSIPCO*, (Morocco), Sep. 2013.

[29] M. Kosunen, V. Turunen, K. Kokkinen, and J. Ryynnen, "Survey and analysis of cyclostationary signal detector implementations on fpga," *IEEE Journal on Emerging and Selected Topics in Circuits and Systems*, vol. 3, pp. 541–551, Dec 2013.

[30] J. Riba, J. Font-Segura, J. Villares, and G. Vzquez, "Frequency-domain glr detection of a second-order cyclostationary signal over fading channels," *IEEE Transactions on Signal Processing*, vol. 62, pp. 1899–1912, April 2014.

[31] P. Urriza, E. Rebeiz, and D. Cabric, "Multiple antenna cyclostationary spectrum sensing based on the cyclic correlation significance test," *IEEE Journal on Selected Areas in Communications*, vol. 31, pp. 2185–2195, November 2013.

[32] R. Tandra and A. Sahai, "Fundamental limits on detection in low snr under noise uncertainty," in *in WirelessCom 2005, Maui, HI*, 2005.

[33] C. Jiang, Y. Li, W. Bai, Y. Yang, and J. Hu, "Statistical matched filter based robust spectrum sensing in noise uncertainty environment," in *Communication Technology (ICCT), 2012 IEEE 14th International Conference on*, pp. 1209–1213, Nov 2012.

[34] D. Bhargavi and C. R. Murthy, "Performance comparison of energy, matched-filter and cyclostationarity-based spectrum sensing," in *Signal Processing Advances in Wireless Communications (SPAWC), 2010 IEEE Eleventh International Workshop on*, pp. 1–5, June 2010.

[35] S. Kapoor, S. Rao, and G. Singh, "Opportunistic spectrum sensing by employing matched filter in cognitive radio network," in *Communication Systems and Network Technologies (CSNT), 2011 International Conference on*, pp. 580–583, June 2011.

[36] L. Cardoso, M. Debbah, P. Bianchi, and J. Najim, "Cooperative spectrum sensing using random matrix theory," in *in Proc. IEEE Int. Symp. Wireless Pervasive Comput. (ISWPC)*, (Greece), pp. 334–338, May 2008.

[37] F. Penna, R. Garello, and M. Spirito, "Cooperative spectrum sensing based on the limiting eigenvalue ratio distribution in wishart matrices," *IEEE Commun. Letters,*, vol. 13, pp. 507–509, July 2009.

[38] Y. Zeng and Y.-C. Liang, "Eigenvalue-based spectrum sensing algorithms for cognitive radio," *IEEE Trans. Commun.*, vol. 57, pp. 1784–1793, June 2009.

[39] R. Zhang, T. J. Lim, Y.-C. Liang, and Y. Zeng, "Multi-antenna based spectrum sensing for cognitive radios: A glrt approach," *IEEE Trans. Comm.*, vol. 58, pp. 84–88, January 2010.

[40] P. Bianchi, M. Debbah, M. Maida, and J. Najim, "Performance of statistical tests for single-source detection using random matrix theory," *IEEE Trans. Inform. Theory,*, vol. 57, pp. 2400–2419, April 2011.

[41] P. Wang, J. Fang, N. Han, and H. Li, "Multiantenna-assisted spectrum sensing for cognitive radio," *Vehicular Technology, IEEE Transactions on*, vol. 59, pp. 1791–1800, May 2010.

[42] B. Nadler, F. Penna, and R. Garello, "Performance of eigenvalue-based signal detectors with known and unknown noise level," in *Communications (ICC), 2011 IEEE International Conference on*, pp. 1–5, June 2011.

[43] L. Wei and O. Tirkkonen, "Spectrum sensing in the presence of multiple primary users," *IEEE Transactions on Communications*, vol. 60, pp. 1268–1277, May 2012.

[44] W. Zhang, G. Abreu, M. Inamori, and Y. Sanada, "Spectrum sensing algorithms via finite random matrices," *IEEE Trans. Commun.*, vol. 60, pp. 164–175, January 2012.

[45] A. M. Tulino and S. Verd?, *Random Matrix Theory and Wireless Communications*. now Publishers Inc., 2004.

[46] R. Couillet and M. Debbah, *Random Matrix Theory for Wireless Communications*. Cambridge University Press, Sep. 2011.

[47] H. Venkataraman and G.-M. Muntean, eds., *COGNITIVE RADIO AND ITS APPLICATION FOR NEXT GENERATION CELLULAR AND WIRELESS NETWORKS*. Springer, 2012.

[48] J. Neel, *Analysis and Design of Cognitive Radio Networks and Distributed Radio Resource Management Algorithms*. PhD thesis, Virginia Polytechnic Institute and State University, September 2006.

[49] R. S. Groups, "Working document towards a preliminary draft new report: Software defined radio in land mobile services (question 230-1/8)," Tech. Rep. 8A/121-E, ITU, Sept. 2004.

[50] I. Joseph Mitola, *Cognitive Radio Architecture: The Engineering Foundations of Radio XML*. 1st ed., Oct. 2006.

[51] A. L. Drozd, I. P. Kasperovich, C. E. Carroll, and A. C. Blackburn, "Computational electromagnetics applied to analyzing the efficient utilization of the rf transmission hyperspace," in *IEEE/ACES International Conference on Wireless Communications and Applied Computational Electromagnetics, 2005.*, pp. 1077–1085, April 2005.

[52] A. Gorcin and H. Arslan, "Signal identification for adaptive spectrum hyperspace access in wireless communications systems," *CoRR*, vol. abs/1501.05819, 2015.

[53] "Multiple access techniques: Fdma, tdma, cdma; system capacity comparisons," in *Mobile Wireless Communications:* (M. Schwartz, ed.), pp. 137–160, Cambridge: Cambridge University Press, 12 2004.

[54] N. Seifi, R. W. Heath, M. Coldrey, and T. Svensson, "Adaptive multicell 3-d beamforming in multiantenna cellular networks," *IEEE Transactions on Vehicular Technology*, vol. 65, pp. 6217–6231, Aug 2016.

[55] B. Cao, H. Liang, J. W. Mark, and Q. Zhang, "Exploiting orthogonally dual-polarized antennas in cooperative cognitive radio networking," *IEEE Journal on Selected Areas in Communications*, vol. 31, pp. 2362–2373, November 2013.

[56] Q. Zhang, B. Cao, Y. Wang, N. Zhang, X. Lin, and L. Sun, "On exploiting polarization for energy-harvesting enabled cooperative cognitive radio networking," *IEEE Wireless Communications*, vol. 20, pp. 116–124, August 2013.

[57] D. N. Hatfield and P. J. Weiser, "Property rights in spectrum: taking the next step," in *First IEEE International Symposium on New Frontiers in Dynamic Spectrum Access Networks, 2005. DySPAN 2005.*, pp. 43–55, Nov 2005.

[58] L. Xu, R. Tonjes, T. Paila, W. Hansmann, M. Frank, and M. Albrecht, "Drive-ing to the internet: Dynamic radio for ip services in vehicular environments," in *Local Computer Networks, 2000. LCN 2000. Proceedings. 25th Annual IEEE Conference on*, pp. 281–289, 2000.

[59] R. Etkin, A. Parekh, and D. Tse, "Spectrum sharing for unlicensed bands," *IEEE Journal on Selected Areas in Communications*, vol. 25, pp. 517–528, April 2007.

[60] W. Lehr and J. Crowcroft, "Managing shared access to a spectrum commons," in *First IEEE International Symposium on New Frontiers in Dynamic Spectrum Access Networks, 2005. DySPAN 2005.*, pp. 420–444, Nov 2005.

[61] A. Goldsmith, S. A. Jafar, I. Maric, and S. Srinivasa, "Breaking spectrum gridlock with cognitive radios: An information theoretic perspective," *Proceedings of the IEEE*, vol. 97, pp. 894–914, May 2009.

[62] FCC, "Establishment of an interference temperature metric to quantify and manage interference and to expand available unlicensed operation in certain fixed, mobile and satellite frequency bands," *FCC 03-289*, November 2003.

[63] H. Du, T. Ratnarajah, M. Pesavento, and C. B. Papadias, "Joint transceiver beamforming in mimo cognitive radio network via second-order cone programming," *IEEE Transactions on Signal Processing*, vol. 60, pp. 781–792, Feb 2012.

[64] M. Vu, N. Devroye, and V. Tarokh, "On the primary exclusive region of cognitive networks," *IEEE Transactions on Wireless Communications*, vol. 8, pp. 3380–3385, July 2009.

[65] Z. Wei, Z. Feng, Q. Zhang, and W. Li, "Three regions for space-time spectrum sensing and access in cognitive radio networks," *IEEE Transactions on Vehicular Technology*, vol. 64, pp. 2448–2462, June 2015.

[66] S. Chatzinotas and B. Ottersten, "Cognitive interference alignment between small cells and a macrocell," in *Telecommunications (ICT), 2012 19th International Conference on*, pp. 1–6, April 2012.

[67] S. A. Jafar, *Interference Alignment: A New Look at Signal Dimensions in a Communication Network*. Now Publishers Inc, 2011.

[68] M. Chiani and A. Giorgetti, "Coexistence between uwb and narrowband wireless communication systems," *Proceedings of the IEEE*, vol. 97, pp. 231–254, Feb 2009.

[69] J. Sachs, I. Maric, and A. Goldsmith, "Cognitive cellular systems within the tv spectrum," in *New Frontiers in Dynamic Spectrum, 2010 IEEE Symposium on*, pp. 1–12, April 2010.

[70] T. Fujii and Y. Suzuki, "Ad-hoc cognitive radio - development to frequency sharing system by using multi-hop network," in *First IEEE International Symposium on New Frontiers in Dynamic Spectrum Access Networks, 2005. DySPAN 2005.*, pp. 589–592, Nov 2005.

[71] M. M. Buddhikot, P. Kolodzy, S. Miller, K. Ryan, and J. Evans, "Dimsumnet: new directions in wireless networking using coordinated dynamic spectrum," in *Sixth IEEE International Symposium on a World of Wireless Mobile and Multimedia Networks*, pp. 78–85, June 2005.

[72] A. P. Hulbert, "Spectrum sharing through beacons," in *2005 IEEE 16th International Symposium on Personal, Indoor and Mobile Radio Communications*, vol. 2, pp. 989–993 Vol. 2, Sept 2005.

[73] S. Mangold, A. Jarosch, and C. Monney, "Operator assisted cognitive radio and dynamic spectrum assignment with dual beacons - detailed evaluation," in *2006 1st International Conference on Communication Systems Software Middleware*, pp. 1–6, 2006.

[74] ITU, "Introduction to cognitive radio systems in the land mobile service.," techreport, International Telecommunication Union., 2011.

[75] O. Sallent, J. Perez-Romero, R. Agusti, and P. Cordier, "Cognitive pilot channel enabling spectrum awareness," in *2009 IEEE International Conference on Communications Workshops*, pp. 1–6, June 2009.

[76] M. Filo, A. Hossain, A. R. Biswas, and R. Piesiewicz, "Cognitive pilot channel: Enabler for radio systems coexistence," in *Cognitive Radio and Advanced Spectrum Management, 2009. CogART 2009. Second International Workshop on*, pp. 17–23, May 2009.

[77] ETSI, "Reconfigurable radio systems (rrs); cognitive pilot channel (cpc)," techreport 102 683, European Telecommunications Standards Institute, 2009.

[78] P. Cordier, P. Houze, S. B. Jemaa, O. Simon, D. Bourse, D. Grandblaise, K. Moessner, J. Luo, C. Kloeck, K. Tsagkaris, R. Agusti, N. Olaziregi, Z. Boufidis, E. Buracchini, P. Goria, and A. Trogolo, "E2r cognitive pilot channel concept," in *15th IST Mobile and Wireless Communications Summit*, (Mykonos, Greece), June 2006.

[79] FCC, "Second report and order and memorandum opinion and order," *FCC 08-260*, November 2008.

[80] OFCOM, "Implementing geolocation," tech. rep., OFCOM, September 2011.

[81] V. Chen, S. Das, L. Zhu, J. Malyar, and P. McCann, "Protocol to access white-space (paws) databases," *Internet Engineering Task Force (IETF)*, May 2015.

[82] T. X. Brown, "An analysis of unlicensed device operation in licensed broadcast service bands," in *First IEEE International Symposium on New Frontiers in Dynamic Spectrum Access Networks, 2005. DySPAN 2005.*, pp. 11–29, Nov 2005.

[83] S. Mangold, Z. Zhong, K. Challapali, and C.-T. Chou, "Spectrum agile radio: radio resource measurements for opportunistic spectrum usage," in *Global Telecommunications Conference, 2004. GLOBECOM '04. IEEE*, vol. 6, pp. 3467–3471 Vol.6, Nov 2004.

[84] B. Wild and K. Ramchandran, "Detecting primary receivers for cognitive radio applications," in *First IEEE International Symposium on New Frontiers in Dynamic Spectrum Access Networks, 2005. DySPAN 2005.*, pp. 124–130, Nov 2005.

[85] T. C. Clancy, "Formalizing the interference temperature model," *Wireless Communications and Mobile Computing*, vol. 7, no. 9, pp. 1077–1086, 2007.

[86] S. M. Kay, *Fundamentals of Statistical Signal Processing: Detection Theory*. Prentice Hall, 1st ed., 1998.

[87] H. Sun, A. Nallanathan, C. X. Wang, and Y. Chen, "Wideband spectrum sensing for cognitive radio networks: a survey," *IEEE Wireless Communications*, vol. 20, pp. 74–81, April 2013.

[88] E. Axell, G. Leus, E. G. Larsson, and H. V. Poor, "Spectrum sensing for cognitive radio : State-of-the-art and recent advances," *IEEE Signal Processing Magazine*, vol. 29, pp. 101–116, May 2012.

[89] R. Umar and A. U. Sheikh, "A comparative study of spectrum awareness techniques for cognitive radio oriented wireless networks," *Physical Communication*, vol. 9, pp. 148 – 170, 2013.

[90] H. Urkowitz, "Energy detection of unknown deterministic signals," *Proceedings of the IEEE*, vol. 55, pp. 523–531, April 1967.

[91] A. Mariani, A. Giorgetti, and M. Chiani, "Effects of noise power estimation on energy detection for cognitive radio applications," *IEEE Transactions on Communications*, vol. 59, pp. 3410–3420, December 2011.

[92] M. Gautier, M. Laugeois, and D. Noguet, "Teager-kaiser energy detector for narrowband wireless microphone spectrum sensing," in *2010 Proceedings of the Fifth International Conference on Cognitive Radio Oriented Wireless Networks and Communications*, pp. 1–5, June 2010.

[93] G. Taricco, "On the accuracy of the gaussian approximation with linear cooperative spectrum sensing over rician fading channels," *IEEE Signal Processing Letters*, vol. 17, pp. 651–654, July 2010.

[94] J. J. Lehtomaki, M. Juntti, H. Saarnisaari, and S. Koivu, "Threshold setting strategies for a quantized total power radiometer," *IEEE Signal Processing Letters*, vol. 12, pp. 796–799, Nov 2005.

[95] R. Tandra and A. Sahai, "Snr walls for signal detection," *IEEE Journal of Selected Topics in Signal Processing*, vol. 2, pp. 4–17, Feb 2008.

[96] S. Bahamou and A. Nafkha, "Noise uncertainty analysis of energy detector: Bounded and unbounded approximation relationship," in *21st European Signal Processing Conference (EUSIPCO 2013)*, pp. 1–4, Sept 2013.

[97] Z. Ye, G. Memik, and J. Grosspietsch, "Energy detection using estimated noise variance for spectrum sensing in cognitive radio networks," in *2008 IEEE Wireless Communications and Networking Conference*, pp. 711–716, March 2008.

[98] Z. Khalaf, A. Nafkha, and J. Palicot, "Enhanced hybrid spectrum sensing architecture for cognitive radio equipment," in *General Assembly and Scientific Symposium, 2011 XXXth URSI*, pp. 1–4, Aug 2011.

[99] H. Teager, "Some observations on oral air flow during phonation," *IEEE Transactions on Acoustics, Speech, and Signal Processing*, vol. 28, pp. 599–601, Oct 1980.

[100] J. F. Kaiser, "On a simple algorithm to calculate the 'energy' of a signal," in *Acoustics, Speech, and Signal Processing, 1990. ICASSP-90., 1990 International Conference on*, pp. 381–384 vol.1, Apr 1990.

[101] D. Dimitriadis, A. Potamianos, and P. Maragos, "A comparison of the squared energy and teager-kaiser operators for short-term energy estimation in additive noise," *IEEE Transactions on Signal Processing*, vol. 57, pp. 2569–2581, July 2009.

[102] W. A. Gardner, "Exploitation of spectral redundancy in cyclostationary signals," *IEEE Signal Processing Magazine*, vol. 8, pp. 14–36, April 1991.

[103] D. Cabric, S. M. Mishra, and R. W. Brodersen, "Implementation issues in spectrum sensing for cognitive radios," in *Signals, Systems and Computers, 2004. Conference Record of the Thirty-Eighth Asilomar Conference on*, vol. 1, pp. 772–776, Nov 2004.

[104] A. Fehske, J. Gaeddert, and J. H. Reed, "A new approach to signal classification using spectral correlation and neural networks," in *First*

IEEE International Symposium on New Frontiers in Dynamic Spectrum Access Networks, 2005. DySPAN 2005., pp. 144–150, Nov 2005.

[105] G. Huang and J. K. Tugnait, "On cyclostationarity based spectrum sensing under uncertain gaussian noise," *IEEE Transactions on Signal Processing*, vol. 61, pp. 2042–2054, April 2013.

[106] L. Safatly, B. Aziz, A. Nafkha, Y. Louet, Y. Nasser, A. El-Hajj, and K. Y. Kabalan, "Blind spectrum sensing using symmetry property of cyclic autocorrelation function: from theory to practice," *EURASIP Journal on Wireless Communications and Networking*, vol. 2014, no. 1, pp. 1–13, 2014.

[107] Y. Li and S. K. Jayaweera, "Dynamic spectrum tracking using energy and cyclostationarity-based multi-variate non-parametric quickest detection for cognitive radios," *IEEE Transactions on Wireless Communications*, vol. 12, pp. 3522–3532, July 2013.

[108] Y. Zeng and Y. C. Liang, "Robustness of the cyclostationary detection to cyclic frequency mismatch," in *21st Annual IEEE International Symposium on Personal, Indoor and Mobile Radio Communications*, pp. 2704–2709, Sept 2010.

[109] L. Ma, Y. Li, and A. Demir, "Matched filtering assisted energy detection for sensing weak primary user signals," in *2012 IEEE International Conference on Acoustics, Speech and Signal Processing (ICASSP)*, pp. 3149–3152, March 2012.

[110] M. Iqbal and A. Ghafoor, "Analysis of multiband joint detection framework for waveform-based sensing in cognitive radios," in *Vehicular Technology Conference (VTC Fall), 2012 IEEE*, pp. 1–5, Sept 2012.

[111] G. Vazquez-Vilar, R. Lopez-Valcarce, and J. Sala, "Multiantenna spectrum sensing exploiting spectral a priori information," *IEEE Transactions on Wireless Communications*, vol. 10, pp. 4345–4355, December 2011.

[112] S. Bokharaiee, H. H. Nguyen, and E. Shwedyk, "Blind spectrum sensing for ofdm-based cognitive radio systems," *IEEE Transactions on Vehicular Technology*, vol. 60, pp. 858–871, March 2011.

[113] H. s. Chen, W. Gao, and D. G. Daut, "Spectrum sensing for ofdm systems employing pilot tones," *IEEE Transactions on Wireless Communications*, vol. 8, pp. 5862–5870, December 2009.

[114] A. Sahai, R. Tandra, S. M. Mishra, and N. Hoven, "Fundamental design tradeoffs in cognitive radio systems," in *Proceedings of the First International Workshop on Technology and Policy for Accessing Spectrum*, TAPAS '06, (New York, NY, USA), ACM, 2006.

[115] Y. Zeng and Y. C. Liang, "Spectrum-sensing algorithms for cognitive radio based on statistical covariances," *IEEE Transactions on Vehicular Technology*, vol. 58, pp. 1804–1815, May 2009.

[116] M. Jin, Y. Li, and H. G. Ryu, "On the performance of covariance based spectrum sensing for cognitive radio," *IEEE Transactions on Signal Processing*, vol. 60, pp. 3670–3682, July 2012.

[117] C. Zhong, M. R. McKay, T. Ratnarajah, and K. K. Wong, "Distribution of the demmel condition number of wishart matrices," *IEEE Transactions on Communications*, vol. 59, pp. 1309–1320, May 2011.

[118] E. J. Candes and M. B. Wakin, "An introduction to compressive sampling," *IEEE Signal Processing Magazine*, vol. 25, pp. 21–30, March 2008.

[119] J. Fang, J. Li, Y. Shen, H. Li, and S. Li, "Super-resolution compressed sensing: An iterative reweighted algorithm for joint parameter learning and sparse signal recovery," *IEEE Signal Processing Letters*, vol. 21, pp. 761–765, June 2014.

[120] F. Fazel, M. Fazel, and M. Stojanovic, "Random access compressed sensing over fading and noisy communication channels," *IEEE Transactions on Wireless Communications*, vol. 12, pp. 2114–2125, May 2013.

[121] Y. Kim, M. S. Nadar, and A. Bilgin, "Wavelet-based compressed sensing using a gaussian scale mixture model," *IEEE Transactions on Image Processing*, vol. 21, pp. 3102–3108, June 2012.

[122] A. M. Madni, "A systems perspective on compressed sensing and its use in reconstructing sparse networks," *IEEE Systems Journal*, vol. 8, pp. 23–27, March 2014.

[123] X. Yang, X. Tao, E. Dutkiewicz, X. Huang, Y. J. Guo, and Q. Cui, "Energy-efficient distributed data storage for wireless sensor networks based on compressed sensing and network coding," *IEEE Transactions on Wireless Communications*, vol. 12, pp. 5087–5099, October 2013.

[124] Z. Tian and G. B. Giannakis, "A wavelet approach to wideband spectrum sensing for cognitive radios," in *2006 1st International Conference on Cognitive Radio Oriented Wireless Networks and Communications*, pp. 1–5, June 2006.

[125] B. Farhang-Boroujeny and R. Kempter, "Multicarrier communication techniques for spectrum sensing and communication in cognitive radios," *IEEE Communications Magazine*, vol. 46, pp. 80–85, April 2008.

[126] T. Erpek, A. Leu, and B. L. Mark, "Spectrum sensing performance in tv bands using the multitaper method," in *2007 IEEE 15th Signal Processing and Communications Applications*, pp. 1–4, June 2007.

[127] Q. T. Zhang, "Theoretical performance and thresholds of the multitaper method for spectrum sensing," *IEEE Transactions on Vehicular Technology*, vol. 60, pp. 2128–2138, Jun 2011.

[128] X. Liu, X. Tan, and A. A. Anghuwo, "Spectrum detection of cognitive radio based on blind signal separation," in *Information, Computing and Telecommunication, 2009. YC-ICT '09. IEEE Youth Conference on*, pp. 166–169, Sept 2009.

[129] C. han Lee and W. Wolf, "Blind signal separation for cognitive radio," *Journal of Signal Processing Systems*, vol. 63, pp. 67–81, April 2011.

[130] N. Khajavi, S. Sadeghi, and S. Sadough, "An improved blind spectrum sensing technique for cognitive radio systems," in *5th International Symposium on Telecommunications*, pp. 13–17, December 2010.

[131] F. Benedetto, G. Giunta, E. Guzzon, and M. Renfors, "Effective monitoring of freeloading user in the presence of active user in cognitive

radio networks," *IEEE Transactions on Vehicular Technology*, vol. 63, pp. 2443–2450, Jun 2014.

[132] T. E. Bogale and L. Vandendorpe, "Moment based spectrum sensing algorithm for cognitive radio networks with noise variance uncertainty," in *Information Sciences and Systems (CISS), 2013 47th Annual Conference on*, pp. 1–5, March 2013.

[133] K. Cao and H. Shao, "Compressive wideband spectrum sensing using high-order statistics for cognitive radio," in *Global High Tech Congress on Electronics (GHTCE), 2013 IEEE*, pp. 187–190, Nov 2013.

[134] X. Chen, H. H. Chen, and W. Meng, "Cooperative communications for cognitive radio networks - from theory to applications," *IEEE Communications Surveys Tutorials*, vol. 16, pp. 1180–1192, Third 2014.

[135] I. F. Akyildiz, B. F. Lo, and R. Balakrishnan, "Cooperative spectrum sensing in cognitive radio networks: A survey," *Phys. Commun.*, vol. 4, pp. 40–62, Mar. 2011.

[136] I. F. Akyildiz, W.-Y. Lee, M. C. Vuran, and S. Mohanty, "Next generation/dynamic spectrum access/cognitive radio wireless networks: A survey," *COMPUTER NETWORKS JOURNAL (ELSEVIER*, vol. 50, pp. 2127–2159, 2006.

[137] E. G. Larsson and P. Stoica, *Space-Time Block Coding for Wireless Communications*. Cambridge University Press, 2008.

[138] R. Zhang and Y. C. Liang, "Exploiting multi-antennas for opportunistic spectrum sharing in cognitive radio networks," *IEEE Journal of Selected Topics in Signal Processing*, vol. 2, pp. 88–102, Feb 2008.

[139] L. Bixio, G. Oliveri, M. Ottonello, M. Raffetto, and C. S. Regazzoni, "Cognitive radios with multiple antennas exploiting spatial opportunities," *IEEE Transactions on Signal Processing*, vol. 58, pp. 4453–4459, Aug 2010.

[140] H. Sarvanko, M. Hyhty, M. Matinmikko, and A. Mmmel, "Exploiting spatial dimension in cognitive radios and networks," in *2011 6th International ICST Conference on Cognitive Radio Oriented Wireless Networks and Communications (CROWNCOM)*, pp. 360–364, June 2011.

[141] H. Islam, Y. c. Liang, and A. T. Hoang, "Joint power control and beamforming for cognitive radio networks," *IEEE Transactions on Wireless Communications*, vol. 7, pp. 2415–2419, July 2008.

[142] R. Zhang, F. Gao, and Y. C. Liang, "Cognitive beamforming made practical: Effective interference channel and learning-throughput tradeoff," in *2009 IEEE 10th Workshop on Signal Processing Advances in Wireless Communications*, pp. 588–592, June 2009.

[143] T. Chen, H. Yuan, T. Zhao, Z. Zhang, and X. Ao, "Joint beamforming and power allocation for secure communication in cognitive radio networks," *IET Communications*, vol. 10, no. 10, pp. 1156–1162, 2016.

[144] A. Pandharipande and J. P. M. G. Linnartz, "Performance analysis of primary user detection in a multiple antenna cognitive radio," in *2007 IEEE International Conference on Communications*, pp. 6482–6486, June 2007.

[145] J. Ma and Y. G. Li, "Soft combination and detection for cooperative spectrum sensing in cognitive radio networks," in *IEEE GLOBECOM 2007 - IEEE Global Telecommunications Conference*, pp. 3139–3143, Nov 2007.

[146] S. H. Hwang, J. H. Baek, and O. A. Dobre, "Spectrum sensing using multiple antenna-aided energy detectors for cognitive radio," in *Electrical and Computer Engineering, 2009. CCECE '09. Canadian Conference on*, pp. 209–212, May 2009.

[147] C. Tepedelenlioglu and R. Challagulla, "Low-complexity multipath diversity through fractional sampling in ofdm," *IEEE Transactions on Signal Processing*, vol. 52, pp. 3104–3116, Nov 2004.

[148] H. Nishimura, M. Inamori, and Y. Sanada, "Sampling rate selection for fractional sampling in ofdm," in *2007 IEEE 18th International Symposium on Personal, Indoor and Mobile Radio Communications*, pp. 1–5, Sept 2007.

[149] B. Li, Q. Wang, G. Lu, Y. Chang, and D. Yang, "Linear mmse frequency domain equalization with colored noise," in *2007 IEEE 66th Vehicular Technology Conference*, pp. 1152–1156, Sept 2007.

[150] O. Tirkkonen and L. Wei, *Foundation of Cognitive Radio Systems*, ch. Exact and Asymptotic Analysis of Largest Eigenvalue Based Spectrum Sensing. InTech, 2012.

[151] L. Wei and O. Tirkkonen, "Cooperative spectrum sensing of ofdm signals using largest eigenvalue distributions," in *IEEE 20th International Symposium on Personal, Indoor and Mobile Radio Communications,*, pp. 2295–2299, Sept 2009.

[152] J. W. Mauchly, "Significance test for sphericity of a normal n-variate distribution," *The Annals of Mathematical Statistics*, vol. 11, pp. 204–209, June 1940.

[153] S. John, "Some optimal multivariate tests," *Biometrika*, vol. 58, no. 1, 1971.

[154] S. Qin, W. Zhang, H. Xiong, and D. Chen, "Cooperative spectrum sensing using finite demmel condition numbers," *Wireless Personal Communications*, vol. 80, no. 1, pp. 335–346, 2015.

[155] J. W. Demmel, "The probability that a numerical analysis problem is difficult," *Mathematics of Computation*, vol. 50, pp. 449–480, APRIL 1988.

[156] L. Wei, M. R. McKay, and O. Tirkkonen, "Exact demmel condition number distribution of complex wishart matrices via the mellin transform," *IEEE Communications Letters*, vol. 15, pp. 175–177, February 2011.

[157] M. Matthaiou, M. McKay, P. Smith, and J. Nossek, "On the condition number distribution of complex wishart matrices," *IEEE Trans. Commun.*, vol. 58, pp. 1705–1717, June 2010.

[158] A. Edelman, "On the distribution of a scaled condition number," *Mathematics of Computation*, vol. 58, pp. 185–190, 1992.

[159] H. Artes, D. Seethaler, and F. Hlawatsch, "Efficient detection algorithms for mimo channels: a geometrical approach to approximate ml detection," *IEEE Trans. Signal Processing*, vol. 51, pp. 2808–2820, Nov 2003.

[160] D. Wubben, R. Bohnke, V. Kuhn, and K. Kammeyer, "Mmse-based lattice-reduction for near-ml detection of mimo systems," in *in Proc. ITG Work. Smart Antennas (WSA)*, (Germany), pp. 106–113, March 2004.

[161] J. Maurer, G. Matz, and D. Seethaler, "Low-complexity and full-diversity mimo detection based on condition number thresholding," in *IEEE Int. Conf. A.S.S.P.*, vol. 3, pp. 61–64, April 2007.

[162] M. Batariere, T. Blankenship, J. Kepler, T. Krauss, I. Lisica, S. Mukthavaram, J. Porter, T. Thomas, and F. W. Vook, "Wideband mimo mobile impulse response measurements at 3.7 ghz," in *in Proc. 55th IEEE Veh. Tech. Conf. (VTC)*, vol. 1, pp. 26–30, 2002.

[163] V. Erceg, P. Soma, D. Baum, and A. J. Paulraj, "Capacity obtained from multiple-input multiple-output channel measurements in fixed wireless environments at 2.5 ghz," in *in Proc. IEEE Int. Conf. Commun. (ICC)*, vol. 1, (New York), pp. 396–400, May 2002.

[164] E. Telatar, "Capacity of multi-antenna gaussian channels," *European Trans. Telecom.*, vol. 10, no. 6, pp. 585–595, 1999.

[165] G. Alfano, A. Lozano, A. M. Tulino, and S. Verdú, "Mutual information and eigenvalue distribution of mimo ricean channels," in *In Proc. Int. Sym. Inf. Theory Applic.*, (Italy), Oct. 2004.

[166] X. Cui, Q. Zhang, and Z. Feng, "Generic procedure for tightly bounding the capacity of mimo correlated rician fading channels," *IEEE Trans. Commun.*, vol. 53, pp. 890–898, May 2005.

[167] M. Kang and M.-S. Alouini, "Capacity of mimo rician channels," *IEEE Trans. Wireless Commun.*, vol. 5, pp. 112–122, Jan 2006.

[168] M. McKay and I. Collings, "General capacity bounds for spatially correlated rician mimo channels," *IEEE Trans. Inform. Theory*, vol. 51, pp. 3121–3145, Sept 2005.

[169] H. Shin, M. Win, J. H. Lee, and M. Chiani, "On the capacity of doubly correlated mimo channels," *IEEE Trans. Wireless Commun.*, vol. 5, pp. 2253–2265, Aug 2006.

[170] A. Maaref and S. Aissa, "Joint and marginal eigenvalue distributions of (non)central complex wishart matrices and pdf-based approach for characterizing the capacity statistics of mimo ricean and rayleigh fading channels," *IEEE Trans. Wireless Commun.*, vol. 6, pp. 3607–3619, October 2007.

[171] A. Zanella, M. Chiani, and M. Win, "A general framework for the distribution of the eigenvalues of wishart matrices," in *In Proc. IEEE Intern. Conf. Commun.*, pp. 1271–1276, May 2008.

[172] S. Jin, X. Gao, and M. McKay, "Ordered eigenvalues of complex noncentral wishart matrices and performance analysis of svd mimo systems," in *In Proc. IEEE Inter. Symp. Inform. Theory*, pp. 1564–1568, July 2006.

[173] L. Ordonez, D. Palomar, and J. Fonollosa, "Ordered eigenvalues of a general class of hermitian random matrices with application to the performance analysis of mimo systems," *IEEE Trans. Signal Processing*, vol. 57, pp. 672–689, Feb 2009.

[174] A. Zanella, M. Chiani, and M. Win, "Mmse reception and successive interference cancellation for mimo systems with high spectral efficiency," *IEEE Trans. Wireless Commun.*, vol. 4, pp. 1244–1253, May 2005.

[175] A. T. James, "Distributions of matrix variates and latent roots derived from normal samples," *The Annals of Mathematical Statistics*, vol. 35, pp. 475–501, June 1964.

[176] M. Chiani, M. Z. Win, and A. Zanella, "On the capacity of spatially correlated mimo rayleigh-fading channels," *IEEE Trans. Inform. Theory*, vol. 49, pp. 2363–2371, Oct. 2003.

[177] M. Kang and M.-S. Alouini, "Largest eigenvalue of complex wishart matrices and performance analysis of mimo mrc systems," *IEEE J. Select. Areas Commun.*, vol. 21, pp. 418–426, Apr 2003.

[178] A. Zanella, M. Chiani, and M. Win, "On the marginal distribution of the eigenvalues of wishart matrices," *IEEE Trans. Commun.*, vol. 57, pp. 1050–1060, April 2009.

[179] I. S. Gradshteyn and I. M. Ryzhik, *Table of Integrals, Series, and Products*. ELSEVIER, seventh ed., 2007.

[180] S. Jin, M. McKay, X. Gao, and I. Collings, "Mimo multichannel beamforming: Ser and outage using new eigenvalue distributions of complex noncentral wishart matrices," *IEEE Trans. Commun.*, vol. 56, pp. 424–434, March 2008.

[181] M. K. Simon, "The nuttall q function - its relation to the marcum q function and its application in digital communication performance evaluation," *IEEE Transactions on Communications,*, vol. 50, pp. 1712–1715, Nov 2002.

[182] M. Matthaiou, D. Laurenson, and C.-X. Wang, "On analytical derivations of the condition number distributions of dual non-central wishart matrices," *IEEE Trans. Wireless Commun.*, vol. 8, pp. 1212–1217, March 2009.

[183] W. Y. Tan and R. P. Gupta, "On approximating the non-central wishart distribution with wishart distribution," *Commun. Stat. Theory Method*, vol. 12, no. 22, pp. 2589–2600, 1983.

[184] A. Zanella, M. Chiani, and M. Win, "Performance of mimo mrc in correlated rayleigh fading environments," in *in Proc. IEEE Veh. Technol. Conf. (VTC)*, vol. 3, pp. 1633–1637, May 2005.

[185] V. A. Marcenko and L. A. Pastur, "Distribution of eigenvalues for some sets of random matrices," *Mathematics of the USSR-Sbornik*, vol. 1, pp. 457–483, April 1967.

[186] C. A. Tracy and H. Widom, "On orthogonal and symplectic matrix ensembles," *Comm. Math. Phys.*, vol. 177, no. 3, pp. 727–754, 1996.

[187] M. Johnstone, "On the distribution of the largest eigenvalue in principal components analysis," *Ann. Statist*, vol. 29, pp. 295–327, 2001.

[188] F. Penna, R. Garello, D. Figlioli, and M. Spirito, "Exact non-asymptotic threshold for eigenvalue-based spectrum sensing," in *in Proc. IEEE 4th Int. Conf. CROWNCOM*, (Germany), pp. 1–5, June 2009.

[189] J. H. Curtiss, "On the distribution of the quotient of two chance variables," *Ann. Math. Statist.*, vol. 12, pp. 409–421, 12 1941.

[190] O. N. Feldheim and S. Sodin, "A universality result for the smallest eigenvalues of certain sample covariance matrices," *Geometric and Functional Analysis*, vol. 20, no. 1, pp. 88–123, 2010.

[191] F. Penna, R. Garello, and M. Spirito, "Probability of missed detection in eigenvalue ratio spectrum sensing," in *Wireless and Mobile Computing, Networking and Communications, 2009. WIMOB 2009. IEEE International Conference on*, pp. 117–122, Oct 2009.

[192] K. Johansson, "Shape fluctuations and random matrices," *Comm. Math. Phys.*, vol. 209, no. 2, pp. 437–476, 2000.

[193] F. Bornemann, "On the numerical evaluation of distributions in random matrix theory: A review with an invitation to experimental mathematics," *Markov Processes Relat. Fields*, vol. 16, pp. 803–866, 2009.

[194] J. Baik, G. Ben Arous, and S. Pch, "Phase transition of the largest eigenvalue for nonnull complex sample covariance matrices," *Ann. Probab.*, vol. 33, pp. 1643–1697, 09 2005.

[195] J. Baik and J. W. Silverstein, "Eigenvalues of large sample covariance matrices of spiked population models," *Journal of Multivariate Analysis*, vol. 97, no. 6, pp. 1382–1408, 2006.

[196] S. Kritchman and B. Nadler, "Determining the number of components in a factor model from limited noisy data," *Chemometrics and Intelligent Laboratory Systems*, vol. 94, pp. 19–32, 2008.

[197] F. Bornemann, "Asymptotic independence of the extreme eigenvalues of gaussian unitary ensemble," *Journal of Mathematical Physics*, vol. 51, 2009.

[198] A. Hachem, Walid; Hardy and J. Najim, "A survey on the eigenvalues local behavior of large complex correlated wishart matrices," *ARXIV*, 09 2015. to be published in the "Proceedings of the Journées MAS 2014".

[199] P. Bianchi, J. Najim, G. Alfano, and M. Debbah, "Asymptotics of eigenbased collaborative sensing," in *IEEE Information Theory Workshop (ITW'09),*, pp. 515–519, Oct 2009.

[200] O. Besson and L. Scharf, "Cfar matched direction detector," *Signal Processing, IEEE Transactions on*, vol. 54, pp. 2840–2844, July 2006.

[201] D. E. Johnson and F. A. Graybill, "An analysis of a two-way model with interaction and no replication," *Journal of the American Statistical Association*, vol. 67, no. 340, pp. 862–868, 1972.

[202] J. R. Schott, "A note on the critical values used in stepwise tests for multiplicative components of interaction," *Communications in Statistics - Theory and Methods*, vol. 15, no. 5, pp. 1561–1570, 1986.

[203] B. Nadler, "On the distribution of the ratio of the largest eigenvalue to the trace of a wishart matrix," *Journal of Multivariate Analysis*, vol. 102, no. 2, pp. 363 – 371, 2011.

[204] L. Wei and O. Tirkkonen, "Analysis of scaled largest eigenvalue based detection for spectrum sensing," in *Communications (ICC), 2011 IEEE International Conference on*, pp. 1–5, June 2011.

[205] L. Wei, O. Tirkkonen, K. D. P. Dharmawansa, and M. R. McKay, "On the exact distribution of the scaled largest eigenvalue," *CoRR*, vol. abs/1202.0754, 2012.

[206] L. Wei, "Non-asymptotic analysis of scaled largest eigenvalue based spectrum sensing," in *Ultra Modern Telecommunications and Control Systems and Workshops (ICUMT), 2012 4th International Congress on*, pp. 955–958, Oct 2012.

[207] T. W. Anderson, "Asymptotic theory for principal component analysis," *Ann. Math. Statist.*, vol. 34, pp. 122–148, 03 1963.

[208] G. Marsaglia, "Ratios of normal variables," *Journal of Statistical Software*, vol. 16, pp. 1–10, May 2006.

[209] E. G. Larsson, O. Edfors, F. Tufvesson, and T. L. Marzetta, "Massive mimo for next generation wireless systems," *IEEE Communications Magazine*, vol. 52, pp. 186–195, February 2014.

[210] F. Boccardi, R. W. Heath, A. Lozano, T. L. Marzetta, and P. Popovski, "Five disruptive technology directions for 5g," *IEEE Communications Magazine*, vol. 52, pp. 74–80, February 2014.

[211] W. H. Chin, Z. Fan, and R. Haines, "Emerging technologies and research challenges for 5g wireless networks," *IEEE Wireless Communications*, vol. 21, pp. 106–112, April 2014.

[212] C. G. Khatri, "Distribution of the largest or the smallest characteristic root under null hypothesis concerning complex multivariate normal populations," *Ann. Math. Statist.*, vol. 35, pp. 1807–1810, 12 1964.

[213] Y. C. Liang, Y. Zeng, E. C. Y. Peh, and A. T. Hoang, "Sensing-throughput tradeoff for cognitive radio networks," *IEEE Transactions on Wireless Communications*, vol. 7, pp. 1326–1337, April 2008.

[214] E. Ahmed, A. M. Eltawil, and A. Sabharwal, "Rate gain region and design tradeoffs for full-duplex wireless communications," *IEEE Transactions on Wireless Communications*, vol. 12, pp. 3556–3565, July 2013.

[215] E. Bjrnson, M. Kountouris, and M. Debbah, "Massive mimo and small cells: Improving energy efficiency by optimal soft-cell coordination," in *Telecommunications (ICT), 2013 20th International Conference on*, pp. 1–5, May 2013.

[216] M. Chiani, M. Win, and H. Shin, "Capacity of mimo systems in the presence of interference," in *In Proc. IEEE GLOBECOM*, (San Francisco), pp. 1–6, Nov 2006.

[217] R. A. Horn and C. R. Johnson, *Matrix Analysis*. Cambridge University Press, 2nd ed., Oct 2012.

[218] S. Kotz and S. Nadarajah, *Extreme Value Distributions: Theory and Applications*. Imperial College Press, 2000.

[219] G. Muraleedharan, C. G. Soares, and C. Lucas, *Characteristic and Moment Generating Functions of Generalised Extreme Value Distribution (GEV)*, ch. 14, pp. 269–276. Nova Science, 2011.